

**SURFACE PROPERTIES AND CATALYTIC ACTIVITY
OF FERROSPINELS CONTAINING
COBALT, NICKEL AND COPPER**

**THESIS SUBMITTED TO THE
COCHIN UNIVERSITY OF SCIENCE AND TECHNOLOGY
IN PARTIAL FULFILMENT OF THE
REQUIREMENTS FOR THE DEGREE OF**

DOCTOR OF PHILOSOPHY

IN

CHEMISTRY

IN THE FACULTY OF SCIENCE

BY

RAMANKUTTY C.G.

**DEPARTMENT OF APPLIED CHEMISTRY
COCHIN UNIVERSITY OF SCIENCE AND TECHNOLOGY
KOCHI - 682 022**

NOVEMBER 2000

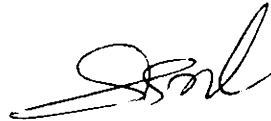
To

The Students of Chemistry

.... not on our merits but on His Grace

CERTIFICATE

This is to certify that the thesis herewith is an authentic record of research work carried out by the author under my supervision, in partial fulfilment of the requirements for the degree of Doctor of Philosophy of Cochin University of Science and Technology, and further that no part thereof has been presented before for any other degree.



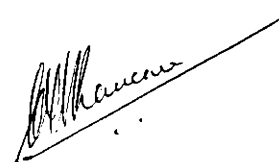
**Dr.S.Sugunan
(Supervising Teacher)
Professor in Physical Chemistry
Department of Applied Chemistry
Cochin University of Science and Technology
Kochi-22**

**Kochi-22
10th November 2000.**

DECLARATION

I hereby declare that the work presented in this thesis entitled, "Surface Properties and Catalytic Activity of Ferrospinels Containing Cobalt, Nickel and Copper" is entirely original and was carried out by me independently under the supervision of Dr. S. Sugunan, Professor in Physical Chemistry, Department of Applied Chemistry, Cochin University of Science and Technology, Kochi-22, India, and has not been included in any other thesis submitted previously for the award of any degree.

Kochi-22
10th November 2000.



RAMANKUTTY C. G.

ACKNOWLEDGEMENT

I express my profound sense of gratitude to Prof. (Dr.) S. Sugunan, Department of Applied Chemistry for accepting me, in spite of my unsuitable age and other commitments, as his student for research. He has been to me a true friend, philosopher and guide. He showed faith in me and often restored my sagging enthusiasm. Words fail me in expressing the depth of my gratitude to him.

I am grateful to Dr. K. K. Mohammed Yusuff, Professor and Head, Department of Applied Chemistry, Cochin University of Science and Technology and to Dr. P. Madhavan Pillai, former Head of the same department, for providing me the necessary facilities. I am deeply indebted to Prof. (Dr.) K. L. Sebastian, presently in IISc, Bangalore, for opening up to me the realms of theoretical chemistry.

I acknowledge my deep sense of gratitude to Dr. B. S. Rao, Deputy Director, Catalysis Division, NCL, Pune for allowing me to utilise the facilities of his laboratory during my short stay at NCL for library work. It is my pleasure to thank Dr. P. P. Bakare, NCL, Pune for the Mossbauer spectra of my samples.

My young colleagues, Dr. K. Sreekumar and Dr. T. M. Jyothi, were great company to me both at CUSAT, Kochi and NCL, Pune. Without their help, my work would not have been easy. I am indeed grateful to each of them. I wish to express my sincere thanks to two of my former students, Dr. Reghunathan Nair and Mr. Jayan for their help in my work.

The faculty members, the office staff and the librarian of the Department of Applied Chemistry have been most cooperative to me and I am grateful to each of them. Special thanks to Dr. P. A. Unnikrishnan for his timely help on all occasions.

My work in the Physical Chemistry lab. would not have been smooth but for the consideration and help rendered by all my colleagues in the lab. I am very grateful to them for their company and cooperation.

My thanks to all my colleagues in U.C.College, Aluva for their encouragement during my research period. I especially thank our Head, Prof. K. George for giving me a free hand to use the department computer for thesis work. I remember with gratitude our former Head, Dr. A. M. Chacko for inspiring me into research. Mr. Varghese Paul and Miss. Amrutha of the ICIT of U.C.College, Aluva, were always ready to rectify computer problems on various occasions and I am grateful to them for the same.

But for the efficiency and speed of N. F. Jose who typed my thesis, it would not have been ready in time. I appreciate the pride he takes in a job well done.

Finally, I would like to apologise to my wife, Gouri and children, Renu and Prabhath for the many hours of my time spent on chemistry in stead of with them and thank them for their tolerance and encouragement.

The financial support granted by ALACHE for thesis preparation is gratefully acknowledged.

C. G. RAMANKUTTY

CONTENTS

CHAPTER I	INTRODUCTION AND LITERATURE SURVEY	
1.0	INTRODUCTION	1
1.1	HETEROGENEOUS CATALYSIS	1
1.1.1	Solid acid-base concept in heterogeneous catalysis	4
1.1.2	Methods of preparation	6
1.1.3	Transition metal oxides as catalysts	9
1.1.4	Sulphate modified oxides as catalysts	11
1.2	SPINEL STRUCTURE	14
1.2.1	Normal and inverse spinels	15
1.2.2	Individual site preference for some cations	17
1.2.3	Ferros spinels	20
1.2.4	Magnetic and electrical properties of ferrites	21
1.2.5	Spinels as catalysts	21
1.3	SURFACE ELECTRON DONOR PROPERTIES	26
1.4	ALCOHOL DECOMPOSITION REACTION	29
1.5	FRIEDEL-CRAFTS ACYLATION REACTION	32
1.6	OBJECTIVES OF THE PRESENT WORK	35
	REFERENCES	37
CHAPTER II	EXPERIMENTAL	
2.1	Catalyst preparation	45
2.2	Catalyst characterisation	46
2.2.1	X-ray diffraction analysis	46
2.2.2	Infrared spectroscopy	48
2.2.3	BET surface area determination	49
2.2.4	Pore volume determination using mercury porosimetry	50
2.2.5	Energy Dispersive X-ray(EDX) fluorescence analysis and Scanning Electron Microscope(SEM)	51

2.2.6	Mossbauer spectroscopy	52
2.2.7	Thermogravimetric analysis	55
2.3	DETERMINATION OF SURFACE ELECTRON-DONOR PROPERTIES	55
2.4	ACIDITY DETERMINATION BY GRAVIMETRIC ADSORPTION OF n-BUTYLAMINE.	56
2.5	VAPOUR-PHASE CYCLOHEXANOL DECOMPOSITION REACTION	57
2.6	LIQUID-PHASE BENZOYLATION REACTIONS	57
	REFERENCES	60
CHAPTER III CHARACTERISATION AND SURFACE PROPERTIES		
RESULTS AND DISCUSSION		
3.1	PHYSICAL CHARACTERISATION	62
3.1.1	X-ray diffraction analysis	62
3.1.2	Infrared spectra	64
3.1.3	Surface area and pore volume distribution	69
3.1.4	Energy Dispersive X-ray (EDX) analysis and Scanning Electron Microgram (SEM)	71
3.1.5	Thermogravimetric Analysis	73
3.1.6	Mossbauer Spectra	74
3.2	SURFACE PROPERTIES - ACIDITY/BASICITY	92
3.2.1	Surface Electron Donating Properties (Evaluation of Lewis basicity)	92
	(i) Simple ferros spinels	96
	(ii) Mixed ferros spinels of Ni-Cu series	98
	(iii) Mixed ferros spinels of Co-Cu series	99
3.2.2	Gravimetric adsorption of n-butylamine followed by TGA	100
3.2.3	Dehydration selectivity in cyclohexanol decomposition Reaction	101

	REFERENCES	109
CHAPTER IV	FRIEDEL-CRAFTS BENZOYLATION REACTION OF TOLUENE AND BENZENE	
4.0	INTRODUCTION	111
4.1	BENZOYLATION OF TOLUENE	111
4.1.1	AFe_2O_4 (A = Ni, Co, Cu)-type systems	113
	(a) Results	113
	(b) Discussion	114
4.1.2	$Ni_{1-x}Cu_xFe_2O_4$ (x = 0.3, 0.5, 0.7)- type systems	117
	(a) Results	117
	(b) Discussion	119
4.1.3	$Co_{1-x}Cu_xFe_2O_4$ (x = 0.3, 0.5, 0.7)- type systems	119
	(a) Results	119
	(b) Discussion	121
4.1.4	Mechanism of benzylation reaction	122
4.2	BENZOYLATION OF BENZENE	126
4.2.1	Results	126
	(a) Simple ferros spinels	128
	(b) Mixed ferros spinels of the Ni-Cu series	128
	(c) Mixed ferros spinels of the Co-Cu series	128
4.2.2	Discussion of results	129
	REFERENCES	134
CHAPTER V	VAPOUR-PHASE CYCLOHEXANOL DECOMPOSITION REACTION	
5.0	INTRODUCTION	135
5.1	DECOMPOSITION OF CYCLOHEXANOL	135
5.1.1	AFe_2O_4 (A = Ni, Co, Cu) – type systems	137
	(a) Results	137
	(b) Discussion	138

5.1.2	$\text{Ni}_{1-x}\text{Cu}_x\text{Fe}_2\text{O}_4$ and $\text{Co}_{1-x}\text{Cu}_x\text{Fe}_2\text{O}_4$ ($x = 0.3, 0.5, 0.7$)- type systems	145
	(a) Results	145
	(b) Discussion	146
5.1.3	Mechanism of cyclohexanol decomposition	148
	(a) Dehydration mechanism	148
	(b) Dehydrogenation mechanism	150
5.1.4	Effect of time on stream	152
5.1.5	Cyclohexanol decomposition and benzylation of toluene-a comparison of rate constants.	152
	REFERENCES	155
CHAPTER VI SUMMARY AND CONCLUSION		
6.1	SUMMARY	158
6.2	CONCLUSIONS	161

PREFACE

Ferrospinel, $A^{\text{II}}\text{Fe}_2\text{O}_4$ have attracted much attention due to their remarkable transport, magnetic and catalytic properties. The catalytic effectiveness of ferrites for many reactions arises because of the ease with which iron can exchange oxidation state between 2 and 3. But, the spinel structure imparts these materials stability to withstand extremely reducing conditions. The reduction of Fe^{3+} to Fe^{2+} takes place without altering the lattice configurations so that, upon reoxidation, the original state is retained.

Ferrites are commonly produced by conventional ceramic processes involving high temperature ($\geq 1200^\circ\text{C}$) solid state reactions between the constituent oxides/carbonates. These methods have some inherent drawbacks such as chemical inhomogeneity, coarser particle size, poor compositional control, etc. These adversely affect the catalytic performance of the ferrites. Recently reported low temperature controlled coprecipitation methods have overcome these drawbacks and produced homogeneous and very fine ferrites powders with high surface areas.

Our work is oriented to evaluate the surface properties and catalytic activities of ferrospinel containing Co, Ni and Cu prepared by the low temperature route. Various physico-chemical methods have been adopted to characterise the systems. The reactions carried out are the Friedel-Crafts benzylation of aromatics and the cyclohexanol decomposition. We have attempted the sulphate modification of the ferrites and have studied the surface and catalytic properties of the sulphated analogues.

The work is presented in six chapters, the last chapter giving the summary and conclusions of the results presented earlier. Our samples prove as potential catalysts for the benzylation of aromatics, for which truly heterogeneous catalysts are rare. Again, the materials show remarkable dehydration/dehydrogenation activities during cyclohexanol decomposition. There is plenty of scope for research in this field, especially in the development of environmentally benign catalysts for acylation reactions.

CHAPTER-I

INTRODUCTION AND LITERATURE SURVEY

1.0 INTRODUCTION

The quality of life is strongly connected to a clean environment. The environmental concerns and regulations have increased very much in the public and in the governments all over the world during the last two decades. Chemical industry has been blamed for producing environmentally hazardous substances which cause acid rain, a reduction in stratospheric ozone levels and so on. The awareness and concern have given impulse for developing cleaner, more efficient and more selective catalysts which play the most important role in chemical industry. Research and development in catalysts are targeted to achieve "100% selectivity!" and "zero emission!" The replacement of homogenous catalyzed processes having many well-known drawbacks with heterogeneous ones is becoming more important in chemical and life science industry.

1.1 HETEROGENEOUS CATALYSIS

There are only very few industrially important homogeneous catalytic processes like (i) alkylations and acylations using Lewis acids such as AlCl_3 and BF_3 , (ii) the WACKER process, (iii) the OXO process and (iv) the MONSANTO process [1]. Nearly eighty percent of heavy industrial chemicals are obtained by heterogeneous catalytic processes. Here the reactants and the catalysts are present in different phases. Commonly the catalyst is a solid and the reactants are either gases or liquids. Rarely the actual catalyst is a liquid at the reaction temperature, in which case, it must be supported on a refractory solid.

A heterogeneous catalyst acts by providing an alternate reaction path with a lower energy of activation. The general steps involved in heterogeneous catalysis are: (i) diffusion of the reactants to the surface of the catalyst, (ii) chemisorption of the reactants on the surface, (iii) reaction at the surface, (iv) desorption of the products from the surface and (v) diffusion of the products away from the catalyst. Of these, chemisorption on the surface followed by reaction at the surface are the most important steps. An effective catalyst must interact with the reactant(s) only just firmly enough to cause chemisorption; strong chemisorption often "poisons" the catalyst.

Heterogeneous catalytic processes have many advantages over the homogeneous ones. The main advantage is that it can be operated continuously in a reactor without interruption. Being in different phases, the separation of the final reaction mass from the catalyst is quite easy. The heterogeneous catalysts need be used only in smaller amounts, are often reusable, are more environmentally benign and have little disposable problems in comparison with homogeneous catalysts.

Most of the solid catalysts are used in three major industries: chemical processing, petroleum refining and pollution control. In terms of physical volume, catalyst consumption continues to be dominated by petroleum refining. But cost-wise, pollution abatement catalysts, being mostly made of costly platinum group metals, match the cost of catalysts consumed in petroleum refining [2]. Every segment of the catalyst business is growing and the world market for heterogeneous catalyst is expected to reach highest peak in the coming years.

The properties of a good catalyst for industrial use may be divided into two categories [3]:

- (i) properties which determine directly catalytic activity and selectivity. Here factors such as bulk and surface chemical composition, local microstructure and phase composition are important.
- (ii) properties which ensure their successful implementation in the catalytic process. Here thermal and mechanical stability, porosity, shape and dimension of catalyst particles enter.

Using a catalytic material in industry often requires a compromise in the properties of the catalysts to produce a material, which meets the contradictory demands imposed by industrial processes. Experiments show that, in the majority of cases, the chemical composition of the catalyst exerts a greater influence on its activity than the method of preparation.

Heterogeneous catalysts are classified into several ways. Based on their physico-chemical nature, they can be classified as follows:

- (1) Metal oxides: Simple metal oxides, mixed metal oxides, supported metal oxides and modified metal oxides.
- (2) Supported metals/bimetallic catalysts.
- (3) Zeolites/molecular sieves
- (4) Clays and hydrotalcites
- (5) Solid supported heteropolyacids.

Reactions on surfaces may be classified in terms of reactant or product classes or on the basis of mechanistic similarities [4]. The latter method is more suitable for applying the principle of surface science studies and also for “designing” new catalysts. The simplest classification is into two main groups:

(1) *acid-base (ionic) reactions*

Catalytic cracking, hydration, dehydration, hydrolysis, isomerisation and a host of other reactions pertain to this type. Acid-base property of a heterogeneous surface is the important factor in determining the catalytic efficiencies for these types of reactions. In acid-catalysed reactions, reactants act as bases toward catalysts which act as acids and in base-catalysed reactions, vice-versa.

(2) *Oxidation-reduction (electronic) reactions:*

Reactions pertaining to this type are those of oxidation, reduction, hydrogenation, dehydrogenation, decomposition of unstable oxygen containing compounds and others. The reactions are catalysed by solid possessing free or easily excited electrons i.e. metals and semiconductors.

Metal catalysts can be supported or unsupported and are primarily used for hydrogenations, isomerisations and oxidative dehydrogenations. Semiconductor oxides are most commonly used in oxidations. These are materials in which the metallic species is relatively easily cycled between two valence states and are exemplified by the transition metal oxides. These are simple or complex oxides which can act as acids or bases as well as redox catalysts.

1.1.1 Solid acid-base concept in heterogeneous catalysis.

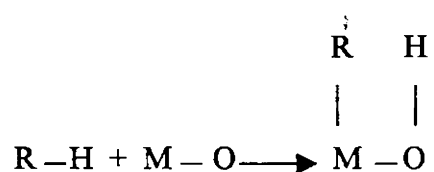
Tanabe [5] defined a solid acid as one on which the colour of a basic indicator changes concomitant with its chemisorption. Following both the Brønsted and Lewis definitions, a solid acid shows a tendency to donate a proton or to accept an electron pair, whereas a solid base tends to accept a proton or to donate an electron pair. An exhaustive list of various solid acids and bases is tabulated by Tanabe [5]. This list of solid acids includes various naturally occurring clay minerals, zeolites, the well-known solid acid namely silica-alumina, various metal oxides, sulphides, sulphates, phosphates and halides. A list of solid superacids i.e. acids stronger than 100% sulphuric acid or having the Hammett acidity function, H_0 less than -11.9, is also given. This includes Nafion, ZSM - 5 zeolite and sulphate-modified zirconia, titania and ferric oxide. However, the classification of solids into solid acids and solid bases may, in several cases, not be meaningful due to large heterogeneity of solid surfaces. The best example is alumina which is a typical amphoteric.

A complete description of acidic and basic properties on solid surfaces requires the determination of the number, strength, type and distribution of the acid and base sites. The exposed cations and anions on oxide surface have long been described as acid-base pair sites.

Several acidic properties originate from local surface defects. Thus the exposed metal cations which are coordinatively unsaturated (CUS) act as Lewis acid sites accepting electrons from adsorbed molecules. The strength of these acid sites depends on the charge and size of the cations. By the hard-soft acid-base (HSAB) concept, cations of higher charge to radius ratio are harder. Surface hydroxyl groups originating from incomplete dehydration exhibit considerable Brønsted acidity. Electron deficient states are also formed by the introduction of foreign cations into the lattice of a solid, which, due to different co-ordination number, are not able to compensate for their positive charge. The stronger acidity of mixed oxides over the single oxides is due to such charge imbalances. Acidic properties can also originate from chemical

modifications of a surface like introducing a ligand having a different electronegativity than the lattice anions [6].

Adsorbed Brønsted acids often dissociate on an oxide surface causing protonation of the surface oxygen anions and coordination of the conjugate base of the acid to surface cations. This reaction is schematically depicted as



The key requirement for such a dissociation of reactants is one of coordination vacancies on the surface metal cations (Lewis acid sites) and surface Brønsted basic sites to abstract and to bind the protons originating from the adsorbate. Experimental evidence suggests that the presence of coordinatively unsaturated (CUS) metal cation rather than CUS-type oxide ion is decisive in such adsorption. Steric arguments also justify this. The smaller neighbouring cations in the lattice may obstruct access to oxide ions less than the larger anions obstruct the cations. Again, the small - sized proton has to bind to the relatively unobstructed oxide anion while the bulky organic conjugate base anion must bind to the more hindered surface metal ion. Small wonder that the co-ordination environment of the surface cation is the critical surface characteristic [4].

Heterogeneous acid catalysis attracted much attention primarily because of its involvement in petroleum refinery. Solid acid catalysts are invariably used in the petroleum cracking process which is the largest among the industrial chemical processes. Extensive studies undertaken in the 1950s revealed that the essential nature of cracking catalysts are acidic. Generation of acidic sites on the solids was extensively studied. As a result, amorphous silica-alumina was utilised as a cracking catalyst for a long time. Presently zeolites (crystalline alumino silicates) have replaced almost all other kinds of catalysts in cracking.

In contrast to these extensive studies on heterogeneous acidic catalysts, fewer efforts have been given to the study of heterogeneous basic catalysts. The first study of heterogeneous basic catalysts, that sodium metal dispersed on alumina acted as effective catalyst for double bond migration of alkenes, was reported by Pines *et al.* [7]. The various types of heterogeneous basic catalysts are [8]:

- (1) Single component metal oxides:- oxides of alkali, alkaline earth and rare earth metals, ThO_2 , ZrO_2 , ZnO and TiO_2 .
- (2) Zeolites :- alkali ion- exchanged and alkali ion- added zeolites.
- (3) Supported alkali metal ions:- alkali metal ions supported on alumina, silica or alkaline earth oxide.
- (4) Clay minerals:- hydrotalcite, chrysotile, sepiolite.
- (5) Non-oxides:- KF supported on alumina, lanthanide imide and nitride on zeolite.

Except for non-oxide catalysts, the basic sites are believed to be surface oxygen atoms. These oxygen atoms would be able to interact attractively with a proton.

Some important solid base catalysed reactions are: double bond migration reactions of unsaturated compounds, alcohol dehydrogenation to aldehydes or ketones, hydrogenation of olefins, amination of conjugated dienes, Meerwein - Ponnendorf - Verley (MPV) reduction, side chain alkylation of aromatics, aldol condensation etc. etc.

1.1.2 Methods of Preparation

The goal of a catalyst manufacturer is to produce and reproduce a commercial product which can be used as a stable, active and selective catalyst. Subtle changes in the preparative details may result in dramatic alteration in the properties of the final catalyst. In spite of numerous studies, the preparation of heterogeneous catalysts with specific properties is still regarded as an art, often kept as a secret by the catalyst manufacturer. However, many preparative routes are sought so as to give catalysts with sufficient surface area, good porosity and suitable mechanical strength.

Schwarz *et al.* [3] divide the preparation of almost all catalysts into two main routes: (i) methods in which the catalytically active phase is generated as a new solid phase by either precipitation or a decomposition reaction. This involves "blending" of

proper reagents from a liquid or solid medium and (ii) methods in which the active phase is introduced and fixed onto a pre-existing solid by suitable impregnation methods. This involves “mounting” of the catalytically active material on a pre-existing support.

;

Between these extremes lie methods which are best characterised as solid transformations and includes dispersion of metals into thin films or colloids. Along the “blending” route, the most common preparation methods are precipitation, co-precipitation, gelation, complexation, crystallization and ceramic methods.

The most common method for preparation of bulk oxide catalysts is the *(co)precipitation* of a precursor phase, usually hydroxides or carbonates, followed by filtration, washing and calcination of the product leading to the oxidic phase. The creation of the precursor solid phase from the liquid medium results from two elementary processes which occur simultaneously or sequentially: (1) nucleation i.e., formation of the smallest elementary particles of the new phase (2) growth or agglomeration of the particles. Factors such as pH, temperature, presence of impurities, nature of reagents etc. are important in determining the morphology, texture and the structure of the precipitates, e.g., under conditions of super-saturation, the rate of nucleation is much faster than rate of crystal growth and leads to numerous yet very small particles. The chemical and physical properties of particles kept in contact with the mother liquor may change due to secondary processes. This ‘aging’ or ‘ripening’ leads to an increase in particle size of precipitates and agglomeration of colloidal particles. A better method of mixing the components is achieved by the continuous homogeneous precipitation where the precipitating agent, usually OH⁻ ions, is slowly and continuously generated by a controlled hydrolysis process such as hydrolysis of urea.

The *co-precipitation* method used to synthesize multi-component systems does not often give homogeneous precipitates due to differences in the solubility between the components. Under conditions of slow precipitation rate or poor mixing, co-precipitation is selective and the coprecipitate is heterogeneous in composition.

A more uniform precipitate is obtained if the metal solution is quickly added to the base with continuous stirring.

In contrast to the (co)precipitation route, the *sol-gel method (gelation)* is a homogeneous process which results in a continuous transformation of a solution into a hydrated solid precursor (hydrogel). Sol-gel methods allow the control of texture, composition and homogeneity of the finished solids. The nanoscale chemistry involved in sol-gel method is a straightforward way to prepare highly divided materials. The method involves the hydrolysis and gelling (by the controlled addition of water) of metal alkoxides or other reactive compounds in alcoholic solutions. The resulting open structure in which the primary units are held together by chemical or dipole forces is imbibed by the solvent. This structure is transformed to the solid phase by high-pressure heating whereby the liquid contained in the gel changes to supercritical vapours. Drying this under supercritical conditions gives aerogels where the solid does not collapse and retains the open structure. These aerogels have high porosity, large surface area, extremely low thermal conductivity and very good textural and structural stability.

Crystallisation has found wide applications in the preparation of homogeneous microporous crystalline solids in which the active phase is distributed uniformly. Such materials are designated as molecular sieves and includes the various zeolites (crystalline aluminosilicates), ALPOs (aluminophosphates) etc. A typical zeolite synthesis involves mixing together alkali, sources of alumina and silica, water and other components in appropriate proportions. The resulting gel is subjected to elevated temperatures in autoclaves for crystallisation, which usually occurs in a time span of several hours to weeks. Zeolite synthesis is, more or less, an art.

The *complexation* method makes use of chemical reactions which transform slowly and without physical discontinuity the homogeneous solution of catalyst precursors into a homogeneous, amorphous phase with either glassy, jelly-like or foamy appearance. This precursor is then dried and decomposed to yield better intermixed and more highly dispersed oxides than those prepared by the usual precipitation route. To obtain smooth gelation, the catalyst precursors are complexed

or chelated with multifunctional organic reagents, yielding three-dimensional organic network with the metallic component entrapped in this structure. Metallic elements are added as water-soluble salts and various α -hydroxy acids (e.g. citric acid) are used as complexing agents.

;

In the high temperature *ceramic method*, the mixed oxide phase results from heating intimately mixed powders at temperatures high enough to allow interdiffusion and solid state reactions. Precursor compounds, such as carbonates and oxalates, that decompose at lower temperature, have also been used instead of the corresponding oxides. This method has the advantage of the extreme simplicity and its use is essential for preparing single phase mixed oxides such as perovskites and spinels. A major shortcoming of the ceramic method is the lack of homogeneity of the materials prepared because the solid state reactions between the precursor oxides occur with very slow rates. Again, the high temperature (about 1300 K) required to complete solid state reactions leads to drastic decrease in surface area of the resulting material by sintering.

1.1.3 Transition metal oxides as catalysts

Not only do the transition metals themselves possess high catalytic activity, but also do their alloys and compounds with non-metals like oxides, sulphides etc. Generally transition metal oxides are active catalysts for oxidation-reduction processes. But these systems also exhibit acido-basic properties, being capable of sorption of acids and/or bases as well as of catalysing some acidic reactions such as dehydration of alcohols, isomerisation of hydrocarbons etc. Usually transition metal oxides are components in catalysts used for reactions such as oxidation, oxidative and non-oxidative dehydrogenation, reduction, ammoxidation, metathesis (production of long chain alkenes) and water gas shift reaction (production of hydrogen). The variable valence of the constituent metal ions enables the oxide to act as a sort of "electron bank." Much work was done by the research group at the Ford Motor Co. (USA) upon chemisorption of CO₂, CO and NO probes on the first row transition metals oxide catalysts within the framework of NO plus CO removal from the exhaust gases of car engines [9]. Again, much work was devoted to the semiconductor aspects of these systems and to the interpretation of simple reactions in terms of the boundary-layer

theory or similar concepts [10]. Many transition metal oxides have n-type or p-type semiconductor properties. On heating in air, n-type oxides lose oxygen. The loss of oxygen by an n-type oxide is made possible by the availability of a lower oxidation state of the metal ion as in TiO_2 , V_2O_5 , CrO_3 , CuO or Fe_2O_3 . The adsorption of oxygen onto a p-type oxide is made possible by the availability of a higher oxidation state for the cation as in Cu_2O , Cr_2O_3 , CoO and NiO [11]. The adsorbed oxygen on a p-type oxide is more active than the lattice oxygen of an n-type oxide. Hence n-type oxides are used for selective oxidation of hydrocarbons, as oxidation on p-type oxides often gives only carbon dioxide and water.

Often transition metal oxides act as a precursor for other catalysts. An example is the doping of molybdenum sulphide with cobalt (II) oxide on an alumina support to make a commercial hydrodesulphurisation (HDS) catalyst [12].

Transition metal oxides also have acid-base properties. Auroux *et al.* [13] studied the adsorption of ammonia and carbon dioxide on various oxides microcalorimetrically and concluded that transition metal oxides are either acidic (A-type) or amphoteric (A-B type). Numerous works were done to correlate the acid-base properties of mixed transition metal oxides with the catalytic activity/selectivity in selective oxidation of hydrocarbons [14-17]. In spite of numerous works no general correlation between acido-basic properties and performance in oxidation reaction has been so far formulated [18].

Titania and zirconia have attracted much attention because these are good supports for metal catalysts and also change to superacids on combining with a small amount of sulphate. TiO_2 is classed as weakly acidic while ZrO_2 as acid-base bifunctional [5]. V_2O_5 , Nb_2O_5 and Ta_2O_5 are typical solid acid catalysts. Oxides of Cr, Mo and W are seldom used as single oxides but are used as mixed oxides with alumina and silica for dehydrogenation, hydrogenation and skeletal isomerisation of hydrocarbons.

Ferric oxide is regarded as weakly acidic and basic and is practically used for oxidation or dehydrogenation reactions as single oxides promoted by alkalies or as

mixed oxides. Typical examples are dehydrogenation of ethylbenzene ($\text{Fe}_2\text{O}_3\text{-K}$), water gas shift reaction ($\text{Fe}_2\text{O}_3\text{-Cr}_2\text{O}_3$), ammoxidation of propylene ($\text{Fe}_2\text{O}_3\text{-Sb}_2\text{O}_5$) and dehydrogenation of methanol ($\text{Fe}_2\text{O}_3\text{-MoO}_3$) [19 a]. Tanabe [19 b] found that Fe_2O_3 prepared from ferric alum is very acidic and active for several reactions. Again Fe_2O_3 obtained by heat-treating of $\text{Fe}_2\text{S}_2\text{O}_7$ showed maximum acidity and catalytic activity at the calcination temperature of 700°C for several reactions [20-24].

CoO and Co_3O_4 are the ordinary oxides of cobalt and Co_3O_4 is one of the most active single metal oxides for oxidation reaction [5].

Non-stoichiometric nickel oxide has high catalytic activity for deep oxidation. NiO mixed with solid acids such as SiO_2 [25], $\text{SiO}_2\text{-Al}_2\text{O}_3$ [26] and NiSO_4 [27] are active for dimerisation of olefins.

Copper oxides CuO and Cu_2O are semiconductors and effective for redox-type reactions such as oxidation or dehydrogenation. Many copper-based catalysts such as CuO-ZnO [28], $\text{Cu-ZnO-Al}_2\text{O}_3$ [29] and CuO-CoO [30] have been reported to be effective for dehydrogenation of cyclohexanol to cyclohexanone.

Transition metal oxides as binary or ternary complex oxides with definite crystal structure show greater structural stability and catalytic activity. Thus single phase complex oxides of formula ABO_3 having the perovskite structure and the general formula AB_2O_4 having the spinel structure have been widely studied for their surface properties and catalytic activities. In the present investigation, iron based spinel oxides of cobalt, nickel and copper are chosen.

1.1.4 Sulphate-modified oxides as catalysts

It is well-known that surface modification of metal oxides with anions, especially sulphate ions, often enhances their acidities and catalytic activities. Sulphation of metal oxides has been most widely studied because some of these are found to be superacidic. The discovery of solid superacids free of halogens can be traced to the study of the effect of anions on the preparation of TiO_2 [31]. Further studies, especially by the researchers of Hokkaido University, reveal that, among the

various sulphate modified oxides, only sulphated ZrO_2 , TiO_2 , HfO_2 and Fe_2O_3 or their binary mixtures and metal promoted sulphated ZrO_2 showed superacidity [32]. Superacids are important catalysts for skeletal isomerisation of *n*-alkanes and alkylation of aliphatics by olefins to produce high octane gasoline components in petroleum industry. Researchers have long been seeking to replace liquid superacids with less corrosive solid superacids and hence there is a great interest in the study of sulphate modified oxides. More than 200 papers and patents on solid superacids (mainly, SO_4^{2-}/ZrO_2 and its modified ones) have been reported since 1990. Nevertheless, not many industrial processes have yet been developed using sulphated metal oxides as catalysts mainly due to catalyst deactivation and low selectivity caused by the strong acidity [33].

The standard procedure of sulphation is the impregnation of the metallic hydroxide or oxide by soaking these with a definite amount of 1N H_2SO_4 or dilute ammonium sulphate solution for a few hours followed by filtration (without washing), drying and calcination. Instead of filtration, evaporation of the solvent to get a dried mass, followed by calcination is also adopted [34]. Generally (not always), sulphation increases the surface area of the catalyst. This is attributed to the inhibition of sintering and the delay in the transition from amorphous to crystalline phase during calcination [32,35].

Many theories are put forward to explain superacidity, but the exact nature of surface acidity in sulphate-modified oxides remains controversial [36]. Some authors [37,38] report that sulphated zirconia has strong Lewis acidity arising from coordinatively unsaturated Zr^{4+} centres, whose positive charge is enhanced by the inductive effect of the neighbouring $S = O$ groups. Some other authors [39,40] report the co-presence of both Lewis (cationic) and Brønsted (protonic) acidities responsible for the peculiar catalytic features of sulphate-doped ZrO_2 . NMR study of acid sites on sulphated zirconia using trimethylphosphine as a probe, supports the latter view [41]. IR studies of adsorbed pyridine show the presence of both Lewis and Brønsted sites on sulphated oxides. The nature of acid sites (Lewis or Brønsted) on sulphated zirconia depends critically on the water content, which, in turn, depends on the history of pretreatment of the sample. The water content of a working catalyst can also be affected by moisture present in feedstocks and by water produced during the reaction [42].

The following models ,I – V, are proposed for the structure of surface sulphate on sulphate-modified zirconia.(Fig. 1.1.1)

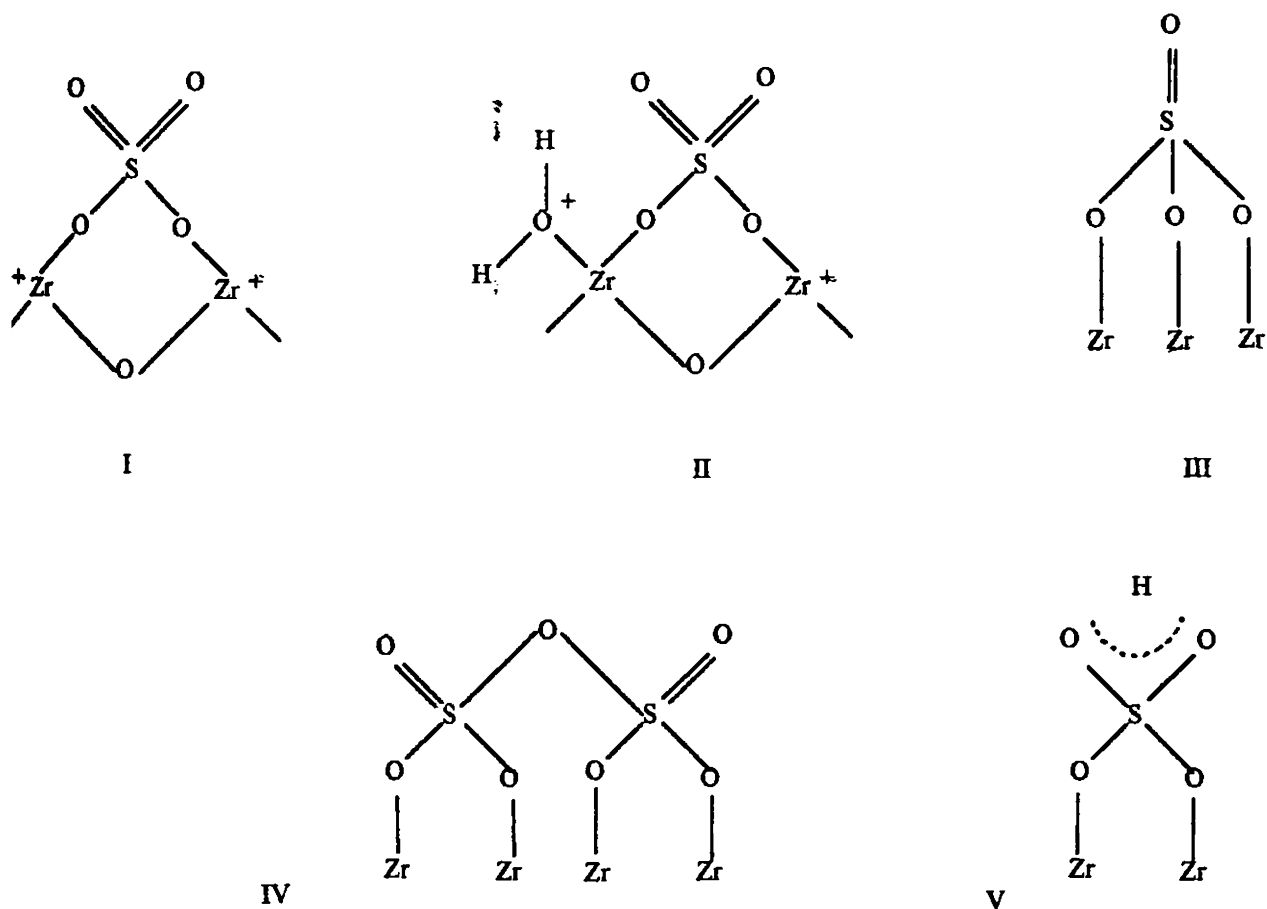


Fig. 1.1.1. Various models proposed for sulphate-modified zirconia.

Model I and II are proposed by Tanabe and coworkers [32,35] for the sulphate modified zirconia in the absence of and in the presence of moisture respectively. Models III, IV and V are proposed by Lavalley and coworkers [38,43,44] for the same catalyst. Model III corresponds to low sulphate loading, IV to high sulphate loading and V to low sulphate loading in presence of moisture. In model V, it appears as if ZrO_2 is modified by bisulphate species (HSO_4^-). In fact, the existence of HSO_4^- on sulphated zirconia has been proved both experimentally [45] and theoretically [46].

The presence of superacidity may be tested by the catalytic activity for low temperature isomerisation of *n*-butane to isobutane reaction, which is catalysed only by superacids. Again , IR spectra of superacidic sulphated oxides typically give a

single strong band near 1380 cm^{-1} , in addition to a number of weak bands in the range, $900\text{-}1100\text{ cm}^{-1}$ [38].

Sulphated oxides are also found to be effective for acylation reactions [47-50]. These are also potential catalysts for hydrocracking of hydrocarbon polymer wastes to $\text{C}_4 - \text{C}_{20}$ liquids with gasoline components exceeding 75% [51]. The surface electron-donor properties and catalytic activities of sulphate modified zirconia [52], samaria [53] and stannic oxide [54] have also been investigated.

Since $\text{SO}_4^{2-}/\text{Fe}_2\text{O}_3$ has superacidic properties and the present work involves investigation of spinel ferrites of Co, Ni and Cu, we took it as an interesting extension work to study the effect of sulphation on these ferrosinels. Literature survey reveals that sulphation studies of spinel-type mixed oxide catalysts have not been so far attempted.

1.2 SPINEL STRUCTURE

Spinel form a large class of compounds whose crystal structure is related to that of the mineral spinel itself, MgAl_2O_4 . The general formula of spinels is AB_2O_4 . The structure can be described in terms of cubic close packing (ccp) of the anions, bound together by suitably placed interstitial cations. Most of the spinels are oxides, some are sulphides, selenides or tellurides and a few are halides. Again the charge distribution of cations can be 2-3 as in MgAl_2O_4 , 2-4 as in Mg_2TiO_4 and 1-6 as in Na_2WO_4 [55]. Of these, 2-3 oxidic spinels are the commercially most important.

The unit cell of spinel structure consists of 8 formula units and hence is represented as $\text{A}_8\text{B}_{16}\text{O}_{32}$. The space group of a spinel is $\text{Fd}\bar{3}\text{m}$. The ccp of 32 oxygen anions will have 64 tetrahedral (T) voids and 32 octahedral (O) voids. Of these, only 8 T-voids and 16 O-voids are occupied by cations in an ordered way. These are called A-sites and B-sites because A cations occupy T-sites and B cations, O-sites. The unit cell of spinel structure is shown in Fig 1.2.1. Here the structure is shown in such a way that the A cations form a supercell fcc unit cell. The cube is divided into 8 octants. The structure within the octants can be imagined as containing AO_4 and B_4O_4 structural units in alternate octants [56]. Fig.1.2.2 shows the arrangement of AO_4 and B_4O_4 units in two neighbouring octants in the unit cell. The atoms are in three sets of special

positions and some typical fractional coordinates of the atoms are (0,0,0) for A, $(\frac{5}{8}, \frac{5}{8}, \frac{5}{8})$ for B and $(\frac{3}{8}, \frac{3}{8}, \frac{3}{8})$ for oxygen. The location of oxygen is an adjustable parameter in the spinel structure and is called the oxygen parameter, u . It has a value 0.375 in the ideal structure. This parameter characterises the difference in the expansion of tetrahedral and octahedral sites in order to accommodate larger cations. In the ideal ccp structure of oxide ions, T-sites can accommodate cations with radii $\leq 0.30 \text{ \AA}$ and the O-sites, cations with radii $\leq 0.55 \text{ \AA}$ [57]. But the cations in the spinels are usually larger than these and hence the T- and O-sites have to expand in the [111] direction (i.e. along the body diagonals of the unit cell) to accommodate the cations. If the expansion of T- and O- sites occurs in the same ratio, u is still 0.375. But usually T-sites expand to a larger extent than the O-sites to produce a non-ideal structure having $u > 0.375$.

Fig 1.2.3 represents the immediate neighbours of an anion in the spinel structure. Each anion is surrounded by one A and three B cations. If 'a' denotes the unit cell edge length, the AX distance is $a(u-\frac{1}{4})\sqrt{3}$, the BX distance is $a(\frac{5}{8} - u)$, the angle AXB is 125° and the angle BXB is 90° , for small deviations from the ideal structure. This means that the BB distance $\frac{\sqrt{2}a}{4}$ is considerably shorter than the AA distance $\frac{\sqrt{3}a}{4}$. As u equals $\frac{3}{8}$ for the ideal spinel structure, we get AX distance as $\frac{\sqrt{3}a}{8}$ and BX distance, $\frac{a}{4}$ [58]

1.2.1 Normal and inverse spinels

The spinel is called "normal" if A cations occupy T-sites and B cations, O-sites. But Barth and Posenjak [59] pointed out a second possibility in which half of the B cations occupy the T-sites and all the A cations together with the other half of the B cations occupy the O-sites. When this is the cation distribution, it is known as an *inverse spinel*. In between these extremes, it is possible to have various degrees of randomization where both types of sites are occupied partly by A cations and partly by B cations. These are known as *random spinels*. (Table 1.2.1). The cation distribution may be described by a parameter λ , defined as the fraction of B atoms in T-sites. For a normal spinel $\lambda = 0$, for an inverse spinel $\lambda = 0.5$ and for a completely random spinel, $\lambda = \frac{1}{3}$ [60].

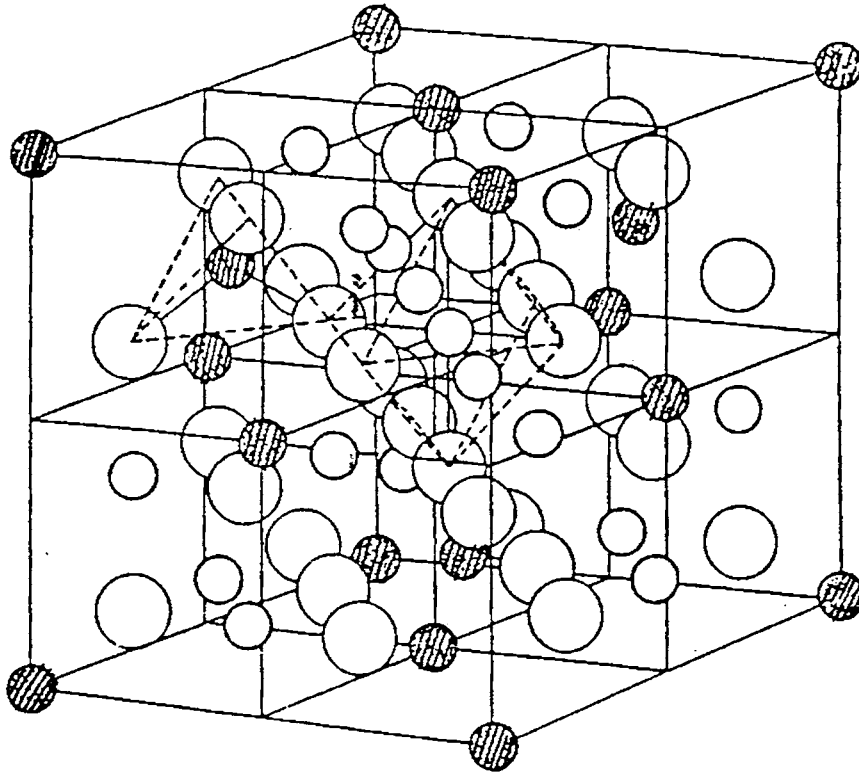


Fig. 1.2.1. The unit cell of an ideal spinel structure. Hatched circles indicate A cations, unhatched circles indicate B cations and large unhatched circles indicate oxygen anions.

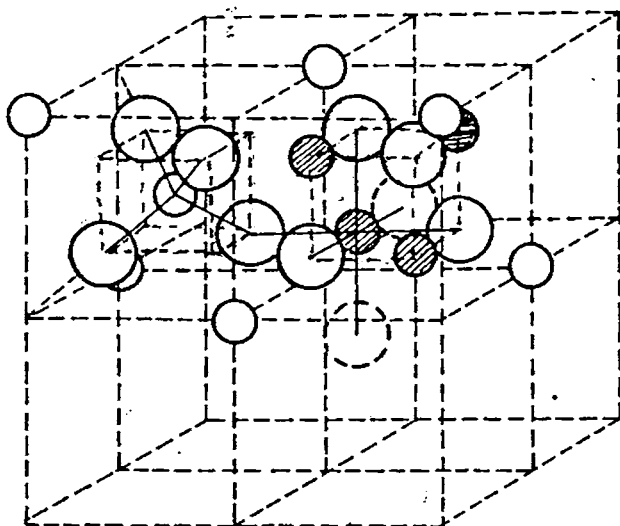


FIG. 1.2.2 Unit cell of the ideal spinel structure
The position of the ions in only two octants shown.
The dashed circles belong to other octants.
Large circles: ANIONS; small hatched circles: B-SITE CATIONS; small unhatched circles: A-SITE CATIONS.

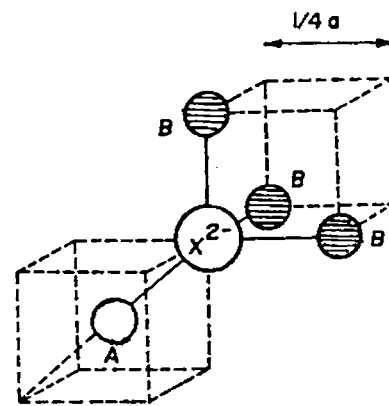


FIG. 1.2.3 The nearest neighbours of anion in the spinel structure. X: ANION; A: A-SITE CATION; B: B-SITE CATION; a: cell edge.

Table 1.2.1. Examples of some normal and inverse spinels.

Type	Structure	Examples
Normal	$(A)_{Tet} [B_2]_{Oct} O_4$	$ZnFe_2O_4$, $MgCr_2O_4$
Inverse	$(B)_{Tet} [AB]_{Oct} O_4$	$NiFe_2O_4$, $CoFe_2O_4$
Random ($0 < x < 1$)	$(A_x B_{1-x})_{Tet} [A_{1-x} B_{1+x}]_{Oct} O_4$	$MnFe_2O_4$, $FeMn_2O_4$

1.2.2 Individual site preference of some cations

The distribution of cations in the available T- and O-holes depends on a number of factors of which the following are important.

(i) Cation size

A greater stability on the lattice is expected if the smaller B cation occupies the smaller T-site. Thus, if the radius of B cation \ll that of A cation, the tendency is towards inverse spinel. But the polarisation effect often outweighs this. Large A^{2+} ions have less polarising influence on oxide ions than the small B^{3+} ions and hence B^{3+} ions in octahedral sites stabilise the structure due to this higher degree of polarisation, favouring normal spinel structure [61].

(ii) Madelung constant

Taking chemical bonding in spinels as purely ionic, the main part of the lattice energy is contributed by the Coulomb energy and Born repulsive energy. The Madelung constant (M) of the spinel structure has been calculated by Verwey, De Boer and Van Santen [62] as a function of the oxygen parameter u and the charge distribution among the A- and B- sites. Their results are represented in Fig. 1.2.4 where M is plotted as a function of u for different values of the average ionic charge on A-sites, q_A . From this figure it is clear that, for electrostatic reasons, it is favourable to have either large ions (high u) with low charge or small ions (low u) with high charge on A - sites. The Madelung constant of inverse 2-3 spinel is hardly affected by the oxygen parameter.

The second energy term is Born repulsion. It is difficult to take this energy term into account due to lack of compressibility data. But, on geometric considerations, it is

concluded that, in normal spinels, the relatively small tripositive ions on B-sites cause anion-anion contact, resulting in a less favourable stacking and a larger edge length. The unit cell edges of normal 2-3 spinels are about 0.8% [63] larger than those of the corresponding inverse spinels.

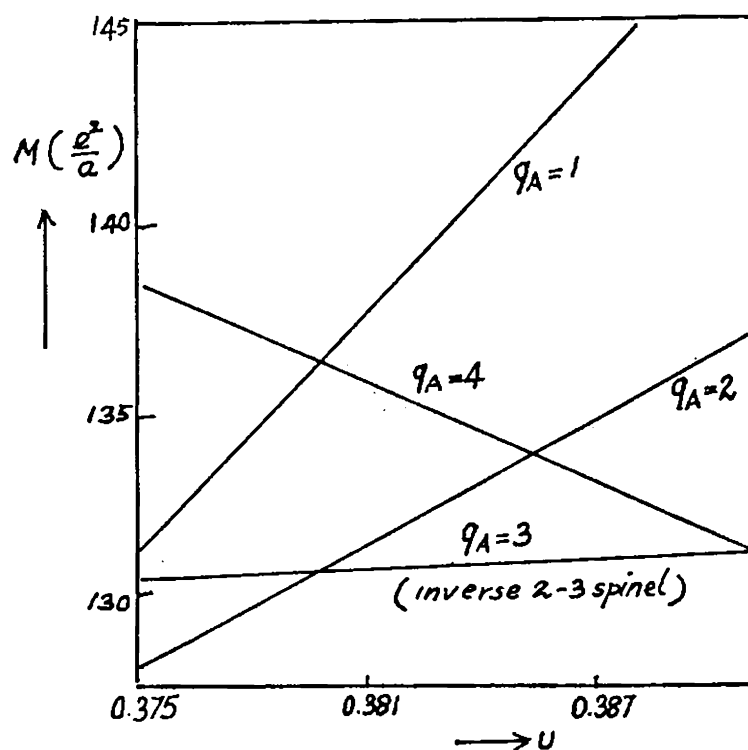


Fig. 1.2.4 The Medulung constant M (in e^2/a units) of the spinel structure as a function of the oxygen parameter u for different values of the average ionic charge on A sites, q_A

Dunitz and Orgel [64] and simultaneously McClare [65] have calculated site preference energies of transition metal ions in oxides using crystal field theory (CFT).

The crystal field stabilisation energies (CFSE) are given in units of Δ_o and Δ_t in Table 1.2.2 and in the units kJ mol^{-1} in Table 1.2.3 respectively, for various d-electron configurations[66].

Table 1.2.2 Crystal Field Stabilisation Energies calculated for different 'd' systems

Configuration	Crystal Field Stabilisation Energy	
	Octahedral field	Tetrahedral field
d^1 and d^6	$0.4 \Delta_o$	$0.6 \Delta_t$
d^2 and d^7	$0.8 \Delta_o$	$1.2 \Delta_t$
d^3 and d^8	$1.2 \Delta_o$	$0.8 \Delta_t$
d^4 and d^9	$0.6 \Delta_o$	$0.4 \Delta_t$
d^5 and d^{10}	0	0

Table 1.2.3 Crystal Field Stabilisation Energies (kJ mol^{-1}) estimated for transition metal oxides, from spectroscopic values of Δ_o and Δ_t (Data from Dunitz and Orgel)

Ion		Octahedral stabilization	Tetrahedral stabilization	Excess Octahedral stabilization
Ti^{3+}	d^1	87.4	58.5	28.9
V^{3+}	d^2	160.1	106.6	53.5
Cr^{3+}	d^3	224.5	66.9	157.6
Mn^{3+}	d^4	135.4	40.1	95.3
$\text{Fe}^{3+}, \text{Mn}^{2+}$	d^5	0	0	0
Fe^{2+}	d^6	49.7	33.0	16.7
Co^{2+}	d^7	92.8	61.9	30.9
Ni^{2+}	d^8	122.1	35.9	86.2
Cu^{2+}	d^9	90.3	26.8	63.5

These data show that d^5 and d^{10} configurations have no site preference while d^3 and d^8 have very large octahedral site preference. Ions with d^4 and d^9 configuration can be stabilised additionally by Jahn-Teller distortions. If the regular O_h symmetry octahedra of surrounding anions is elongated or compressed in the c direction to give D_{4h} symmetry, the doublet (e_g) and triplet (t_{2g}) levels split. The splitting of the doublet is larger. It is clear that, in the case of elongation, the d_{z^2} orbital is stabilised compared to the $d_{x^2-y^2}$ orbital. So metal ions with d^4 and d^9 configuration have an extra stabilisation equal to half the splitting of the doublet. $Fe[CuFe]O_4$ and $Zn[Mn_2^{3+}]O_4$ are examples of tetragonally distorted spinels with $c/a > 1$ (c and a are the unit cell edges along the z and x directions).

Partial covalent bonding using hybrid orbitals can influence site preference of cations. d^{10} ions show a marked tetrahedral site preference as they can use sp^3 orbitals to form covalent bonds with the p -orbital of oxide ion. Examples are Zn^{2+} and Cd^{2+} ions. $ZnFe_2O_4$ and $CdFe_2O_4$ are the only known normal ferros spinels.

Blasse [67] derived site preference of cations on the basis of the Molecular Orbital Theory (equivalent to the Ligand Field Theory) which takes into account both covalency and crystal field stabilisation energy simultaneously. According to Blasse's approach, d^3 ions have the strongest O-site preference while d^5, d^6, d^7, d^9 , or d^{10} ions prefer T-sites. d^0, d^1, d^2, d^4 and d^8 ions do not show any pronounced site preference.

When the various factors as mentioned above are counterbalancing there can be a completely random arrangement of metal ions among the eight T-sites and sixteen O-sites.

1.2.3 Ferros spinels

Spinel oxides containing iron are called ferros spinels. The interesting electrical and magnetic properties of these compounds are governed critically by their chemical composition. Hence preparation of ferrite composites, with specific properties has gained much importance. Simple ferros spinels ($A^{II}Fe_2O_4$) as well as mixed ferros spinels ($A^{II}_{1-x}B^{II}_xFe_2O_4$) are known.

1.2.4 Magnetic and Electrical properties of ferrites

Historically ferrites attracted the attention of physicists and technologists since they are magnetic semiconductors. Ferrites exhibit ferrimagnetic behaviour and are widely used as magnetic materials in various electronic devices. Due to occupancy of cations in two crystallographically different sites (i.e. octahedral B and tetrahedral A sites) three kinds of magnetic interactions are possible between the metallic ions, through the intermediate O^{2-} ions, by superexchange mechanism, namely, A-A interactions, B-B interactions and A - B interactions. These interaction energies are negative and induce an antiparallel orientation. Calculations show that A-B interactions are the strongest and hence, for inverse spinels, the resultant magnetic moment is that of the divalent metal ion in B sites. This can be explained by taking magnetite (Fe_3O_4) as a specific example. It has the inverse spinel cation distribution, $(Fe^{3+})_{tet} [Fe^{2+} Fe^{3+}]_{oct} O_4$. The spins of A site and B site Fe^{3+} ions mutually cancel due to negative A-B interaction and the resultant moment is only due to the Fe^{2+} ions in the B sites. But in $ZnFe_2O_4$, a normal spinel, there can be neither A-B nor A-A interaction as Zn^{2+} is a non- magnetic ion. Therefore, the only prevalent interaction is B-B between Fe^{3+} ions, which is antiferromagnetic [68]. The other normal ferrite $CdFe_2O_4$ also exhibits similar behaviour.

Spinel ferrites in general are semiconductors with conductivity ranging between 10^2 and 10^{-11} $ohm^{-1}cm^{-1}$. The low electrical conductivity compared to conventional metallic magnetic materials is responsible for their wide use at microwave frequencies. Ni-Zn ferrites have been found to be one of the most versatile ferrites for general use. This microwave behaviour of Ni-Zn ferrites strongly depends on their composition [69]. Co-Zn ferrites [70] and lithium ferrites [71] were also extensively studied in technological fields.

1.2.5 Spinel as Catalysts

Spinel show interesting catalytic properties. In these compounds the properties are controlled by the nature of the ions, their charge and site distribution among the T - and O - sites. The catalytic activity of spinels containing transition metal ions is influenced both by the redox properties and the acid-base properties of these ions .Correlation between catalytic activities and the electric or magnetic properties of

spinel is often found; this is a direct consequence of the dependence of both properties on cation distribution among the T- and O- sites. Beaufils and Barbaux [72] have shown, from surface neutron differential diffraction (SDD) studies, that the surfaces of ideal normal spinels consist of a mixture of (111) and (110) planes. In the case of a distorted spinel like γ - alumina, it is suggested that nearly 80% of the exposed faces are of the (110) type. Probing the surface of solids has become more accurate after introducing Low Energy Ion Scattering (LEIS) technique in catalytic field. The most characteristic feature of this technique is that the peaks in the spectra result from scattering by topmost atomic layer only. Jacobs *et al.* [73], in a recent work, applied this technique to evaluate spinel surface composition. Their work clearly revealed that octahedral sites are exposed almost exclusively at the surface of spinel oxide powders and the catalytic activity of many such systems is mainly due to octahedral cations. Similar conclusions have been made earlier with regard to oxidation reactions [74]. The fact that tetrahedral sites are not active could originate from stronger metal-oxygen bonds due to the lower valency and coordination number.

Catalytic activities of spinels have been well-established for reactions like oxidative dehydrogenation of hydrocarbons, hydrodesulphurisation of petroleum crudes, treatment of automobile exhaust gases, oxidation of carbon monoxide, hydrogen and methane etc. Unlike single oxides, spinel-type binary and ternary oxides show extra structural stability, greater activity and reusability as catalysts. Among the spinel compounds, ferrites have been used as effective catalysts for a number of industrially important reactions as mentioned above. The catalytic effectiveness of ferrites arises because of the ease with which iron can exchange its oxidation state between 2 and 3. Another important attribute, from the commercial standpoint, is their stability under extremely reducing conditions, which is due to the spinel structure. Thus reduction of Fe^{3+} to Fe^{2+} takes place without altering the lattice configurations so that upon reoxidation, the original state is retained [75].

Spinel ferrites are well-known as effective catalysts for the oxidative dehydrogenation (OXD) of hydrocarbons containing 4 to 6 carbon atoms. The first use of magnesium ferrite for this purpose was reported in a patent granted to Bajars, Croce and Gabliks [76]. Zinc-chromium-ferrite showed high conversion and

selectivity for the OXD of butene to butadiene [77]. Massoth and Scapiello [78] probed the catalyst function in the above case by measuring catalyst weight loss in a reducing atmosphere of either hydrogen or butene in a flow type microbalance reactor and also proposed a mechanism for the reaction. They found that the spinel ferrites were less reducible than Fe_2O_3 in hydrogen and underwent only surface reduction in butene maintaining the chemical and structural stability of the bulk. The same reaction was also investigated over MgFe_2O_4 catalyst using deuterium and ^{14}C labelled isotopic tracers to unravel its kinetics and mechanism [79]. The results showed that the reaction was zero order in oxygen and first order in butene at low partial pressure of butene and that a modified Massoth-Scapiello mechanism was operative.

The spinels ACr_2O_4 and AFe_2O_4 where $\text{A} = \text{Ni, Co or Mn}$ have been found to be active for the non-selective oxidation of propylene to CO_2 and water, the normal Cr (III) spinels being more active than the inverse Fe(III) spinels [80].

Decomposition of alcohols is another class of reactions catalysed by oxidic spinels. The decomposition of propan-2-ol to acetone was studied over chromite spinels of Zn, Co and Cu [81]. The results showed that CuCr_2O_4 was the most effective catalyst and the dehydration activity was only meagre. The same decomposition was studied over $\text{MgAl}_{2-x}\text{Fe}_x\text{O}_4$ ($x \leq 0.4$ and $x \geq 1.3$) systems [75]. Here the catalysts showed both dehydration and dehydrogenation activities for $x > 0.02$. The important conclusion was that, the dehydration as well as the electrical and magnetic properties are influenced by a fundamental property of the spinel system, namely, the symmetry of the catalytically active Fe^{3+} site. Dube and Darshane investigated the spinel systems, $\text{Zn}_{1-x}\text{Cu}_x\text{MnFeO}_4$ ($0 \leq x \leq 1$) [82] and $\text{Co}_{1+x}\text{Fe}_{2-2x}\text{Ti}_x\text{O}_4$ [83] by various physico-chemical methods and correlated the physical properties with their catalytic behaviour in benzyl alcohol decomposition. It was found that Cu-rich catalysts were always more active than Zn-rich catalysts and that CoFe_2O_4 was a better catalyst than Co_2TiO_4 . Cyclohexanol decomposition was also studied using $\text{Zn}_x\text{Ni}_{1-x}\text{Fe}_2\text{O}_4$ ($0 \leq x \leq 1$) [84] and $\text{Mg}_{1-x}\text{Zn}_x\text{Al}_2\text{O}_4$ ($0 \leq x \leq 1$) [85] spinel systems and the results were correlated with structural parameters.

Perhaps the most widely studied reaction using spinel catalysts is the catalytic selective oxidation of carbon monoxide. Selective removal of carbon monoxide from CO/H₂ mixed gas is a key step for fuel cell or sensor technology. A possible approach includes selective catalytic oxidation [86,87]. Among metal oxides, cobalt oxide of the spinel type (Co₃O₄) is the most active catalyst for oxidation of CO. The active cobalt species for selective oxidation of CO has been found to be Co³⁺_{oh}, after investigating the catalytic activities of ZnCo₂O₄, CoAl₂O₄, CoFe₂O₄ of the spinel type [87]. The same conclusion has been confirmed by X-ray photoelectron spectroscopy (XPS) on cobalt spinel oxides such as Zn_xCo_{3-x}O₄ (x = 0 – 1), Al_xCo_{3-x}O₄ (x = 1 – 2.5) and Fe_xCo_{3-x}O₄ (x = 1 – 2.5) [88].

Maltha *et al.* [89] investigated the active sites in the spinels Mn₃O₄ and Co₃O₄ in the selective reduction of nitrobenzene to nitrosobenzene by substitution of Mn or Co ions in T-sites and/or in O-sites by redox inactive ions like Zn and Al. The totally substituted spinels ZnMn₂O₄, CoAl₂O₄ and ZnCo₂O₄ showed that the Mn and Co ions in octahedral positions were responsible for the activity of the reaction. MnAl₂O₄ however showed some activity for the reaction which should be due to surface enrichment and/or oxidative transfer of manganese from T - to O - sites. The same team of researchers studied the cation distribution in the spinels, Zn_{1-x}Mn_xAl₂O₄ (0 ≤ x ≤ 1) by X- ray diffraction and MAS-NMR [90] which gave evidence for oxidative transfer of manganese as Mn³⁺ into O-sites. The compounds showed a defect spinel structure containing Mn³⁺ and cation vacancies, with average valence of Mn close to 2.8.

Production of methyl formate (MF) is a synthetically important reaction and is usually achieved by the dehydrocoupling of methanol using copper containing catalysts. MF was produced in about 50% yield with methanol conversion above 60% at 320°C in patent literature [91,92]. Sato *et al.* [93] prepared CuO - Al₂O₃ systems with different Cu/Al ratios by the amorphous citrate process and examined their catalytic activities for the dehydrocoupling of methanol to methyl formate. CuO - Al₂O₃ samples calcined at temperatures below 1000°C are partially reduced during the catalytic reaction and the selectivity to MF decreases with increasing Cu (0) content. This is because Cu (0) decomposes MF to methanol and CO above 210°C. On the other hand, CuAl₂O₄ samples calcined at 1100°C showed the highest activity for the

formation of MF at a temperature of 310°C. The Cu (II) species in CuAl_2O_4 were found to be effective sites for the reaction above 250°C.

Spinel catalysts also find use in higher alcohol synthesis. e.g., a commercial Zn/Cr spinel methanol synthesis catalyst (Englehard Zn - 0312) has been promoted with various amounts of K and tested for isobutanol synthesis [94]. An equimolar mixture of methanol and isobutanol is an ideal feedstock for producing the high octane petrol additive, methyl tertiary butyl ether (MTBE). The use of 3 wt % K- containing catalysts resulted in the lowest methanol- to- isobutanol mole ratio of 1.5, which is close to the desired ratio of 1 for MTBE synthesis.

Heterogeneous decomposition of H_2O_2 is a convenient alternative method to electrolysis of water, for the production and storage of oxygen gas. The usual peroxide decomposition catalysts like silver oxide, platinum black etc. are expensive. Various ferros spinels have been reported as effective catalysts for H_2O_2 decomposition [95-99]. Spinel of general formula $\text{M}_x\text{Fe}_{3-x}\text{O}_4$ where $\text{M} = \text{Co}, \text{Ni}$ or Cu and $0 \leq x \leq 3$ have been found to be very active for peroxide decomposition in alkaline media, with the activity following the order, $\text{Co} > \text{Cu} > \text{Ni}$ [96-98]. Sengupta and Lahiri [99] investigated the intrinsic catalytic activity of several coprecipitated $\text{Mn}_x\text{Fe}_{3-x}\text{O}_4$ specimens having x varying between 0.5 to 2.5, towards hydrogen peroxide decomposition in neutral media. $\text{Mn}_{2.5}\text{Fe}_{0.5}\text{O}_4$ has been found to be more active and CoFe_2O_4 as much active as the noble metal catalysts for the above reaction in neutral media [99].

Liquid phase Friedel -Crafts alkylation of benzene with benzyl chloride has been studied using $\text{CuCr}_{2-x}\text{Fe}_x\text{O}_4$ spinel catalysts [100]. CuCr_2O_4 gave no reaction but the yield of the product diphenylmethane increased with iron content in the spinel, reaching a maximum with CuFe_2O_4 . Presence of strong Lewis acid sites as proved by DRIFT spectra of adsorbed pyridine on the spinels was suggested as mainly responsible for the good catalytic performance.

The catalytic activity of a series of ferrites of the general formula $\text{Zn}_{1-x}\text{Co}_x\text{Fe}_2\text{O}_4$ ($0 \leq x \leq 1$), prepared by 'soft' chemical route has been investigated for

aniline alkylation reaction using methanol and dimethyl carbonate (DMC) as the alkylating agents [101-102]. Methanol showed high N-monoalkylation selectivity compared to DMC and the most active and stable catalyst has been found to be $Zn_{0.8}Co_{0.2}Fe_2O_4$. The above catalysts are also found to be very effective, $CoFe_2O_4$ being the best, for the alkylation of phenol to o-cresol and 2,6-xyleneol [103]. The kinetic parameters of N-monoalkylation of aniline with methanol over the above mentioned catalysts have also been determined [104].

In addition to the above mentioned reactions, lot of other reactions are also catalysed by spinel type oxides. e.g. Ferrospinels, especially of Co, Ni and Cu, have been widely patented as alternate catalysts to noble metals for purification of automobile exhausts. Another example is the hydrodesulphurisation of petroleum crude with $CoFe_2O_4$ and $NiFe_2O_4$ [105].

1.3 SURFACE ELECTRON DONOR PROPERTIES

Study of electron-donor (ED) properties of metal oxides by the adsorption of electron acceptors (EA) of varying electron affinity values has been a well-established technique.

It was already known that acidic centres of the Lewis type on active aluminas could promote the formation of positive radical ions from aromatic hydrocarbons in presence of molecular oxygen [106]. But the first experimental evidence for the presence of electron-donor sites on metal oxides was obtained by Flockhart *et al.* [107] by studying the esr spectrum of tetracyanoethylene (TCNE) on alumina. The dipolar nature of aluminas has been confirmed by Flockhart *et al.* [108-109] using the electron acceptor perylene and the electron-donor, TCNE. When TCNE was adsorbed on the surface, the corresponding anion radical was formed. The electron-donor sites were associated with surface hydroxyl groups and with defect centres involving oxide ions. Similar studies to determine the number of electron-donor sites were done on many single and two-component metal oxides [110-113].

The above studies were limited to determining the number of electron-donor sites only. The first systematic study of determining the strength and distribution of

electron-donor sites by adsorption of several electron acceptors over a range of electron affinity values, was done by Meguro and Esumi [114-115]. They studied alumina, titania and zirconia-titania by adsorption of four electron acceptors namely 7,7,8,8 - tetracyanoquinodimethane (TCNQ), 2,5 - dichloro-p- benzoquinone (DCQ), p-dinitrobenzene (PDNB) and m-dinitrobenzene (MDNB) whose electron affinity values varied from 2.84 to 1.26 eV, using esr spectrometer.

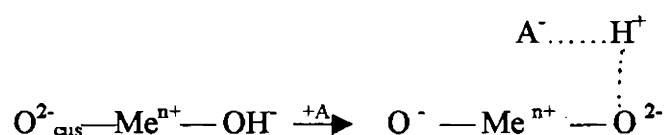
The electron donor strength of metal oxides can be defined as the conversion power of an electron acceptor adsorbed on the surface into its anion radical [115]. If a strong EA is adsorbed on the metal oxide, its anion radical is formed at every donor site present on the metal oxide surface. On the other hand, if a weak EA is adsorbed, the formation of anion radical will be expected only at the strong donor sites. Finally, in the case of very weak EA adsorption, the anion radical will not be formed even at the strongest donor sites. Therefore, the electron donor strength of a metal oxide can be expressed as the limiting electron affinity value at which free anion radical formation is not observed at the metal oxide surface. It was concluded that the ED strength of alumina and titania is similar and stronger than that of zirconia-titania.

The metal oxides, after adsorption of EA from acetonitrile solution, developed characteristic colours due to the charge transfer (CT) spectra of the adsorbed species. These coloured samples showed unresolved esr bands proving the existence of radical ions. Radical concentrations were calculated by comparison of the areas obtained by double integration of the esr signals of the sample and a standard reference. It was found that the limiting radical concentration was proportional to the limiting amount of EA adsorbed and these decreased with decrease in the electron affinity values of the EA. A plot of logarithm of the limiting radical concentration for a given oxide vs. the electron affinity of the EA was linear. This was interpreted in terms of the distribution of strength of the ED sites; the greater the gradient of these plots, the wider the distribution. Alumina showed a wider distribution compared to titania or zirconia-titania.

ED sites come from two sources: electrons trapped in intrinsic defects (created only at high activation temperatures) and the other, surface hydroxyl or oxide ions. The ionisation potential of hydroxyl ions is comparatively small (about 2.6 eV in gas

phase) and, therefore, a process of the type, $\text{OH}^- + \text{A} \rightarrow \text{OH} + \text{A}^-$, where A is the EA, can be included [114].

Cordischi *et al.* [116,117] studied the esr hyperfine splitting parameters of adsorbed nitrobenzene radical anions on several metal oxides activated below 1200 K. They found evidence for a dual quality for the ED sites, as consisting of a coordinatively unsaturated oxide ion ($\text{O}_{\text{cus}}^{2-}$) associated with a nearby OH^- group (Bronsted acid site) whose proton interacts with the radical formed.



(Me^{n+} = surface cation, A = EA molecule)

Esumi *et al.* [118] investigated the ED property of zirconia at various calcining temperatures (300 -1000°C) by means of adsorption of TCNQ and found that the radical concentration decreased with increasing calcining temperatures, reached a minimum at 700°C and then increased. The behaviour was interpreted in terms of two different ED sites, surface OH^- ions at low temperatures and surface oxide ions at high temperatures. From the ratio of radical concentration to the amount adsorbed, it was proved that surface oxide ions were much stronger ED sites than surface OH^- ions. The same team [119] also studied the adsorption of various EAs on titania and could determine that the limit of electron transfer from titania surface to the acceptor ranged between 1.77 to 1.26 eV in the electron affinity of the acceptor.

Adsorption of EAs from non-aqueous solutions onto solid surfaces shows various solvent effects. Hosaka and Meguro [120] studied the solvent effect of several aromatic solvents on the CT adsorption of TCNQ onto various kinds of oxides. Two different types of influence on radical concentrations were noticed - (i) in insulators (magnesia, alumina and silica) the radical concentration decreased with decreasing ionisation potential of the aromatic solvent and (ii) in n-type semiconductors (zinc oxide and titania), no regular relation between ionisation potential of solvents and radical concentration was observed. The electron-donor-acceptor interactions on alumina and titania were probed by means of TCNQ adsorption from solvents of

varying basicities and also acidities and the Drago correlation [121] of the heats of acid-base interactions was applied to the results [122,123]. The adsorption of tetrachloro-*p*-benzoquinone (chloranil) from basic and acidic solvents was also studied on the same metal oxides [124]. The basic solvents used were acetonitrile, ethyl acetate and 1,4-dioxane and the acidic solvents were dichloromethane and chloroform.

The amount of EA adsorbed decreased with increase of acid-base interactions between the basic solvent and EA and also decreased with an increase in acid-base interaction between the acidic solvent and electron donor sites of the metal oxides.

Esumi *et al.* [125] measured the zeta potentials of metal oxides such as alumina and titania by adsorption of TCNQ from organic solvents of varying basicities and found that the zeta potentials decreased in the order: acetonitrile > ethyl acetate > 1,4-dioxane, the order of increased basic strength of the solvents.

The acid-base and electron-donor properties of rare earth oxides such as Pr_6O_{11} [126], CeO_2 [127], Dy_2O_3 [128], Y_2O_3 [129-130], Sm_2O_3 [131], La_2O_3 [132] and Nd_2O_3 [133-134] and their mixed oxides with alumina were investigated as a function of composition and activation temperature. The extent of electron transfer was characterised by magnetic measurements. Again, surface properties and catalytic activities of mixed oxides such as $\text{CeO}_2\text{-ZrO}_2$ [135], $\text{Y}_2\text{O}_3\text{-ZrO}_2$ [136,137], $\text{La}_2\text{O}_3\text{-ZnO}$ [138] and $\text{Al}_2\text{O}_3\text{-CeO}_2\text{-Dy}_2\text{O}_3$ [139] were also investigated.

1.4 ALCOHOL DECOMPOSITION REACTION

It has been well-established that the acidic, basic and redox nature of catalysts are the most important properties in metal oxide catalysis. Various physico-chemical methods of determining acidity and basicity of solids have been reviewed by Kijenski and Baiker [6] who also pointed out that every method has one or other limitation. The most sensitive probe of catalysts performance will continue to be the rate and selectivity of a chemical test reaction. In this context, alcohol decomposition has been widely studied because it is a simple method to determine the functionality of an oxide catalyst.

There are two basic modes of reaction during alcohol decomposition - (a) dehydration to form an olefin and water and (b) dehydrogenation to form an aldehyde

(in the case of primary alcohols) or a ketone (in the case of secondary alcohol) and hydrogen. At higher temperatures, decomposition may involve carbon-carbon bond cleavage giving products like CO, CO₂ etc. At near ambient temperatures, ether can be a major product. The most widely studied alcohol decomposition reactions are those of isopropanol and of cyclohexanol.

According to the generally accepted concept, dehydration is an acidic reaction whereas dehydrogenation activity is due to the combined effect of both acidic and basic sites on the system. Isopropanol decomposes to give propene by dehydration and acetone by dehydrogenation. From a mechanistic point of view, Ai *et al.* [14, 140,141] assumed that the dehydration of isopropanol is catalysed by an acid site whereas the dehydrogenation is catalysed by both acidic and basic sites through a concerted mechanism. Consequently, the dehydration rate is regarded as a measure of the acidity of the catalyst while the ratio of the dehydrogenation rate to the dehydration rate, as a measure of the basicity. However, the widely documented correlation found for alcohol dehydration is not so clear for alcohol dehydrogenation [142]. Often redox properties of catalysts are responsible for their oxidation activity and may predominate over their acid-base properties. According to Krylov [143] dehydrogenation is expected to be catalysed by p-type semiconductors and dehydration by n-type semiconductors.

The mechanism of alcohol dehydration can be any one among E1, E2 or E1cB as outlined in the following scheme: [144] (Fig. 1.4.1)

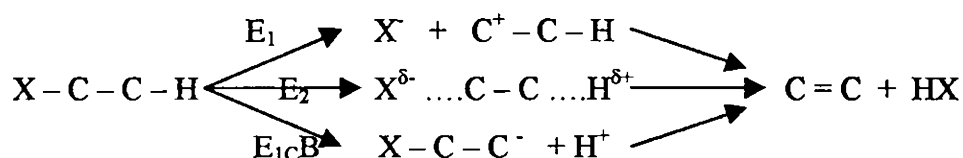


Fig. 1.4.1. Three possible routes of dehydration reaction.

In E1, C-OH bond rupture occurs with carbonium ion formation, the latter being capable of positional and geometrical isomerisation, all possible alkenes being

formed. In E2, the reaction is concerted, single step, with no intermediate formed. Saytzeff alkene orientation occurs from 2-ols, i.e. there are more alk-2-enes than alk-1-enes. In E1cB, C-H bond reapture occurs via the most acidic proton. Hofmann orientation of alkenes occurs, i.e. alk-1-enes predominate and there is a tendency for dehydrogenation to occur. The above categories are not clear cut and quite often intermediate situations can occur. The nature of alcohol is of importance and the order of ease of dehydration is tertiary > secondary > primary. Tertiary alcohols tend to react by the E1 mechanism due to the higher stability of tertiary carbonium ion.

Gervasini and Auroux [13] made a 'direct' measurement of acidity and basicity of a large series of metal oxides microcalorimetrically by adsorption of probe molecules NH_3 and CO_2 . The same authors [145] made an 'indirect' measurement of acidity and basicity of the same series of oxides from the selectivities of isopropanol decomposition and attempted to correlate these with the 'direct' values. A relationship was found between the strength of the acid sites microcalorimetrically evaluated and the activation energy for the dehydration reaction. But there was no correlation between the strength of acid or basic sites or both of them and dehydrogenation parameters.

By using temperature-programmed desorption-mass spectrometry (TPD-MS) technique with pyridine (PY), 2,6 dimethylpyridine (DMPY) and CO_2 , the decomposition of 1-phenylethanol and 2-propanol have been studied over several oxide catalysts and the results correlated with acid-base properties [142]. It is known that DMPY is selectively adsorbed on Brønsted sites, but not on Lewis sites whereas PY is adsorbed on both Brønsted and Lewis sites. As expected, the dehydration activity was appreciably correlated to Brønsted acidity and total acidity. Bezouhanova *et al.* [146] recommend dehydration activity of cyclohexanol decomposition as a simple method of determining Brønsted acid sites on a catalyst surface.

The results of cyclohexanol decomposition have also been interpreted similar to the case of isopropanol. Dehydration of cyclohexanol gives cyclohexene while dehydrogenation gives cyclohexanone. The cyclohexene activity is related to the

surface acidity and the ratio of cyclohexanone to cyclohexene activity to the surface basicity [147].

Most of the research work seeking to relate dehydration/dehydrogenation activity with surface acid - base properties has involved mixed rather than single oxides as the former provides a means of varying acidity through composition changes. Iron oxide possesses inherent dehydrogenation properties but it was reported that in the presence of Al_2O_3 these properties are lost and it becomes a dehydration catalyst [148].

Decomposition of isopropanol was carried out on the solid solution system $\text{MgAl}_{2-x}\text{Fe}_x\text{O}_4$ by Narasimhan *et al.* [75]. The system exhibited both dehydration and dehydrogenation activities. It was predicted that Fe^{3+} sites act as the active sites for the adsorption of alcohol while the Fe^{3+} site may be reduced to Fe^{2+} during adsorption and subsequent reaction. However, it regains the Fe^{3+} state by diffusing the electron to an adjacent Fe^{3+} ion. In a similar way $\text{Ga}_{1-x}\text{Fe}_x\text{CuMnO}_4$ spinel system has been studied for the decomposition of 1-octanol by Dube *et al.* [149]. They observed that increase of Fe^{3+} ions at the A site increased the octyl alcohol decomposition rate. According to them, when Fe^{3+} replaces Ga^{3+} ions, the number of active centres for the adsorption of alcohol molecule increases due to the hopping of A site ion between +2 and +3 states.

Cyclohexanol decomposition has been investigated over the catalyst system $\text{Mg}_{1-x}\text{Zn}_x\text{Al}_2\text{O}_4$ ($0 \leq x \leq 1$) [150] and also over $\text{Zn}_x\text{Ni}_{1-x}\text{Fe}_2\text{O}_4$ [151]. Costa *et al.* [152] by means of deuterium labelling experiments, have shown that the gas-phase dehydration of cyclohexanol over a solid zirconium phosphate catalyst, involves a long-lived carbocation intermediate and that the reaction proceeds via the E1 mechanistic route.

1.5 FRIEDEL – CRAFTS ACYLATION REACTIONS

Acylation and alkylation using Lewis acid catalysts such as AlCl_3 , FeCl_3 etc. and Brønsted acid catalysts such as $\text{CF}_3\text{SO}_3\text{H}$, FSO_3H etc. are important in organic synthesis and the chemical industry. Acylations are involved in the manufacture of weed killers, dye intermediates etc. while alkylations are involved in manufacturing such important chemicals as p-xylene, ethylbenzene, cumene etc. However, these homogeneous catalytic processes have several disadvantages like the use of large

amounts of catalysts, unwanted isomerisations, corrosion of the reactors, environmental pollution by acidic waste water and spent catalysts, difficulty of catalytic recovery and so on. To eliminate these disadvantages, the use of solid acid catalysts have been attempted. Considerable body of literature exists concerning alkylation using solid acid catalysts. But, relatively few reports exist regarding heterogeneous acylation reactions.

Solid acids such as heteropolyacids [153], activated iron sulphate [154] and iron oxide [155] have been attempted for acylations; but it was found that these catalysts dissolved into the reaction mixture during reaction and did not act as true heterogeneous catalysts.

The first report of a truly heterogeneous catalyst for acylation was probably due to Tanabe [47], who demonstrated that sulphated zirconia was an efficient catalyst for the acylation of chlorobenzene with *o*-chlorobenzoyl chloride. Hino and Arata [48] found the solid superacid, sulphated zirconia, to act as a true and active heterogeneous catalyst for the acetylation and benzoylation of toluene with acetic and benzoic acids and benzoic anhydride. The isomer distribution of the methylbenzophenones was para > ortho >> meta, similar to the case with homogeneous acylations or alkylations. The authors suggested that the adsorption site of the catalyst could be a strong Lewis acid site at Zr^{4+} created by the inductive effect of $S = O$ or a Brønsted site formed by the adsorption of water on Zr^{4+} . The same team of researchers [49] reported that alumina sulphated by 2.5 M H_2SO_4 followed by calcination functioned as a true and very active heterogeneous catalyst for benzoylation of toluene with benzoyl chloride or benzoic anhydride. The same reaction was found to be catalysed by several superacidic sulphated oxides and metal oxide-supported WO_3 [156]. In most cases, the reaction showed a continual increase of yield with time, proving them to be heterogeneously catalytic. In the cases of SO_4/Fe_2O_3 and WO_3/Fe_2O_3 , however, the reaction failed to proceed further after 30-60 minutes, with benzoyl chloride as the acylating agent. In the latter two cases, the deep brown colour of the reaction mixture was indicative of the dissolution of Fe_2O_3 as $FeCl_3$, which caused homogeneous catalysis. The catalytic performance of Al-promoted sulphated zirconia and sulphated titania for benzoylation of toluene with benzoyl chloride has been investigated [157]. A superacidic

perfluororesin sulphonic acid (Nafion-H) has been reported to be catalytically active for several types of acylation reactions [158].

Benzoylation of toluene [159] and selective benzoylation of o-xylene to 3,4-dimethylbenzophenone [160] have been reported over zeolite catalysts.

Acylation of aromatics was studied using rare earth (Sc,La,Nd) ion-exchanged K10 montmorillonite clay as the catalyst [161]. The reaction rate was found to increase with substrates containing electron-donating groups. Thus benzoylation of anisole took place giving high yield of products while benzene failed to react. Electron-donating groups stabilise the benzoyl cation intermediate, PhCO^+

Laszlo and Mathy [162] found that transitional metal-exchanged K10 montmorillonite clay was quite effective for Friedel - Crafts alkylation of aromatics; Zr^{4+} and Ti^{4+} , in general, giving the best results.

The liquid phase Friedel-Crafts benzoylation of benzene has been investigated using $\text{CuCr}_{2-x}\text{Fe}_x\text{O}_4$ spinel catalysts [163]. DRIFT spectra of adsorbed pyridine showed the presence of both Lewis and Brønsted acidic sites on the surface of the spinels. The number of Lewis acid sites increased as the iron content of the system increased. Conductivity measurements showed that all the catalysts are semiconductors, with the activation energy (band gap) decreasing with the iron content. CuFe_2O_4 gave the highest yield of products. The Lewis acidity of the catalysts, coupled with the low value of activation energy has been suggested as mainly responsible for the good catalytic performance. Due to the generally unreliable kinetic behaviour of Friedel-Crafts systems, very few kinetic rate studies of alkylations and acylations were ever undertaken for the homogeneous systems [164], let alone for the heterogeneous ones.

It is presumed that the heterogeneous Friedel-Crafts reaction proceeds through the carbocation or the acyl cation as the intermediate. In the case of superacidic catalysts, the Brønsted acid site can be the active site to produce these intermediate cations. In other situations, strong Lewis sites are responsible for producing these cationic intermediates.

1.6 OBJECTIVES OF THE PRESENT WORK

By and large, ferrites are commonly produced by conventional ceramic processes involving high temperature ($\geq 1200^\circ\text{C}$) solid state reactions between the constituent oxides/carbonates. These methods have some inherent drawbacks such as poor compositional control, chemical inhomogeneity, coarser particle size etc. Wet chemical methods such as hot (100°C) coprecipitation, sol-gel method etc. have overcome these drawbacks and produced fine and homogeneous ferrite powders. Recently there are reports of preparing spinel ferrites by the low temperature controlled chemical coprecipitation method using aqueous solutions of the metallic nitrates and sodium hydroxide as the precipitating agent [165]. So, in this work we prepared some ferros spinels containing Co, Ni and Cu, by adopting this soft chemical route. Two series of ferros spinels of formula $\text{Ni}_{1-x}\text{Cu}_x\text{Fe}_2\text{O}_4$ and $\text{Co}_{1-x}\text{Cu}_x\text{Fe}_2\text{O}_4$ where x varies as 0, 0.3, 0.5, 0.7 and 1 were prepared. All these systems have the inverse spinel structure and only the Co-Cu or Ni-Cu ratio varies in the octahedral sites as x varies. The acido - basic and redox properties of the systems also vary with x .

The discussion of results has been done after sub-dividing the catalytic systems into simple ferros spinels, AFe_2O_4 ($\text{A} = \text{Co}, \text{Ni}$ and Cu) and mixed ferros spinels of the Ni-Cu series and the Co-Cu series ($x = 0.3, 0.5$ and 0.7). Following the discovery of superacidity in sulphated metal oxides, especially ZrO_2 , much work has been done on modifying metal oxides with anions like sulphate, phosphate etc. Since sulphated Fe_2O_3 is one among the solid superacids reported, we have taken up in this work, the modification of the ferros spinel systems with sulphate ion and investigating their properties. The main objectives of the present work are the following:

- To prepare ferros spinels of Co, Ni and Cu by low temperature co-precipitation methods and also their sulphated analogues and characterise these by various physico-chemical methods like XRD, EDX, BET surface area, FTIR, Mossbauer, TGA etc.
- To study the effect of copper substitution in the spinel matrix of nickel and cobalt ferros spinels.

- To evaluate the surface basicity using electron acceptors of various electron affinity values.
- To study the vapour -phase cyclohexanol decomposition reaction and correlate the results with surface acid-base and redox properties.
- To evaluate the surface acidity by gravimetric adsorption of n-butylamine followed by TGA and also by the dehydration selectivity of cyclohexanol decomposition.
- To assess the catalytic activity by studying the Friedel-Crafts benzylation reaction of toluene.
- Sulphation of oxides is known to create new active sites. So another objective is to prepare sulphate-modified analogues of all samples under study and explore their surface properties and catalytic activities.
- To explore the effect of activation temperature on the properties of the catalysts by doing the above studies at activation temperatures of 300° C and 500° C.
- To reaffirm the trends in benzylation of toluene by doing the benzylation of benzene with the ferrosin samples.

REFERENCES

1. R. H. Perry and D. W. Green, "Perry's Chemical Engineers' Handbook", Seventh Edition, McGraw-Hill, 1977, p.23
2. F. Greek, Chemical and Engineering News, 67(22) (1989) 29
3. J. A. Schwarz, C. Contescu and A. Contescu, Chem.Rev., 95 (1995) 477.
4. M. A. Barteau, Chem.Rev., 96 (1996) 1413
5. K. Tanabe, M. Misono, Y. Ono and H. Hattori, "New Solid Acids and Bases", Kodansha, Tokyo, 1989, p.1
6. J. Kijenski and A. Baiker, Catal. Today, 5 (1989) 1
7. H. Pines, J. A. Vaseley and V. N. Ipatieff, J. Am. Chem. Soc., 77 (1961) 6314
8. H. Hattori, Chem. Rev., 95 (1995) 537
9. J. L. G. Fierro and J. F. Garcia De La Banda, Catal. Rev.- Sci. Eng., 28 (2&3) (1986) 265
10. A. Clark, "The Theory of Adsorption and Catalysis", Academic Press, New York and London, 1970, ch.8
11. R. L. Augustine, "Heterogeneous Catalysis for the Synthetic Chemist", Marcel Dekker, Inc., 1996, p.180
12. T. W. Swaddle, "Inorganic Chemistry", Academic Press, 1997, p.122
13. A. Auroux and A. Gervasini, J. Phys. Chem., 94 (1990) 6371
14. M. Ai and S. Susuki, J. Catal., 30 (1973) 362
15. Yu. Belokopytov, K. M. Kholyavalenko, M. Ya. Rubanic, Kin. i Kataliz (russ.), 14 (1973) 1280.
16. Yu. Belokopytov, K. M. Kholyavalenko, M. Ya. Rubanic, Kataliz i Katalizatory, Vol.8 (Russ), Naukovaya Dumka, Kiev (1971) 13
17. P. Forzati, F. Trifiro and P. L. Villa, J. Catal., 52 (1978) 389
18. B. Grzybowska – Swierkosz, "Catalysis by Acids and Bases", (Editors: B.Imelik *et al.*), Elsevier, 1985, p. 45
19. (a) K. Tanabe, M. Misono, Y. Ono and H. Hattori, 'New Solid Acids and Bases', Kodansha, Tokyo, 1989, p.70; (b) A. Koyo, T. Yamaguchi, K. Tanabe, J. Catal., 83 (1983) 99

20. K. Arata, K. Sato and I. Toyoshima, *J. Catal.*, 42 (1976) 221
21. K. Arata, K. Yabe and I. Toyoshima, *J.Catal.*, 44 (1976) 385
22. K. Arata and I. Toyoshima, *J.Catal.*, 47 (1977) 109
23. K. Arata, A. Fukui and I. Toyoshima, *J. Chem. Soc., Chem. Commun.*, (1978) 121
24. K. Arata and M. Hino, *Bull. Chem. Soc. Jpn.*, 53 (1980) 535
25. K. Kimura, H. Ai, A. Ozaki, *J.Catal.*, 18 (1970) 271
26. H. Uchida, H. Imai, *Bull. Chem. Soc. Jpn.*, 35 (1962) 995
27. K. Mayura and A. Ozaki, *Bull. Chem. Soc. Jpn.*, 46 (1973) 351
28. Y. M. Lin, I. Wang and C. T. Yeh, *Appl.Catal.*, 41 (1988) 53
29. Ch. Sivaraj, B. M. Reddy and P. K. Rao, *Appl. Catal.*, 45 (1988) 11L
30. Mitsubishi Chem. Ind. Ltd., *Jpn, Patent 136241* (1980)
31. K. Tanabe, M. Itoh, K. Morishige and H. Hattori, in "Preparation of Catalysts", (B. Delmon, P. A. Jacob, G. Poncelet, eds.), Elsevier, Amsterdam, 1976, p.65
32. K. Arata, *Adv. Catal.*, 37 (1990) 165
33. K. Tanabe and W. F. Holderich, *Appl. Catal.*, 181 (1999) 399
34. D. Farcasiu and J Qi Li, *Appl. Catal.*, 128 (1995) 97
35. K. Arata and M. Hino, *Mater. Chem. Phys.*, 26 (1990) 213
36. E. Iglesia, S. L. Solid and G. M. Kramer, *J.Catal.*, 144 (1993) 238
37. T. Jin, T. Yamaguchi and K. Tanabe, *J. Phys. Chem.*, 90 (1986) 4794
38. M. Bensitel, O. Saur, J. C. Lavalley and B. A. Morrow, *Mater. Chem. Phys.*, 19 (1988) 147
39. V. S. Komarov and M. F. Sinilo, *Kinet. Catal. (Engl. Edit.)*, 29 (1988) 701
40. P. Nascimento, C. Akrotopoulou, M. Oszagyan, G. Coudurier, C. Travers, J. F. Joly and J. C. Vedrine, 10th Int. Congr. Catalysis (Budapest, July 1992) Contr. 080
41. J. H. Lunsford, H. Sang, S. M. Campbell, C. H. Liang and R. G. Anthony, *Catal. Lett.*, 27 (1994) 305
42. X. Song and A. Sayari, *Catal. Rev. – Sci. Eng.*, 38(3) (1996) 329
43. O. Saur, M. Bensitel, A. B. M. Saad, J. C. Lavalley, C. P. Tripp and B. A. Morrow, *J. Catal.*, 99 (1986) 104

44. B. A. Morrow, R. A. McFarlane, M. Lion and J. C. Lavalley, *J. Catal.*, 107 (1987) 232
45. A. Clearfield, G. P. D. Serrette, A. H. Khazi – Syed, *Catal. Today*, 20 (1994) 295
46. F. Babou, B. Bigot and P. Sautet, *J. Phys. Chem.*, 97 (1993) 11501
47. K. Tanabe, *Meter. Chem. Phys.*, 13 (1985) 347
48. M. Hino and K. Arata, *J. Chem. Soc., Chem. Commun.*, (1985) 112
49. K. Arata and M. Hino, *Appl. Catal.*, 59 (1990) 197
50. Y. Xia, W. Hua and Zi Gao, *Catal. Lett.*, 55 (1998) 101
51. K. R. Venkatesh, J. Hu, J. W. Tierney and I. Wender, *Prepr. Am. Chem. Soc. Div. Fuel Chem.*, 40 (1995) 788
52. S. Sugunan, C. R. K. Seena and T. M. Jyothi, *React. Kinet. Catal. Lett.*, 67, 1 (1999) 49
53. S. Sugunan and C. R. Kumaree Seena, *Indian J. Chem.*, 37A (1998) 438
54. S. Sugunan and C. R. Kumaree Seena, *Indian J. Chem.*, 37A (1998) 669
55. A. R. West, “Solid State Chemistry and its Applications”, John Wiley, New York, 1989, p. 569
56. D. K. Chakrabarthy, “Solid State Chemistry”, New Age International, New Delhi, 1996, p. 53
57. B. Viswanathan, “Ferrite Materials – Science and Technology”, (B. Viswanathan and V. R. K. Murthy eds.), Narosha, New Delhi, 1990, p. 4
58. G. Blasse, *Philips Research Reports Supplements*, 3 (1964) 2
59. T. F. W. Barth and E. Posenjak, *Zs. Kristallographie*, 84 (1952) 325
60. A. F. Wells, “Structural Inorganic Chemistry”, 4th Edition, ELBS, London, 1979, p. 491
61. B. Viswanathan, “Ferrite materials – Science and Technology”, (B. Viswanathan and V. R. K. Murthy, eds.), Narosha, New Delhi, 1990, p.5
62. E. J. W. Verwey, F. de Boer and J. H. van Santen, *J. Chem. Phys.*, 16 (1948) 1091
63. G. Blasse, *Philips Research Supplements*, 3, (1964) 7
64. J. D. Dunitz and L. E. Orgel, *Phys. Chem. Solids*, 3 (1957) 318
65. D. S. Mc Clare, *Phys. Chem. Solids*, 3 (1957) 311

66. A. R. West, "Solid State Chemistry and its Applications", John Wiley, New York, 1989, p.313
67. G. Blasse, Philips Research Reports, Supplement, 3 (1964) 13
68. B. Viswanathan, "Ferrite materials – Science and Technology", (B. Viswanathan and V. R. K. Murthy, eds.), Narosha, New Delhi, 1990, p.9
69. V. R. K. Murthy, Ph.D Thesis, Department of Physics, Indian Institute of Technology, Madras, India (1981)
70. O. S. Josyulu, Ph.D Thesis, Department of Physics, Indian Institute of Technology, Madras, India (1981)
71. R. Raman, Ph.D Thesis, Indian Institute of Technology, Madras, India (1989)
72. J. P. Beaufils and Y. Barbaux, J. Appl. Crystallogr., 15 (1982) 301
73. J. P. Jacobs, A. Maltha, J. G. H. Reintjes, J. Drimal, V. Ponc and H. H. Brongersma, J. Catal., 147 (1994) 294
74. J. Ziolkowski and Y. Barbaux, J. Mol. Catal., 67 (1991) 199
75. C. S. Narasimhan and C. S. Swamy, Appl. Catal., 2 (1982) 315
76. L. Bajars, J. L. Croce and M. Gabliks, U. S. Patent 3,284,536 (1966)
77. R. J. Rennard Jr and W. L. Kehl, J. Catal., 21 (1971) 282
78. F. E. Massoth and D. A. Scarpiello, J. Catal., 21 (1971) 294
79. M. A. Gibson and J. W. Hightower, J. Catal., 41 (1976) 420
80. L. Zanderighi, M. P. Faedda and S. Carra, J. Catal., 35 (1974) 127
81. V. Krishnasamy and S. Chokkalingam, J. Indian. Chem. Soc., 59 (1982) 641
82. G. R. Dube and V. S. Darshane, J. Chem. Soc. Faraday Trans., 88(9) (1992) 1299
83. G. R. Dube and V. S. Darshane, Bull. Chem. Soc. Jpn., 64 (1991) 2449
84. N. J. Jabarathinam and V. Krishnasamy, in: "Catalysis: Present and Future", Intermediate Series on Chemical Engineering , (P. Kanta Rao and R. S. Beniwal, eds), Publications and Information Directorate and Wiley Eastern Ltd., New Delhi, 1995, p. 288
85. M. V. Joshi, S. G. Oak and V. S. Darshane, in: "Catalysis: Modern Trends", (N. M. Gupta and D. K. Chakrabarthy eds.), Narosha, New Delhi, 1995, p. 275
86. S. H. Oh and R. M. Sinkevitch, J. Catal., 142 (1993) 254

87. T. Takada, S. Kasahara, K. Omata and M. Yamada, *Nippon Kagaku Kaishi*, (1994) 793
88. K. Omata, T. Takada, S. Kasahara and M. Yamada, *Appl. Catal.*, 146 (1996) 255
89. A. Maltha, H. F. Kist, B. Brunet, J. Ziolkowski, H. Onishi, Y. Iwasawa and V. Ponec, *J. Catal.*, 149 (1994) 356
90. J. Ziolkowski, A. M. Maltha, H. Kist, E. J. Grootendorst, H.J. M. de Groot and V. Ponec, *J. Catal.*, 160 (1996) 148
91. Mitsubishi Gas Chemical Co., Japan Patent 46,821 (1978)
92. Mitsubishi Gas Chemical Co., Japan Patent 33,418 (1984)
93. S. Sato, M. Iijima, T. Nakayama, T. Sodesawa and F. Nozaki, *J. Catal.*, 169 (1997) 447
94. W. S. Epling, G. B. Hoflund, W. M. Hart and D. M. Minahan, *J. Catal.*, 169 (1997) 438
95. H. M. Cota, J. Katan, M. Chin and F. J. Schoenweis, *Nature*, London, 203 (1964) 1281
96. J. R. Goldstein and A. C. C. Tseung, *J. Catal.*, 32 (1974) 452
97. A. I. Onuchukwu, *J. Chem. Soc. Faraday Trans.*, I 80 (1984) 1447
98. A. I. Onuchukwu and A. B. Zuru, *Mater. Chem. Phys.*, 15 (1986) 131
99. S. K. Sengupta and P. Lahiri, *Indian J. of Technol.*, 30 (1992) 172;
P. Lahiri and S. K. Sengupta, *Can. J. Chem.*, 69 (1991) 33
100. S. P. Ghorpade, V. S. Darshane and S. G. Dixit, *Appl. Catal.*, 166 (1988) 135
101. K. Sreekumar, T. M. Jyothi, M. B. Talwar, B. P. Kiran, B. S. Rao and S. Sugunan, *J. Mol. Catal.*, 152 (2000) 225
102. K. Sreekumar, T. Mathew, S. P. Mirajkar, S. Sugunan and B. S. Rao, *Appl. Catal.*, 201 (2000) L1
103. B. S. Rao, K. Sreekumar T. M. Jyothi, Indian Patent No. 2707/98, (1998)
104. K. Sreekumar, T. M. Jyothi, C. G. Ramankutty, B. S. Rao and S. Sugunan, *React. Kinet. Catal. Lett.*, 70,1 (2000) 161
105. P. N. Rylader. Jr and W. J. Zimmerschied, *U. S. Pat.* 2, 805 (1957) 187
106. R. K. Merrifield and W. D. Phillips, *J. Am. Chem. Soc.* 80 (1958) 2778

107. B. D. Flockhart, C. Naccache, J. A. N. Scott and R. C. Pink, *Chemical Communications*, 11 (1965)
108. B. D. Flockhart, J. A. N. Scott and R. C. Pink, *Trans. Faraday Soc.*, 62 (1966) 370
109. B. D. Flockhart, I. R. Leith and R. C. Pink, *Trans. Faraday Soc.*, 65 (1969) 542
110. A.J. Tench and R. L. Nelson, *Trans. Faraday Soc.*, 63 (1967) 2254
111. M. Che, C. Naccache and B. Imelik, *J. Catal.*, 24 (1972) 328
112. H. Hosaka, T. Fujiwara and K. Meguro, *Bull. Chem. Soc. Jpn.*, 44 (1971) 2616
113. H. Hosaka, N. Kawashima and K. Meguro, *Bull. Chem. Soc. Jpn.*, 45 (1972) 3371
114. K. Meguro and K. Esumi, *J. Colloid Interface Sci.*, 59,(1) (1977) 93
115. K. Esumi and K. Meguro, *J. Colloid Interface Sci.*, 66 (1978) 192
116. D. Cordischi and V. Indovina, *J. Chem. Soc. Faraday Trans.*, 72(10) (1976) 2341
117. D. Cordischi, V. Indovina and A. Cinimo, *J. Chem. Soc. Faraday* 1, 70 (1974) 2189
118. K. Esumi and K. Meguro, *Bull. Chem. Soc. Jpn.*, 55 (1982) 315
119. K. Esumi and K. Meguro, *Bull. Chem. Soc. Jpn.*, 55 (1982) 1647
120. H. Hosaka and K. Meguro, *Colloids and Polymer Sci.*, 252 (1974) 322
121. R. S. Drago, L B. Parr and C. S. Chamberlain, *J. Am. Chem. Soc.*, 99 (1977) 3203
122. K. Esumi, K. Miyata and K. Meguro, *Bull. Chem. Soc. Jpn.*, 58 (1985) 3524
123. K. Esumi, K. Miyata and F. Waki and K. Meguro, *Colloids and Surfaces*, 20 (1986) 81
124. K. Esumi, K. Miyata, F. Waki and K. Meguro, *Bull. Chem. Soc. Jpn.*, 59 (1986) 3363
125. K. Esumi, K. Magara and K. Meguro, *J. Colloid Interface Sci.*, 141, (2) (1991) 578
126. S. Sugunan, G. D. Devikarani and P. A. Unnikrishnan, *J. Mater. Sci. Technol.*, 10 (1994) 425
127. S. Sugunan and J. M. Jalaja, *Collect. Czech. Chem. Commun.*, 59 (1994) 2605

128. S. Sugunan K. B. Sherley and G. D. Devikarani, *React. Kinet. Catal. Lett.*, 51(2) (1993) 525
129. S. Sugunan and G. D. Devikarani, *J. Mater. Sci. Lett.*, 10 (1991) 887
130. S. Sugunan, G. D. Devikarani and P. A. Unnikrishnan, *Indian J. Eng. Mater. Sci.*, 12 (1995) 245
131. S. Sugunan and J. J. Malayan, *J. Adhesion Sci. Technol.*, 9(1) (1995) 73
132. S. Sugunan and K. B. Sherley, *Indian J. Chem.*, 32(A) (1993) 689
133. S. Sugunan and G. D. Devikarani, *Indian J. Chem.*, 32(A) (1993) 993
134. S. Sugunan and G. D. Devikarani *J. Mater. Sci.*, 29 (1993) 4811
135. S. Sugunan and B. Varghese, *Indian J. Chem.*, 37A (1998) 806
136. S. Sugunan and Anto Paul, *React. Kinet. Catal. Lett.*, 65 (2) (1998) 343
137. S. Sugunan and Anto Paul, *Indian J. Chem.*, 36A (1997) 1068
138. S. Sugunan and Binsy Varghese, *React. Kinet. Catal. Lett.*, 62 (1) (1997) 157
139. S. Sugunan and Bindu Jacob, *Indian J. Eng. Mater. Sci.*, 4 (1997) 120
140. M. Ai, *J. Catal.*, 40 (1975) 318
141. M. Ai, *Bull. Chem. Soc. Jpn.*, 50 (1977) 2597
142. M. A. Aramendia, V. Borau, I. M. Garcia, C. Jimenez, A. Marinas, J. M. Marinas, A. Porras and F. J. Urbano, *Appl. Catal.*, 184 (1999) 115
143. O. V. Krylov, "Catalysis by Non-metals", Academic Press, New York.
144. H. Vinek, H. Noller, M. Ebel and K. Schwarz, *J. Chem. Soc., Faraday Trans. I*, 73 (1977) 734
145. A. Auroux and A. Gervasini, *J. Catal.*, 131 (1991) 190
146. C. P. Bezouhanova and M. A. Al-Zihari, *Catal. Lett.*, 11 (1991) 245
147. D. Martin and D. Duprez, *J. Mol. Catal.*, 118 (1997) 113
148. R. Venkatachalam and J. C. Kuriakose, *Proc. Natl. Acad. Sci., India, Sect. A1* (1977) 245
149. G. R. Dube and V. S. Darshane, *J. Mol. Catal.*, 79 (1993) 285
150. M. V. Joshi, S. G. Oak and V. S. Darshane, in "Catalysis: Modern Trends" (N. M. Gupta and D. K. Chakrabarthy ,eds.), Narosha Publishing House, New Delhi, 1995, p. 275

151. N. J. Jabarathinam and V. Krishnasamy in, "Catalysis – Present and Future", edited by P. Kanta Rao and B. S. Benwal, Publication And Information Directorate & Wiley Eastern Ltd., New Delhi , 1995, p. 288
152. M. C. C. Costa, L. F. Hudson, R. A. W. Johnstone, J. Y. Liu and D. Whittaker, J. Mol. Catal., 142 (1999) 349
153. K. Nomiya, Y. Sugana, S. Sosa and M. Miwa, Bull. Chem. Soc. Jpn, 53 (1980) 2089
154. K. Arata and M. Hino, Bull. Chem. Soc. Jpn, 53 (1980) 446
155. K. Arata and M. Hino, Chem. Lett., (1980) 1479
156. K. Arata H. Nakamura and M. Shouji, Appl. Catal., 197 (2000) 213
157. Y. Xia, W. Hua and Z. Gao, Catal. Lett., 55 (1998) 101
158. G. A. Olah, P. S. Iyer and G. K. Surya Prakash, Synthesis, (1986) 513
159. A. P. Singh, D. Bhattacharya and S. Sharma, J. Mol. Catal., 102 (1995) 139
160. B. Jacob, S. Sugunan and A. P. Singh, J. Mol. Catal., 139 (1999) 43
161. D. B. Barbier, A. Dormond and F. D. Montagne, J. Mol. Catal., 149 (1999) 215.
162. P. Zaszlo and A. Mathy, Helvetica Chimica Acta, 70 (1987) 577
163. S. P. Ghorpade, V. S. Darshane and S. G. Dixit, Appl. Catal., 166 (1998) 135
164. G. A. Olah, S. Kobayashi and M. Tashiro, J. Am. Chem. Soc., 94 (1972) 7448
165. P. S. Anilkumar, J. J. Shrotri S. D. Kulkarni, C. E. Deshpande and S. K. Date, Mater. Lett., 27 (1996) 293

CHAPTER-II
EXPERIMENTAL

2.1 CATALYST PREPARATION

Two series of ferros spinels of formulae $\text{Ni}_{1-x}\text{Cu}_x\text{Fe}_2\text{O}_4$ and $\text{Co}_{1-x}\text{Cu}_x\text{Fe}_2\text{O}_4$ ($x = 0, 0.3, 0.5, 0.7$ and 1) and their sulphated analogues were prepared for the present work. Their compositions and cation distributions are summarised in the following table.

Table 2.1 Catalyst compositions and cation distributions of ferros spinels containing Co, Ni and Cu.

x	composition	Cation at	
		Tetraherdal site	Octahedral site
	Simple ferros spinels		
0	NiFe_2O_4	Fe^{3+}	$\text{Fe}^{3+} \text{Ni}^{2+}$
0	CoFe_2O_4	Fe^{3+}	$\text{Fe}^{3+} \text{Co}^{2+}$
1	CuFe_2O_4	Fe^{3+}	$\text{Fe}^{3+} \text{Cu}^{2+}$
	Mixed Ferros spinels		
	i) Ni – Cu series		
0.3	$\text{Ni}_{0.7}\text{Cu}_{0.3}\text{Fe}_2\text{O}_4$	Fe^{3+}	$\text{Fe}^{3+} \text{Ni}_{0.7}^{2+} \text{Cu}_{0.3}^{2+}$
0.5	$\text{Ni}_{0.5}\text{Cu}_{0.5}\text{Fe}_2\text{O}_4$	Fe^{3+}	$\text{Fe}^{3+} \text{Ni}_{0.5}^{2+} \text{Cu}_{0.5}^{2+}$
0.7	$\text{Ni}_{0.3}\text{Cu}_{0.7}\text{Fe}_2\text{O}_4$	Fe^{3+}	$\text{Fe}^{3+} \text{Ni}_{0.3}^{2+} \text{Cu}_{0.7}^{2+}$
	ii) Co – Cu series		
0.3	$\text{Co}_{0.7}\text{Cu}_{0.3}\text{Fe}_2\text{O}_4$	Fe^{3+}	$\text{Fe}^{3+} \text{Co}_{0.7}^{2+} \text{Cu}_{0.3}^{2+}$
0.5	$\text{Co}_{0.5}\text{Cu}_{0.5}\text{Fe}_2\text{O}_4$	Fe^{3+}	$\text{Fe}^{3+} \text{Co}_{0.5}^{2+} \text{Cu}_{0.5}^{2+}$
0.7	$\text{Co}_{0.3}\text{Cu}_{0.7}\text{Fe}_2\text{O}_4$	Fe^{3+}	$\text{Fe}^{3+} \text{Co}_{0.3}^{2+} \text{Cu}_{0.7}^{2+}$

Preparation of these systems was done by the ‘soft’ chemical route reported by Date *et al.* [1]. Extra pure grade $\text{Ni}(\text{NO}_3)_2 \cdot 6\text{H}_2\text{O}$, $\text{Co}(\text{NO}_3)_2 \cdot 6\text{H}_2\text{O}$, $\text{Cu}(\text{NO}_3)_2 \cdot 3\text{H}_2\text{O}$ and $\text{Fe}(\text{NO}_3)_3 \cdot 9\text{H}_2\text{O}$ from Merck were used as such, without further purification. Metals were coprecipitated as their hydroxides from their nitrate solutions using sodium hydroxide as the precipitating alkali. Stoichiometric masses of the nitrates

were accurately weighed out and dissolved in distilled water to the following molarities.

1. ferric nitrate : 2.6 M
2. cobalt nitrate : 3.4 M
3. Nickel nitrate: 3.4 M ;
4. Copper nitrate: 3.4 M

Solutions of the metal nitrates were mixed thoroughly and the mixture was added rapidly to stoichiometric amount of 5.3M NaOH solution with stirring. Temperature of the slurry rose to 45-50°C due to the exothermic nature of the precipitation reaction. The pH of the final slurry was carefully adjusted between 10 and 11. The precipitate was kept overnight for aging and then washed several times (about 10-12 washings) with distilled water until free from nitrate ion and alkali. It was filtered and then dried in an air oven at 120°C for 48 hours and was calcined at 300°C for 3 hours to achieve transformation into spinel phase. The dried materials were powdered and sieved below 75 µm mesh.

Sulphation of spinel samples was done by the standard 'impregnation' method. 30 g of each of the spinel oxide samples was immersed in 150 ml of 0.2 M $(\text{NH}_4)_2\text{SO}_4$ solution and mechanically agitated for 4 hours. The mixture was kept overnight and filtered without washing. It was then dried at 120°C for 24 hours, powdered and sieved below 75 µm mesh.

2.2 CATALYST CHARACTERISATION

The prepared catalyst samples were characterized by adopting a variety of physico-chemical methods. Before each characterization, the samples were activated for 3 hours at temperatures of 300°C or 500°C. A brief discussion of each method of characterisation along with the experimental aspects adopted is presented below.

2.2.1 X-ray Diffraction analysis

X-ray diffraction (XRD) by crystals is the most widely employed method for determining the three dimensional structure of solid substances. Complete determination of crystal structure by locating the coordinates of all the atoms needs good single crystals at least of the size of about 1 mm. Most commonly found solids

are however, polycrystalline, meaning that each particle is made up of a large number of randomly oriented tiny crystals [2]. It is possible to get important structural information by recording the X-ray diffraction pattern of powdered polycrystalline samples by the powder diffractometer method.

Monochromatic X-rays (like Cu K_{α} or Mo K_{α} source) are reflected by families of planes in the polycrystalline material when the Bragg equation, $2d \sin \theta = n\lambda$, is fulfilled, where d is the interplanar spacing, θ is the angle between the planes and the X-ray beam (Bragg angle), λ is the X-ray wave length, and n is an integer called the order of reflection. Families of planes are identified by a system of Miller indices, hkl . These are integers and correspond to the number of times a family of planes strike the a , b , and c edges of the unit cell.

Powder diffractometer can produce accurate data in less than half an hour. The specimen for diffraction studies is prepared by packing the powder into the window of an aluminium holder backed by a glass slide. The plate containing the specimen is rotated and the diffracted X-rays are detected using a proportional counter or scintillation counter, rotating at twice the speed of the specimen. The usual scan speed is $2^{\circ} 2\theta$ per minute. The X-rays reaching the detector are registered and displayed on a paper chart recorder as series of peaks on top of background due to 'white' radiation, together with a scale of 2θ . The Bragg angles are simply read off the diffractometer trace and rough values of relative intensity are derived from peak heights above background.

Every crystalline substance has a unique X-ray powder pattern because line positions depend on unit cell size, and line intensity depends on the type of atoms present and on their arrangement in the crystal. Materials are identified from these values in conjunction with the 'Joint Committee on Powder Diffraction Standards' (JCPDS) Powder Diffraction File. This contains sets of cards containing X-ray data for most known crystalline phases. The data include d -spacing and relative intensity (I/I_0) values, Miller indices, unit cell dimensions etc. The appropriate Data Card is retrieved and the experimental data, especially those of the three strongest peaks are matched with the standard values [3].

Powder diffractometer method has many other applications than qualitative phase analysis. Some of these are quantitative phase analysis, determination of unit cell parameters, study of preferred orientation and the determination of particle size [3].

Rough estimate of particle size less than 0.1 μm diameter can be obtained from the amount of line broadening using the relation,

$$t = \lambda / B \cos \theta$$

where B = line width (Full Width-Half Maximum) of the strongest peak (in radians), θ =Bragg angle and t = the crystal diameter. The line broadening gives the size of the crystals and not the size of the particles since a particle may contain a number of crystals [4].

The diffractometer traces of the catalyst samples were taken using RIGAKU D/MAX-C instrument.

2.2.2 Infrared Spectroscopy

Infrared (IR) spectroscopy has been widely used in catalysis for identifying the structural features of the catalyst itself, as well as for identifying the adsorbed species and reaction intermediates on the catalyst surface. Conventional dispersive infrared spectrometers are gradually being replaced by Fourier Transform Infrared (FTIR) instruments due to many added advantages like improved spectral quality, higher sensitivity, suitability for use in the low frequency region ($<600 \text{ cm}^{-1}$) etc. In FTIR, a polychromatic incoming infrared beam passes through an interferometer, the sample and reaches the detector to produce an interferogram where the spectral information is in the line domain. It is converted to frequency domain spectral data using Fast Fourier Transform done with a computer attached to the instrument. The sampling of solids for infrared studies are most commonly done as KBr pellets or wafers.

The introduction of Diffuse Reflectance Infrared Fourier Transform Spectroscopy (DRIFTS) by Fuller and Griffiths [5] in 1978 has revolutionised the

application of IR spectroscopy to yield valuable spectroscopic information inherent in a mid-IR ($4000\text{-}200\text{ cm}^{-1}$) spectrum. Diffuse reflectance differs from ordinary reflectance, in that, here, the angular distribution of the reflected radiations is independent of the angle of incidence. A diffuse reflectance spectrum is obtained by the collection and analysis of surface-reflected electromagnetic radiation as a function of frequency using Fourier Transform technique. Thus it is more sensitive to surface species than the bulk of particles and hence is most suitable to explore the surface chemistry of high surface area powders. DRIFTS enables the rapid identification of powders with little or no sample preparation and a very little (about 0.1 mg) amount of the sample. Thus, for a variety of reasons, DRIFTS is becoming the single most important technique of studying the surfaces of catalyst powders [6].

The IR spectra of the catalyst samples have been taken in order to identify sulphation and to reaffirm the identification of the spinel phase. Ferrospinels typically give two absorption bands below 1000 cm^{-1} [7] and sulphated samples typically show a number of weak bands in the range $900\text{-}1100\text{ cm}^{-1}$ and sometimes, a strong band near 1380 cm^{-1} [8].

The FTIR spectra were taken using Shimadzu FTIR-8101 and the DRIFT spectra were taken using a DR-IR (Shimadzu).

2.2.3 BET Surface area determination

The Brunauer, Emmett and Teller (BET) method [9] has been adopted as a standard procedure for surface area determination of powdered catalysts. The BET theory of adsorption is an extension of Langmuir model to multilayer adsorption. The basic assumptions of the BET model are (i) the heat of adsorption for an adsorbate-adsorbent system does not change with surface coverage which means that all the adsorption sites on a given surface are energetically homogeneous (ii) the adsorption is multilayer and the heat of adsorption of the second and the subsequent layers are the same as the heat of condensation of the adsorbate and (iii) the model assumes a dynamic equilibrium within each layer.

The BET equation is conveniently expressed in the form ,

$$p/[v(p_0 - p)] = 1/[Cv_m] + [(C - 1)/(v_m C)](p/p_0)$$

where C = a constant for a given system at a given temperature and related to the heat of adsorption, v = the volume adsorbed at equilibrium pressure p , v_m = volume of the adsorbate necessary to form a monolayer on the surface, and p_0 = saturated vapour pressure of the adsorbate.

This equation predicts a linear plot (BET plot) between the experimental $p/[v(p_0 - p)]$ and p/p_0 values with slope equal to $(C - 1)/(v_m C)$ and y- intercept equal to $1/(Cv_m)$. From the slope and intercept, v_m can be calculated. The specific surface area of the sample is then calculated using the relation,

Surface area ($\text{m}^2 \text{g}^{-1}$) = $v_m N_0 a_m / (22414 \text{ wt})$ where a_m = average area occupied by the adsorbate molecule,

N_0 = Avagadro number and

wt = mass of the solid sample used for surface area measurements.

Adsorption of nitrogen gas at its boiling point is generally used for surface area measurements using BET method, a_m for N_2 being taken as 0.162 nm^2 . The linearity of BET plot is severely restricted to within the p/p_0 range of 0.05 - 0.30. A very high or very low C value will create considerable error in calculating the effective adsorbate cross-sectional area. High C values are likely to be associated either with localised monolayer adsorption or with micropore filling. Best results are obtained if C values are within the approximate range 80-120 [10].

The surface areas of all the catalyst samples have been measured by BET nitrogen adsorption at liquid N_2 temperature using the Micromeritics Gemini Analyser.

2.2.4 Pore Volume determination using mercury porosimetry

Dubin [11] has classified pores according to their diameters as micropores ($<20 \text{ \AA}$), macropores ($>200 \text{ \AA}$), and intermediate pores, now called mesopores (between 20 and 200 \AA). The pore size can be determined either from an adsorption isotherm or by using a mercury porosimeter. The underlying principle of mercury

porosimeter is to relate the force necessary to intrude a non-wetting liquid like mercury, to the average radius of the pores which are filled. The number of these pores is related to the volume of mercury needed to fill pores of certain average diameter. The relationship among the pressure(ΔP), surface tension(γ), contact angle (θ) and pore radius(r_p) is given by [12],

$$\Delta P = - 2 \gamma \cos \theta / r_p$$

. For mercury, $\gamma = 480 \text{ dyne cm}^{-1}$ and $\theta = 140^\circ$ so that the above equation enables one to calculate the pressure that will be needed to force mercury into pores of radius r_p . The apparatus consists of a calibrated piston pump, connected to a thermostated high pressure cell and a pressure gauge. The zero penetration volume is noted when the pressure just begins to rise. Usually these instruments are automated such that the volume and pressure signals drive an X-Y recorder or the data are collected on computer for post-run processing and manipulation.

The pore volumes of the catalyst specimens were determined using a Quantachrome mercury porosimeter.

2.2.5 Energy Dispersive X-ray (EDX) fluorescence analysis and Scanning Electron Microscope (SEM)

Energy dispersive X-ray (EDX) fluorescence analysis is a relatively new analytical technique used for qualitative and quantitative elemental analysis of solid specimens. As the name implies, it separates the characteristic X-rays on the basis of their photon energies rather than on their wave lengths. The instrumentation has been made possible due to the simultaneous development of the Si(Li) detector, the multi-channel pulse height analyser and powerful microcomputers [13].

The Si(Li) detector cooled by liquid N_2 receives undispersed characteristic X-rays from a fluorescing specimen. The amplified detector output is then digitised and the pulses accumulated in channels, each channel representing a small range of energy. For quantitative analysis, data are transferred to a computer for the calculation of elemental concentrations. For qualitative analysis the data may be displayed in a number of ways, eg, as a series of peaks (intensity vs. energy) on a cathode ray oscilloscope.

The compact geometry of the spectrometer allows the use of low power X-ray tubes and results in specimen preparation not being very critical. The simultaneous measurement and display of the energy spectrum result in rapid quantitative and qualitative elemental analysis. However, the method has some limitation, mainly imposed by the Si(Li) detector. The technique cannot detect elements lighter than sodium and the resolution of low energy radiation is poor. Again, it is not possible to achieve high sensitivities of weak peaks when strong ones are also present.

Scanning Electron microscopy (SEM) is based on the strong interaction of electrons with matter and their appreciable scattering by quite small atomic clusters. Electrons can be conveniently deflected and focused by electric or magnetic fields so that magnified real-space images can be formed in addition to simple diffraction patterns. In SEM, the electron optics act before the specimen is reached to convert the beam into a fine probe which can be as small as 100 \AA in diameter at the specimen surface [14]. This enables very impressive, in-focus images to be obtained from the highly irregular structures typical of catalyst specimens. The technique is of great interest in catalysis particularly because of its high spatial resolution. However, a serious drawback is that, the result need not be really representative of the whole sample. This can be overcome by making many analyses at different locations of the sample particles and for many catalyst particles.

SEM analysis was done using Stereoscan 440: Cambridge, U.K Scanning Electron Microscope.

2.2.6 Mossbauer spectroscopy.

Mossbauer spectroscopy has matured into an important technique for catalyst characterisation, although its application is limited to a small number of Mossbauer - active elements among which iron, tin, europium, iridium, ruthenium, antimony, platinum and gold are probably the most relevant for catalysis [15]. This technique yields information's like oxidation state, magnetic properties and lattice symmetry of these elements in catalyst specimens. The use of specimens in the form of micro

crystallites ensures that the information obtained bears considerable significance to the chemical state of the surface of the catalyst [16]. The great advantage of Mossbauer spectroscopy is that its γ -ray photons 'see' inside reactors to reveal catalyst chemistry and structure under *in situ* conditions of high temperature and pressure.

Mossbauer spectroscopy is based on Mossbauer effect, the recoil-free γ -ray emission and resonant absorption as achieved by putting the emitting and absorbing nuclei within a rigid solid matrix. Its importance lies in the very narrow line width of the γ -ray spectrum. Consequently it is able to probe the minor variations in nuclear energy levels resulting from any discrete changes in the chemical state and/or environment of the Mossbauer nucleus.

The most widely studied Mossbauer isotope is ^{57}Fe having a natural abundance of around 2%. The Mossbauer spectrometer essentially consists of a γ -ray source attached to a Doppler-shifting device, the sample (absorber) and a detector (G.M counter) which is connected to an amplifier and then to a pulse generator. The source of γ -rays is excited ^{57}Fe nuclei, produced by the decay of ^{57}Co isotope. These excited ^{57}Fe nuclei, in turn, decay in various modes emitting γ -rays of which the 14.4 keV γ -ray is of interest in Mossbauer spectroscopy. For scanning the minor energy changes in the sample nuclei, the source γ -ray energy is modified by Doppler shift generated by the controlled movement of the source. Thus Mossbauer spectrum consists of a plot of counts vs the applied Doppler velocity in the range of -10 to +10 mm s^{-1} .

The three important Mossbauer parameters are (i) isomer shift, (ii) the electric quadrupole splitting, ΔE_Q and (iii) the magnetic hyperfine splitting.

The isomer shift, δ , is the consequence of the Coulomb interaction between the positively charged nucleus and the negatively charged s-electrons which have definite density within the nuclear volume. Since the size of the nucleus in the excited state differs from that in the ground state, the Coulomb interaction energies are different as well. The isomer shift, therefore, is a measure of the s-electron

density at the nucleus, and yields useful information on the oxidation state of the iron in the absorber. Isomer shifts are expressed in velocity units, mm/s, and are given with respect to the peak position of a reference such as metallic iron or sodium nitroprusside.

The electric quadrupole splitting, ΔE_Q is caused by the interaction of the electric quadrupole moment of the nucleus with an electric field gradient (EFG). The nucleus of iron in the excited state has the shape of an ellipsoid and possesses an electric quadrupole moment. The origin of EFG is twofold. It is caused by asymmetrically distributed electrons in incompletely filled shells of the atom itself and by charges on neighbouring ions. If the symmetry of the electrons is spherical and that of the surrounding ions is cubic, EFG vanishes.

The magnetic hyperfine splitting, also known as the Zeeman effect, arises from the interaction between the nuclear magnetic dipole moment and the magnetic field H at the nucleus. This interaction gives rise to six transitions (magnetic sextuplet) with the separation between the corresponding peaks in the spectrum proportional to the magnetic field at the nucleus.

Often, all these three interactions occur simultaneously. In catalysts, the usual situation is that the quadrupole interaction is much smaller than the magnetic interaction. Again, Mossbauer lines may be broad, overlapping and ill-resolved and various curve fitting methods are then used to sort out the situation.

Yet another application of Mossbauer spectroscopy is to determine particle size. If the particle size is very small, a ferro or ferrimagnetic specimen fails to show magnetic splitting at room temperature. This is because the thermal excitations of energy kT at room temperature are energetic enough to decouple the magnetisation from the lattice causing the magnetisation vector of each particle to fluctuate rapidly over all directions. Thus the Mossbauer nucleus feels an average magnetisation of zero and a singlet or a doublet (in the case of quadrupolar splitting) Mossbauer spectrum, characteristic of superparamagnetic substance, results [17]. Now the particle size can be determined by studying the Mossbauer spectrum of the

superparamagnetic substance at varying temperatures and/or applied magnetic fields [17]. Shift from superparamagnetic singlet to ferro or ferrimagnetic sextet Mossbauer spectra is often found as the measuring temperature is lowered because the critical particle size to maintain magnetic property becomes smaller at lower temperatures [18].

The Mossbauer spectra of the catalyst samples have been taken using the constant acceleration type Austin (USA) S-600 Mossbauer spectrometer.

2.2.7 Thermogravimetric analysis (TGA)

Thermogravimetry is a technique where the weight of a sample can be followed over a period of time while its temperature is being raised linearly. Recording analytical balances with provision for controlled heating of a sample are called thermobalances. In a thermogravimetric curve the horizontal portions point out the regions where there is no weight change, whereas the weight loss is indicated by the curved portions. In the derivative thermogravimetric curve (DTG), dips correspond to weight loss and plateaus correspond to no weight change.

The TGA of catalyst samples has been done using TGA – 50 (Shimadzu) at the rate of heating of 10° per minute.

2.3 DETERMINATION OF SURFACE ELECTRON-DONOR PROPERTIES

(a) Reagents and purification methods:

The electron acceptors used in the study are:

7,7,8,8 -tetracyanoquinodimethane (TCNQ)

2,3,5,6 -tetrachloro-p-benzoquinone (chloranil) and
p-dinitrobenzene.

TCNQ was obtained from Merck -Schuchardt and was purified by repeated recrystallisation from acetonitrile [19]. Chloranil was obtained from Sisco research laboratories Pvt. Ltd. and was purified by recrystallisation from benzene [20]. p - Dinitrobenzene was supplied by Koch Light laboratories Ltd. and was purified by recrystallisation from chloroform [21].

Acetonitrile was used as the solvent. SQ grade acetonitrile obtained from Qualigens Fine Chemicals was first dried by passing through a column filled with silica gel 60-120 mesh size activated at 110° C for 2 hours. It was then distilled with anhydrous phosphorus pentoxide and the fraction distilling between 80-82°C was collected [22].

(b) Method adopted for adsorption studies:

The catalyst was activated at a particular temperature for 3 hours prior to each experiment. Adsorption study was carried out over 0.5 g catalyst placed in a cylindrical glass vessel fitted with a mercury sealed stirrer. Before sealing, the sample was outgassed at 10 torr for one hour. 10 ml of solution of an electron acceptor in acetonitrile was then admitted to the catalyst. Stirring was continued for 4 hours in a mechanically driven stirrer at 28° C in a thermostated bath and the oxide was collected by centrifuging the solution. The amount of electron acceptor adsorbed was determined from the difference in the concentration of the electron acceptor in solution before and after adsorption, which was measured by means of a Shimadzu UV - VIS spectrophotometer. The λ_{max} of electron acceptors in acetonitrile are 393.5 nm for TCNQ, 288 nm for chloranil and 262 nm for p-dinitrobenzene. From the absorbance vs. concentration linear plots, any unknown concentrations have been determined.

2.4 ACIDITY DETERMINATION BY GRAVIMETRIC ADSORPTION OF n-BUTYLAMINE

Determination of the strength of the acidic sites exposed on the solid surface as well as their distribution is a necessary requirement to understand the catalytic properties of solid acids. Among all the physico-chemical methods of determining acidity as reviewed by Kijenski and Baiker [23], temperature-programmed desorption and calorimetric measurements are the most promising. However, the gravimetric adsorption of n-butylamine followed by TGA is a very simple method to determine strength and distribution of acid sites on catalyst surfaces [24,25].

Catalysts were kept in a desiccator saturated with n-butylamine vapour at room temperature for 48 hours. Then the weight loss of the adsorbed sample was

measured by TGA (Shimadzu TGA-50) operating between 40 to 600° C at a rate of 20° /minute. The weight loss between 150-300, 301-450 and 451-600°C are considered to be measures of weak, medium and strong acid sites, respectively.

2.5 VAPOUR-PHASE CYCLOHEXANOL DECOMPOSITION REACTION

Cyclohexanol from Merck was used as such without further purification. The reaction was done at atmospheric pressure in a fixed bed, vertical, down-flow, integral silica reactor placed inside a double-zone furnace (Solelem - France). Schematic diagram of the reactor set up is shown in Fig 2.4.1 The catalysts were pressed, pelletised and broken into uniform pieces and sieved to obtain catalyst particles of size 10-20 mesh. Exactly 3 g catalyst was charged each time in the centre of the reactor in such a way that the catalyst was sandwiched between the layers of inert porcelain beads. The upper portion of the reactor served as a vapouriser cum pre-heater. All heating and temperature measurements were carried out using 'Aplab' temperature controller and indicator instruments.

A thermocouple was positioned at the centre of the catalyst bed to monitor the exact temperature of the catalyst bed. The catalysts were activated in the reactor itself at 573K in a sufficient flow of dry air or at least 3 hours before each run. The liquid reactant was fed by a syringe pump (ISCO Model 500 D). The products of the reaction were collected downstream from the reactor in a receiver connected through a cold water circulating condenser. Products were collected at various time intervals and analysed by gas chromatography (Shimadzu, Model 15A, HP ultra capillary column, FID detector, N₂ carrier gas, injection port temperature 250° C, column temperature 80°C, detector temperature 250° C.) Identification of products was done by comparing the GC retention times of expected products with those of standard chemicals.

2.6 LIQUID-PHASE BENZOYLATION REACTIONS

Toluene and benzene from Qualigens Fine Chemicals were purified according to the standard procedure [26]. Benzoyl chloride from Merck was used as such. A mixture of toluene and benzoyl chloride in the molar ratio 3.6:1 (toluene: 10 ml, benzoyl chloride : 3 ml) is refluxed at the b.p of the mixture with 0.100 g of the

activated catalyst sample for 30 minutes. The products were analysed using gas chromatography.(Chemito 8510, SE 30 column, FID detector, N₂ carrier gas, injection port temperature 250°C, column temperature programmed as 100°C for 2 minutes followed by heating at the rate 7° per minute upto 170°C, detector temperature 250°C). The products were identified by GC – MS.

Similarly a mixture of benzene and benzoyl chloride in the molar ratio 4.3:1 (benzene: 10 ml and benzoyl chloride : 3 ml) is refluxed at the boiling point of the mixture with 0.150 g of the activated catalyst sample for 1.5 hours. The products were analysed using gas chromatography, with details the same as for the previous benzoylation.

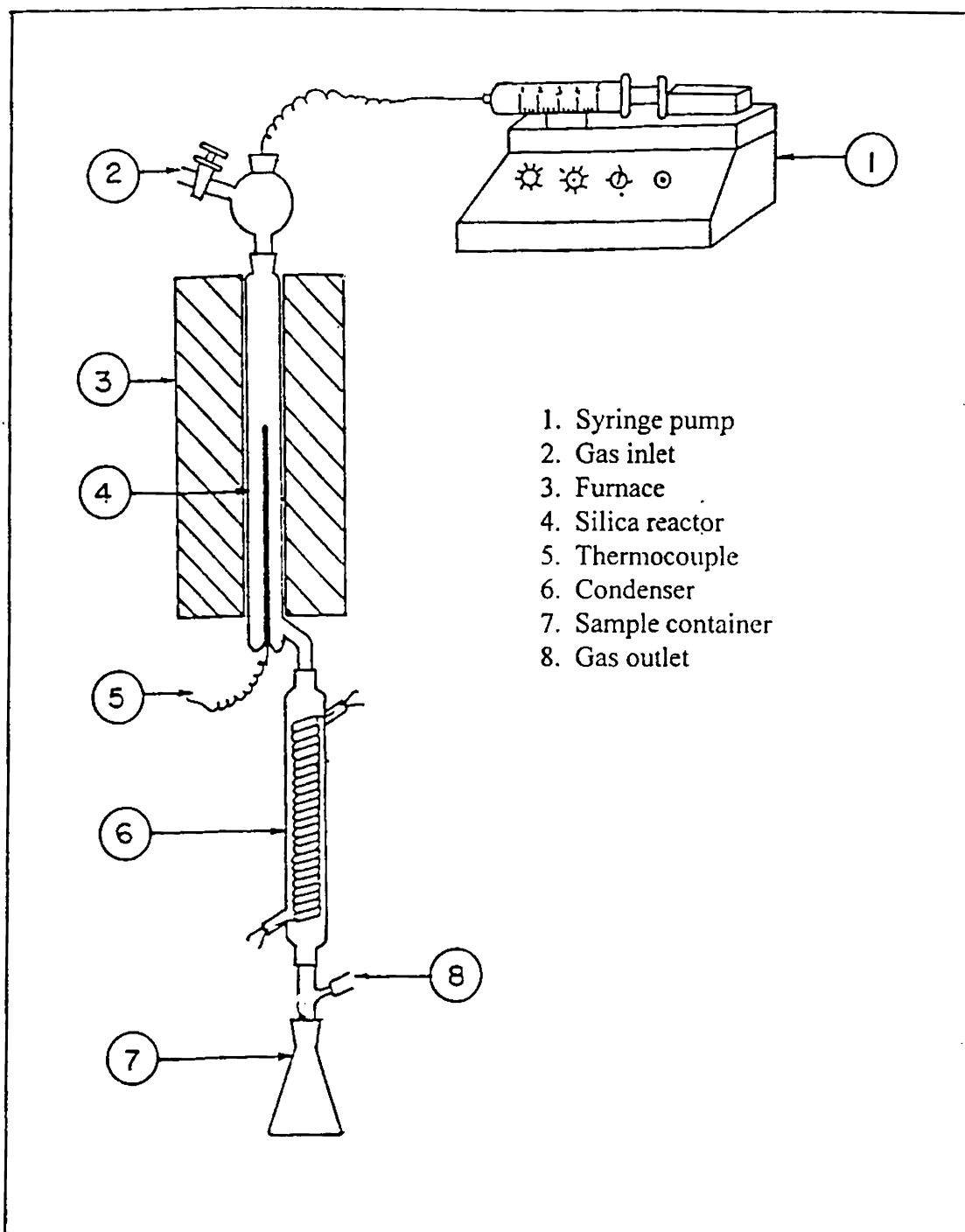


Fig. 2.4.1 Reactor set-up for reactions carried out at atmospheric pressure

REFERENCES

1. P.S. Anilkumar, J. J. Shrotri, S. D. Kulkarni, C. E. Deshpande and S. K. Date, *Materials Letters*, 27 (1996) 293
2. D. K. Chakrabarthy, "Solid State Chemistry", New Age International Ltd., New Delhi, 1996, p.14
3. Clive Whiston, "X-ray Methods – Analytical Chemistry by Open Learning", (F. E. Prichard, Editor), John Wiley, 1987, ch. 3
4. H. Lipson and H. Steeple, "Interpretation of X-ray Powder Diffraction Patterns", Macmillan, London, 1970, p. 261
5. M. P. Fuller and P. R. Griffiths, *Anal. Chem.*, 58 (1978) 1906
6. J. P. Blitz, Diffuse Reflectance Spectroscopy in "Modern Techniques in Applied Molecular Spectroscopy", edited by F. M. Mirabella, John Wiley, New York, 1998, p. 213
7. R. D. Waldon, *Phys. Rev.*, 99 (1955) 1727
8. M. Bensitel, O. Saur, J. C. Lavalley and B. A. Morrow, *Mater. Chem. Phys.*, 19 (1988) 147
9. S. Brunauer, P. H. Emmett and E. Teller, *J. Am. Chem. Soc.*, 60 (1938) 309
10. K. S. W. Sing in "Characterisation of Catalysts", edited by J. M. Thomas and R. M. Lambert, John Wiley, New York, 1980, p. 20
11. M. M. Dubinin, *Chem. Rev.*, 60 (1960) 235
12. D. K. Chakrabarthy, "Adsorption and Catalysis by Solids", Wiley Eastern Ltd., New Delhi, 1991, p. 73
13. Clive Whiston, "X-ray Methods – Analytical Chemistry by Open Learning", John Wiley, New York, 1991, p. 296
14. A. Howie in "Characterisation of Catalysts", edited by J. M. Thomas and R. M. Lambert, John Wiley, New York, 1980, p. 89
15. N. N. Greenwood and T. C. Gibb, "Mossbauer Spectroscopy", Chapman and Hall, London, 1971
16. W. Jones in "Characterisation of Catalysts" edited by J. M. Thomas and R. M. Lambert, John Wiley, New York, 1980, p. 114
17. J. W. Niemantsverdriet and W. N. Delgass, *Topics in Catalysis*, 8 (1999) 133
18. J. G. Lee, J. Y. Park and C. S. Kin, *J. Mater. Sci.*, 33 (1998) 3965
19. D. S. Acker and W. R. Hertler, *J. Am. Chem. Soc.*, 84 (1962) 3370

20. L. F. Fiesser and M. Fiesser, "Reagents for Organic Synthesis", John Wiley, New York, 1967, p. 125
21. B. S. Furness, A. J. Hannaford, V. Rogers, P. W. G. Smith and A. R. Tatchell, "Vogel's text book of Practical Organic Chemistry", 4th Edition, ELBS, London, 1978, p. 708
22. A. I. Vogel, "A Text Book of Practical Organic Chemistry", 3rd Edition, ELBS, London, 1973, p. 407
23. J. Kijenski and A. Baiker, *Catal. Today*, 5 (1989) 1
24. J. C. Wu, C. S. Chung, C. L. Ay and I. Wang, *J. Catal.*, 87 (1984) 98
25. N. J. Jebarathinam and V. Krishnaswamy, "Catalysis – Present and Future" edited by P. Kanta Rao and B. S. Benwal, Publication and Information Directorate and Wiley Eastern Ltd., New Delhi, 1995, p. 288
26. A. I. Vogel, "A Text Book of Practical Organic Chemistry", 3rd Edition, ELBS, London, 1973, p. 177

CHAPTER-III
CHARACTERISATION AND SURFACE PROPERTIES
RESULTS AND DISCUSSION

3.1 PHYSICAL CHARACTERISATION

The catalyst samples prepared were characterised by adopting various physical methods such as X-ray diffraction analysis, infrared spectra, BET surface area, pore volume measurements, Energy Dispersive X-ray (EDX) analysis, Mossbauer spectra etc. The results of each method and their interpretations are given below.

3.1.1 X-ray diffraction analysis

The X-ray diffraction analysis of the catalyst samples has been done using RIGAKU D/MAX-C powder diffractometer and a few diffractometer traces are given in Fig 3.1.1.& Fig.3.1.2. The experimental d_{hkl} values for the simple ferros spinels, agree very closely with the standard values given in the JCPDS Data Cards for these systems (Table 3.1.1). This identifies and confirms the spinel phase of the samples.

Table 3.1.1 Experimental and standard X-ray powder diffraction data for the first three strong lines for the ferros spinels of Co, Ni and Cu.

System	JCPDS data		Experimental data, d_{hkl} (Å °)	hkl
	I/I ₀	d_{hkl} (Å °)		
NiFe ₂ O ₄	100	2.51	2.51	311
	40	1.48	1.47	440
	30	1.61	1.60	511
CoFe ₂ O ₄	100	2.52	2.51	311
	64	1.48	1.48	440
	40	1.61	1.60	511
CuFe ₂ O ₄	100	2.52	2.50	311
	60	1.48	1.48	440
	50	2.96	2.96	220

The mixed ferros spinels of the Ni-Cu series and the Co-Cu series are treated as solid solutions obtained by the substitution of Ni or Co of NiFe_2O_4 or CoFe_2O_4 with Cu ions. In interpreting the XRD of such substitutions, the substitutional site can be considered as 'statistically' occupied i.e., by a sort of 'composite atom' made up of the appropriate portions of the atoms involved [1]. There is a linear relation (Vegard's law) existing between the lattice parameters and the composition of the solid solution [2]. Thus the pattern of the solid solution is expected to be intermediate between those of the pure substances. The fact that the mixed ferrites of the Ni-Cu series and the Co-Cu series give almost identical XRD patterns with those of NiFe_2O_4 or CoFe_2O_4 proves that the Cu substitution does not change the site occupancy and that the mixed ferrites have the same inverse spinel structure as the pure ferrites. It is interesting to observe that the XRD data of all the samples are very much alike. This is an expected result. In the powder diffraction pattern, the line position depends on unit cell edge length and the line intensities depend on the type of atoms present and their arrangement in the crystal. In the present systems studied, the compositional differences are due to different proportions of the atoms Ni, Co or Cu. These have close atomic numbers and hence close X-ray atomic scattering factors. Naturally, the lattice parameters are also expected to be very close to one another. These parameters for the ferros spinels of Ni, Co and Cu are given in Table 3.1.2 [3]. The slight elongation of the CuFe_2O_4 unit cell along the z-direction is due to Jahn-Teller distortion.

Table 3.1.2: Lattice parameters of the ferros spinels of Ni, Co and Cu

Lattice parameters	NiFe_2O_4	CoFe_2O_4	CuFe_2O_4
System	Cubic	Cubic	Cubic
Space Group	Fd3m	Fd3m	Fd3m
Unit cell Edge length (Å)	a = 8.325	a = 8.380	a = 8.220 c = 8.710

The XRD patterns of sulphated samples do not show differences from those of the unmodified samples. Components in a mixture occurring below about 5% by mass would be insufficient to give measurable diffraction lines [4]. As sulphate loading is very much less than 5%, it is not expected to cause changes in XRD patterns. As temperature of calcination increases, the XRD peaks become sharper. This is illustrated in Fig.3.1.3. for NiFe_2O_4 . This is because the samples become more crystalline with calcination temperature.

The average particle diameter (t) has been calculated from the glancing angle (θ), peak width (B) of the strongest peak in the XRD pattern and the wavelength (λ) of the X-ray used, using the relation, $t = \lambda/(B \cos \theta)$, and a few values are given in Table 3.1.3. These results show that copper-containing ferros spinels have relatively smaller particle size while CoFe_2O_4 has the highest particle size.

Table 3.1.3: Average particle diameters of the catalyst systems from XRD data.

System	Average particle diameter (nm)
NiFe_2O_4	25
CoFe_2O_4	26
CuFe_2O_4	16
$\text{Ni}_{0.3}\text{Cu}_{0.7}\text{Fe}_2\text{O}_4$	15
$\text{SO}_4^{2-}/\text{Ni}_{0.3}\text{Cu}_{0.7}\text{Fe}_2\text{O}_4$	18

3.1.2 Infrared spectra

The Diffuse Reflectance Infrared Fourier Transform (DRIFT) and Fourier Transform Infrared (FT-IR) spectra of the samples have been taken to supplement identification of the spinel phase and to confirm sulphate loading. Some of these spectra are shown in Fig. 3.1.4 – Fig. 3.1.8.

The DRIFT spectra, taken in the $400\text{-}1000\text{ cm}^{-1}$ wave number region, typically show two strong infrared bands ν_1 and ν_2 around 700 cm^{-1} and 500 cm^{-1}

respectively. The first important paper on the infrared spectra of spinels was published in 1955 by Waldron [5] who, giving experimental data on seven ferrite spinels, showed that two absorption bands below 1000 cm^{-1} were a common feature of all the ferrites. He also assigned, based on a simplified theoretical treatment, the high frequency band near 700 cm^{-1} to the tetrahedral M-O group stretching vibration and the low frequency band near 500 cm^{-1} to the octahedral M-O group vibration. The basis of Waldron's description is as follows:

In the spinel lattice, every oxygen anion is bonded to three octahedral and one tetrahedral cation (Fig. 3.1.9)

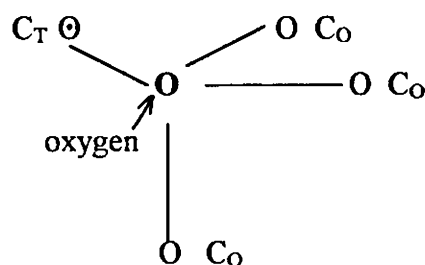


Fig 3.1.9 The nearest cationic neighbours of the oxygen anion in the spinel lattice. C_O : octahedral cation, C_T : tetrahedral cation.

The three octahedral bonds are perpendicular to one another and thus provide an isotropic force field in which the oxygen would be free to oscillate in the three directions if the tetrahedral bond was absent. The tetrahedral cation C_T introduces a supplementary restoring force in a preferential direction along the $C_T - O$ bond. This is responsible for the ν_1 mode in which the oxygen is forced to oscillate along the $C_T - O$ bond, and thus appears as a stretching vibration of the tetrahedral group. The highest restoring force is directed along the $C_T - O$ bond and the corresponding vibration i.e. a stretching vibration of the tetrahedral group is assigned to the high-frequency absorption band. If we now consider an oxygen vibration at right angle with the preceding one, the restoring force due to the tetrahedral cation C_T will be negligible. This leads to the lower frequency ν_2 mode, which may be considered as a stretching frequency of the octahedral group.

Waldron's assignment is fairly acceptable for all inverse spinels, where cations with +3 oxidation state is present in tetrahedral sites and cations with +2 and +3 oxidation states, in octahedral sites. Waldron's interpretations have been supported by White *et al.* [6] who applied group theory to the classification of the vibrational modes of the spinels. However, an opposite opinion has been raised by Preudhomme and Tarte [7], according to which, in the case of normal spinels, the high frequency band should be assigned to the stretching vibration of the octahedral group, since the tetrahedral site is solely occupied by +2 cations and hence the $C_T - O$ bonding force will be less than the $C_O - O$ bonding force.

Sulphate loading of the spinel samples has been qualitatively confirmed from their infrared spectra which always showed additional bands in the range 1200-1000 cm^{-1} for the sulphated samples (e.g., Fig 3.1.5 & 3.1.6). Such bands are characteristic of the sulphate group in ionic sulphates [8].

High resolution of these bands shows four absorptions - two strong ones near 1100 cm^{-1} and 1050 cm^{-1} and two weak ones near 1150 cm^{-1} and 990 cm^{-1} , which sometimes only appear as shoulders (Fig. 3.1.7 & 3.1.8).

Infrared spectra of sulphated metal oxides, especially the superacidic sulphated ZrO_2 , HfO_2 , TiO_2 , Fe_2O_3 and SnO_2 have been the subject of detailed study for explaining the cause of superacidity and for proposing structure models for the surface sulphated species [9-13].

A common feature of all superacidic sulphated oxides is the presence of a strong band near 1400 cm^{-1} and a number of bands at lower wave numbers in the range 1150-1000 cm^{-1} [11]. The strong band near 1400 cm^{-1} representing the asymmetric stretching frequency of S=O is often regarded as the characteristic band of sulphate-promoted superacids [14,15]. The presence of this band and hence superacidity, depends very critically on the water content of the sulphated oxides. Thus, calcination temperature of the catalyst and the precautions taken to keep the samples always in a dry condition are very crucial in generating superacidity. On most oxides which are hydrated or slightly dehydrated, surface sulphates are in

highly ionic form and give several ν_{S-O} bands localised at $\bar{\nu} \leq 1200 \text{ cm}^{-1}$, reminiscent of crystalline inorganic sulphates or sulphato complexes. In contrast, sulphates at the surfaces of oxides brought *in vacuo* to medium-high dehydration stage possess a highly covalent character, reminiscent of covalent organic sulphates. Only such sulphates give ν_{S-O} stretching bands near 1400 cm^{-1} , besides a number of lower frequency bands at $\bar{\nu} \leq 1150$ due to ν_{S-O} stretching modes. The IR spectra of sulphated zirconia are much more complex in having many bands in the $1400\text{-}800 \text{ cm}^{-1}$ spectral region, suggesting several surface species to be present, whereas the IR spectra of sulphated titania or alumina are simpler, suggesting only a single surface species [9]. For sulphated alumina, there is an intense sharp band at 1380 cm^{-1} and an intense but broad band near 1045 cm^{-1} . For sulphated titania, there is a similar sharp peak at 1370 cm^{-1} and a broad doublet at 1045 and 1005 cm^{-1} in addition to a weak band at 1110 cm^{-1} [9].

The various structural models suggested for sulphate species on zirconia have been reviewed by Song and Sayari [13]. Pyridine adsorption studies followed by IR spectrum show that there are both new Lewis and Brønsted sites created on sulphated oxides [16]. The mechanism of superacidity in sulphate-modified oxides remains controversial. Tanabe [17] attributed superacidity to an enhanced Lewis acidity of the Zr^{4+} ions arising from the inductive effect of neighbouring $\text{S}=\text{O}$ groups. ^{31}P MAS NMR spectral studies of sulphated zirconia reveal that strongly acidic protons are responsible for superacidity [18]. But these strong Brønsted sites require the presence of adjacent Lewis acid centres.

The effect of hydration on sulphated zirconia has been investigated by Morterra *et al.* [19] using infrared spectroscopy. In a medium-high dehydration stage, the IR spectra showed a strong band at 1370 cm^{-1} , a broad unresolved band centred at 1200 cm^{-1} and a broad partially resolved band at $1000\text{-}1050 \text{ cm}^{-1}$. With increasing doses of water vapour admitted, the IR spectra showed that the strong band at 1370 cm^{-1} gradually disappeared and the lower frequency bands transformed into three bands at 1240 cm^{-1} , 1130 cm^{-1} and 1070 cm^{-1} with a weak shoulder appearing at 1000 cm^{-1} . Such an IR pattern is typical of sulphato complexes

in a bidentate configuration with C_{2v} symmetry [20]. Also a new band centred at 1650 cm^{-1} appeared. This was due to δ_{HOH} band of undissociated water molecules.

It was noticed that the IR spectra of sulphated alumina or titania also changed with presence of H_2^{18}O at 20° C and the new spectra resembled that of the traditional bidentate type sulphate species [9]. The authors propose that, in the absence of water, the sulphate has a structure resembling $(\text{MO})_3\text{S}=\text{O}$ ($\text{M} = \text{Al}$ or Ti) [Structure I] whereas, in presence of H_2O or excess surface OH groups, this is converted to $(\text{MO})_2\text{SO}(\text{OH})$ [structure II], thus accounting for the increased Brønsted acidity. (Fig. 3.1.10)

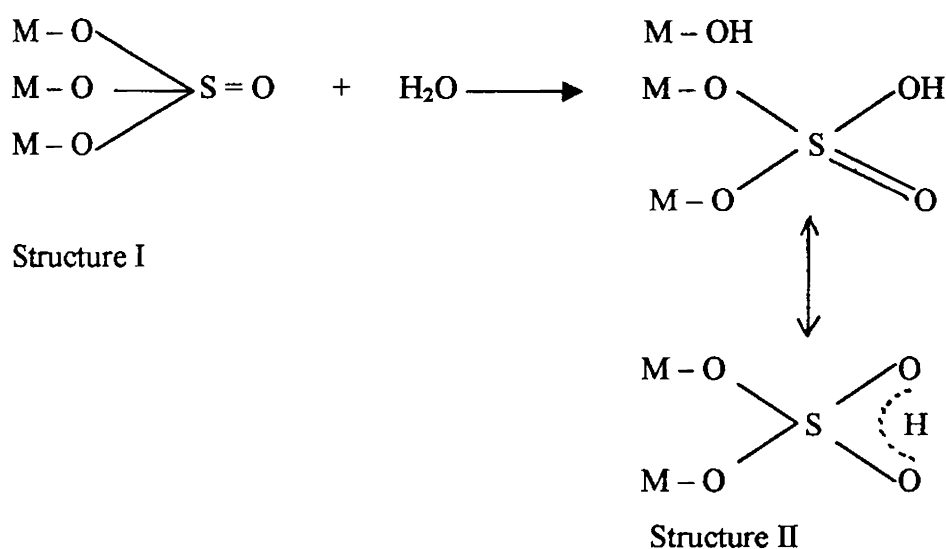


Fig.3.1.10. Structure of surface sulphate accounting for the increased Brønsted acidity.

The IR spectra of structure II are very close to those reported for bidentate metal sulphates.

Returning to our IR spectra (Fig 3.1.7 & 3.1.8), the above discussion leads us to the following conclusions.

(i) Lack of IR band near 1400 cm^{-1} reveals that none of the sulphated spinel samples under study possess superacidic qualities. This is explained by the fact that much of the characterisation and catalytic studies of the systems were done at the activation temperature of 300°C . At this temperature, the samples are still sufficiently hydrated. Broad XRD peaks show lack of sufficient crystallinity at 300°C (Fig. 3.1.3). Again

T.G studies (Fig. 3.1.16) reveal that complete dehydration of sulphated samples occur just above 300°C. Finally, no special precautions, other than keeping in a desiccator, were taken (like keeping *in vacuo* in sealed tubes) to keep the catalyst samples perfectly dry before the various studies were done. The IR band at 1613 cm⁻¹ (Fig. 3.1.8.) is due to δ_{HOH} vibration of undissociated water molecule; its intensity diminishes as the activation temperature is increased to 500°C.

(ii) The structure model of the sulphate species on our samples is suggested to be the hydrogenosulphate modified form, II (Fig. 3.1.10). The IR spectra of structure II closely resemble that of the bidentate sulphate complex as having bands around 1150 cm⁻¹, 1130 cm⁻¹, 1070 cm⁻¹, and a shoulder at 980 cm⁻¹. Our spectral bands also closely agree with these. The bisulphate model is preferred as it can also account for the enhanced Brønsted acidity evinced by the sulphated samples during decomposition of cyclohexanol (Chapter V).

3.1.3 Surface Area and Pore Volume distribution

The BET surface areas of all the catalytic systems calcined at 300°C and 500°C were measured using the Micromeritics Gemini Analyser. The results are given in Table 3.1.4 and the trends are shown graphically in Fig. 3.1.11 & 3.1.12. These data show that incorporation of copper into the ferros spinel systems of nickel and cobalt increases the surface areas of the systems calcined at 300°C while decreases the surface areas at the calcination temperature of 500°C. This is a direct consequence of the fact that, among the ferros spinels of Ni, Co and Cu, CuFe₂O₄ has the highest surface area at 300°C while, the same CuFe₂O₄ has the lowest surface area at 500°C. Surface areas of sulphated systems are invariably higher than those of the unmodified samples except for CuFe₂O₄ and Co_{0.3}Cu_{0.7}Fe₂O₄. It has been shown that sulphation inhibits sintering of the metallic oxide and delays the transition from amorphous to crystalline phase [13]. Here also, the large surface areas of sulphated samples have been related to retardation of crystallisation into the spinel phase. It is interesting to observe that CuFe₂O₄ having the highest surface area among the simple ferros spinels, also has the lowest average particle size, as calculated from XRD line broadening. Keeping other factors aside, a finely divided catalyst sample will, not only have a higher surface area, but also a higher catalytic activity as was shown for

finely divided TiO_2 [21]. The decrease in surface area with calcination temperature is partly due to completion of dehydration of the surface hydroxyl groups concomitant with the completion of crystallisation and growth of crystallite size and partly due to sintering.

Table 3.1.4. BET surface areas of the ferrosipinel systems.

Catalyst Systems	x	Surface area (m^2/g)			
		Unmodified		modified with sulphate	
		300° C	500° C	300° C	500° C
$\text{Ni}_{1-x}\text{Cu}_x\text{Fe}_2\text{O}_4$	0	152.85	45.14	196.34	77.92
	0.3	177.01	39.16	202.88	71.80
	0.5	183.20	28.78	211.52	38.90
	0.7	174.40	25.82	193.49	38.02
	1.0	187.87	19.77	187.66	32.49
$\text{Co}_{1-x}\text{Cu}_x\text{Fe}_2\text{O}_4$	0	94.58	32.16	107.37	46.29
	0.3	137.15	23.07	152.34	34.40
	0.5	134.41	26.00	154.66	40.00
	0.7	167.50	30.00	162.66	46.51
	1.0	187.87	19.77	187.66	32.49

The availability of active centres as well as the transport of reactant and product molecules to and from the active surface can be accomplished by a proper pore size distribution. Thus the knowledge of porous structure parameters of catalysts is indispensable for their use in industrial processes, where resistance to flow should be as low as possible. The pore volumes of catalyst samples have been determined using mercury porosimeter and the values for three types of NiFe_2O_4 systems are given in Table 3.1.5. The differential pore volume curves are given in Fig. 3.1.13.

The pore size range, over which the major pore volume distribution occurs as inferred from these graphs, is also given in the Table 3.1.5

Table 3.1.5 Pore volume and pore size distribution of NiFe₂O₄ samples.

System	Pore Volume (cm ³ g ⁻¹)	Major pore size distribution (Å°)
NiFe ₂ O ₄ activated at 300°C	0.5283	20-50
NiFe ₂ O ₄ activated at 500°C	0.5108	50-150
SO ₄ ²⁻ /NiFe ₂ O ₄ activated at 300°C	0.4077	18-30

Both the pore volume and pore size decrease with sulphation for a given catalyst at a given calcination temperature. This is due to the preferential attachment of sulphate at the corners and edges of the pores. This amounts to partial filling of the pores, reducing their effective radii and volumes. The pore volume decreases while the average pore size increases with increase of calcination temperature. The decrease in pore volume is due to the decrease in the number of pores as the crystallites agglomerate by virtue of enhanced crystallisation and sintering. The increase in pore size is due to the increased dehydration of the surface hydroxyl groups, thus enlarging the surviving pores.

3.1.4 Energy Dispersive X-ray (EDX) analysis and Scanning Electron Microgram (SEM)

The compositions of the ferrosinell samples prepared have been checked by EDX analysis and the results for a few samples are given in Table 3.1.6

Table 3.1.6 :- Energy Dispersive X- Ray analysis (EDX) data.

System	EDX weight %	Theoretical weight %
CoFe_2O_4	Co : 34.20, Fe : 65.80	Co : 34.50, Fe : 65.50
CuFe_2O_4	Cu : 35.24, Fe : 64.76	Cu : 36.30, Fe : 63.70
NiFe_2O_4	Ni : 32.19, Fe : 67.81	Ni : 34.40, Fe : 65.60
$\text{Ni}_{0.3}\text{Cu}_{0.7}\text{Fe}_2\text{O}_4$	Ni : 9.73, Cu : 25.88, Fe : 64.38	Ni : 10.10, Cu : 25.60, Fe : 64.30
$\text{SO}_4^{2-}/\text{Ni}_{0.3}\text{Cu}_{0.7}\text{Fe}_2\text{O}_4$	Ni : 9.14, Cu : 25.01, Fe : 64.94, S : 0.90	-
$\text{SO}_4^{2-}/\text{NiFe}_2\text{O}_4$	Ni : 31.94, Fe : 67.08, S : 0.98	-

There is good agreement between the experimental weight percentage of the elements and the theoretically expected weight percentage calculated from the stoichiometric formulae. Sulphate loading has been to an extent of about 1% by mass of sulphur. In the study of sulphated zirconia, sulphur content usually varies in the range 0.8 to 3 weight % [13]. The nature of sulphur species rather than the sulphur content is important in influencing catalytic activity. For sulphated zirconia, Chen *et al.* [22] found that the maximum rate of n-butane isomerisation (a test reaction for superacidity) occurred with the catalyst sample activated at 650°C, containing 1 % by mass of sulphur. Calculation shows that 1 % by mass of sulphur corresponds to a sulphate uptake of about 250 $\mu\text{mol g}^{-1}$. This, in turn, corresponds to about half monolayer coverage (about 2 sulphur atoms per nm^2) in a sample of surface area 100 $\text{m}^2 \text{g}^{-1}$ [11].

SCM photograph of CoFe_2O_4 calcined at 300°C is given in Fig.3.1.14. The small particle size (about 250 Å diameter) of the sample is evident from this photograph.

3.1.5 Thermogravimetric Analysis

Thermogravimetric analysis curve (TG) along with the corresponding derivative curve (DTG) for the systems NiFe_2O_4 and $\text{SO}_4^{2-}/\text{NiFe}_2\text{O}_4$ are shown in Fig. 3.1.15 and Fig. 3.1.16 respectively.

As shown in these figures, the TG curve involves a plot of % weight loss of the samples against the temperature while the DTG curve involves a plot of the corresponding derivative of the % weight loss vs. temperature.

In the TG curve of NiFe_2O_4 , the initial weight loss taking place below 100°C is due to the loss of physisorbed water. The weight loss occurring between about 180 to 300°C corresponds to the removal of chemisorbed water out of the surface hydroxyl groups as the system gets more and more dehydrated into the oxidic spinel phase. This dehydration occurs at two distinct temperature ranges, around 180°C and 280°C , as shown by the dips in the DTG curve. A similar behaviour was observed by Morishige *et al.* [23] who reported two distinct peaks around 240°C and 300°C in their graphical differentiation spectra of the TG curves for chemisorbed water desorption and assigned both peaks to surface hydroxyls. From 300°C onwards, the weight loss of the sample is very small and both the TG and DTG curves are almost horizontal to the temperature axis (Fig.3.1.15), proving the stability of the spinel phase.

The TG curve for sulphated NiFe_2O_4 (Fig.3.1.16) also starts with an initial sharp weight loss. But, here, it occurs in a sharper manner and over a wider range (from room temperature to about 130°C). This is accounted for by the loss of physisorbed water as well as loss of ammonia out of the decomposition of ammonium sulphate, the sulphating agent. Here the dehydration is delayed to a higher temperature and occurs in the range 280 - 350°C , the dip in the DTG curve being centred at 320°C . This can be explained by accepting the fact that sulphation delays transformation from amorphous to crystalline phase. Both the TG and DTG curves are almost horizontal from about 400 to 700°C proving the thermal stability of

the sulphated phase. But a new weight loss develops from 700°C and continues up to 800°C. This should be due to the decomposition of the sulphate into SO₃/SO₂ vapours. Similar weight loss for sulphated metal oxides have been observed by Saur *et al.* [9], who noticed a weight loss between 650 to 720°C for sulphated titania and between 650 to 800°C for sulphated alumina. The samples after calcination to such high temperatures did not give IR bands for sulphate, proving the loss of sulphate by decomposition [9].

3.1.6 MOSSBAUER SPECTRA

The room temperature Mossbauer spectra of the simple ferros spinels of Co, Ni and Cu and the mixed ferros spinels, Ni_{0.5}Cu_{0.5}Fe₂O₄ and Co_{0.5}Cu_{0.5}Fe₂O₄, calcined at 300°C are given in Fig 3.1.17 (a to e). The important Mossbauer parameters are summarised in Table 3.1.7

Table 3.1.7 Mossbauer Parameters of Ferros spinel samples.

System*	Isomer shift w.r.t. natural Fe (± 0.02 mm/s)	ΔE_Q (± 0.02 mm/s)	Line width (FWHM) (± 0.02 mm/s)
NiFe ₂ O ₄	0.34	0.60	0.58
CuFe ₂ O ₄	0.34	0.74	0.56
Ni _{0.5} Cu _{0.5} Fe ₂ O ₄	0.36	0.84	0.81
Co _{0.5} Cu _{0.5} Fe ₂ O ₄	0.35	0.70	0.54

* Activation temperature : 300 ° C

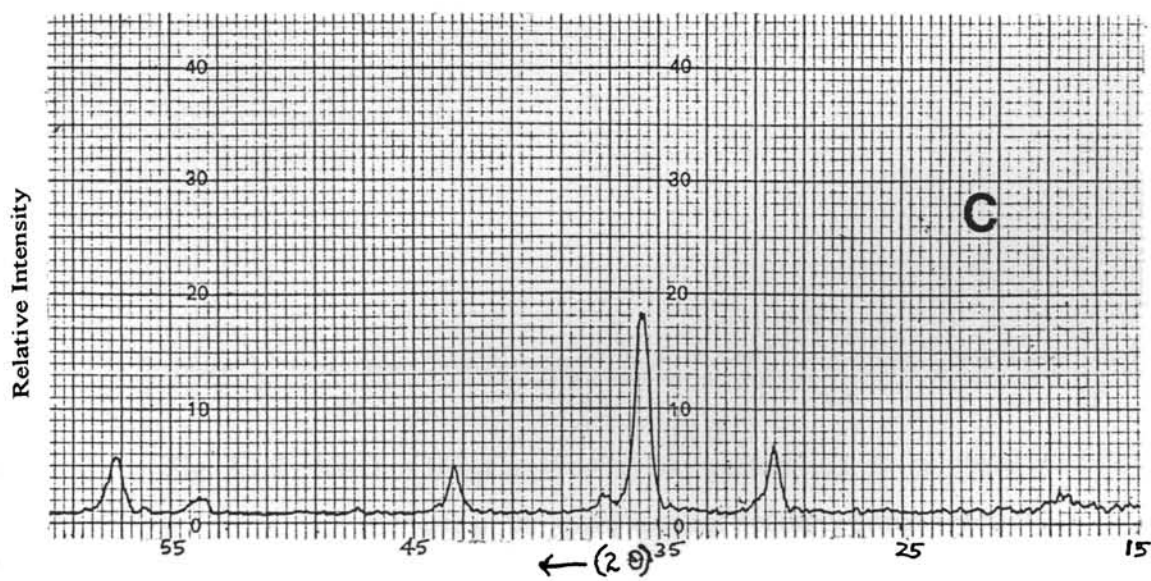
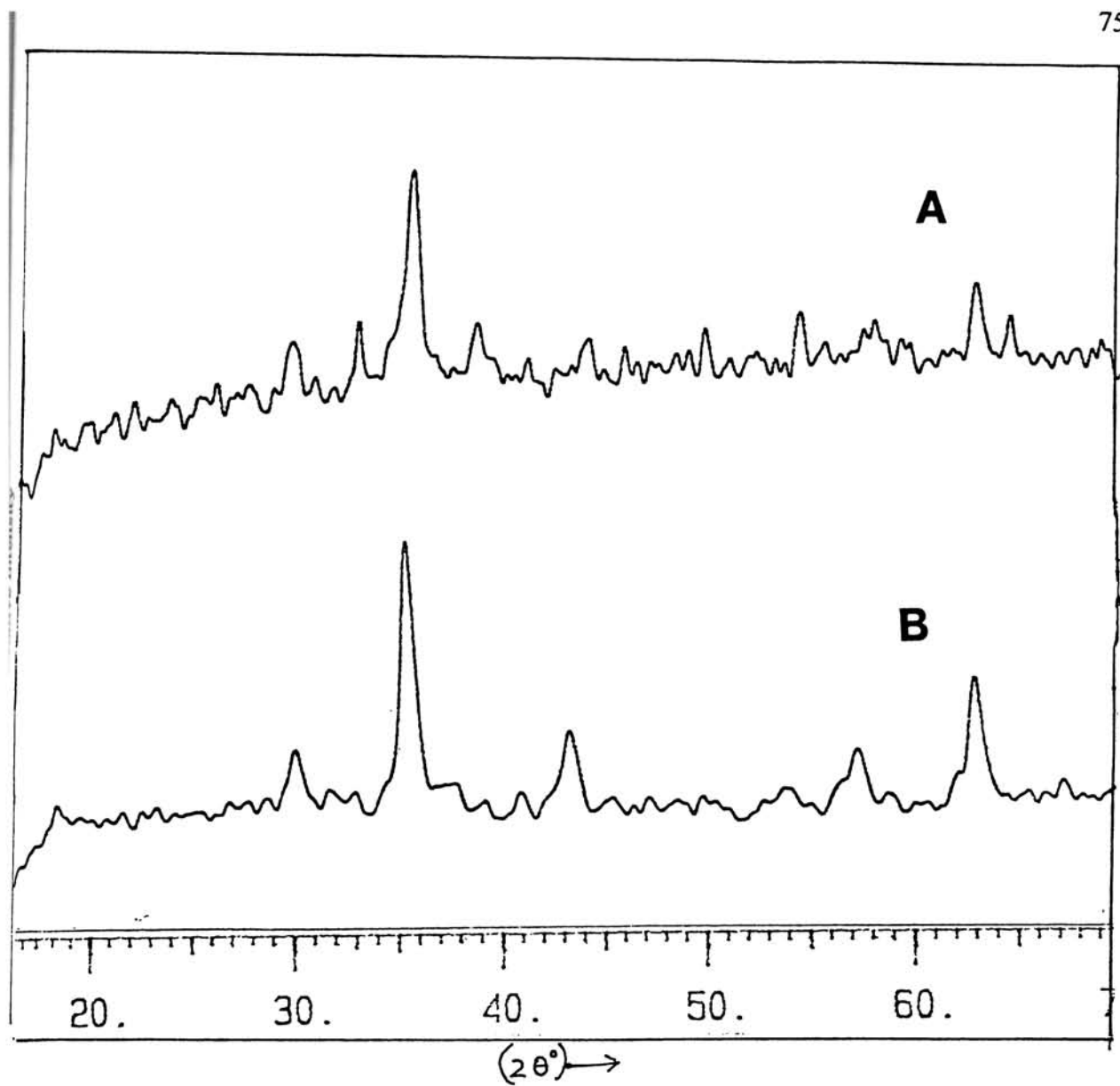


Fig. 3.1.1 XRD of simple ferrites:- A. CuFe_2O_4 B. NiFe_2O_4 C. CoFe_2O_4

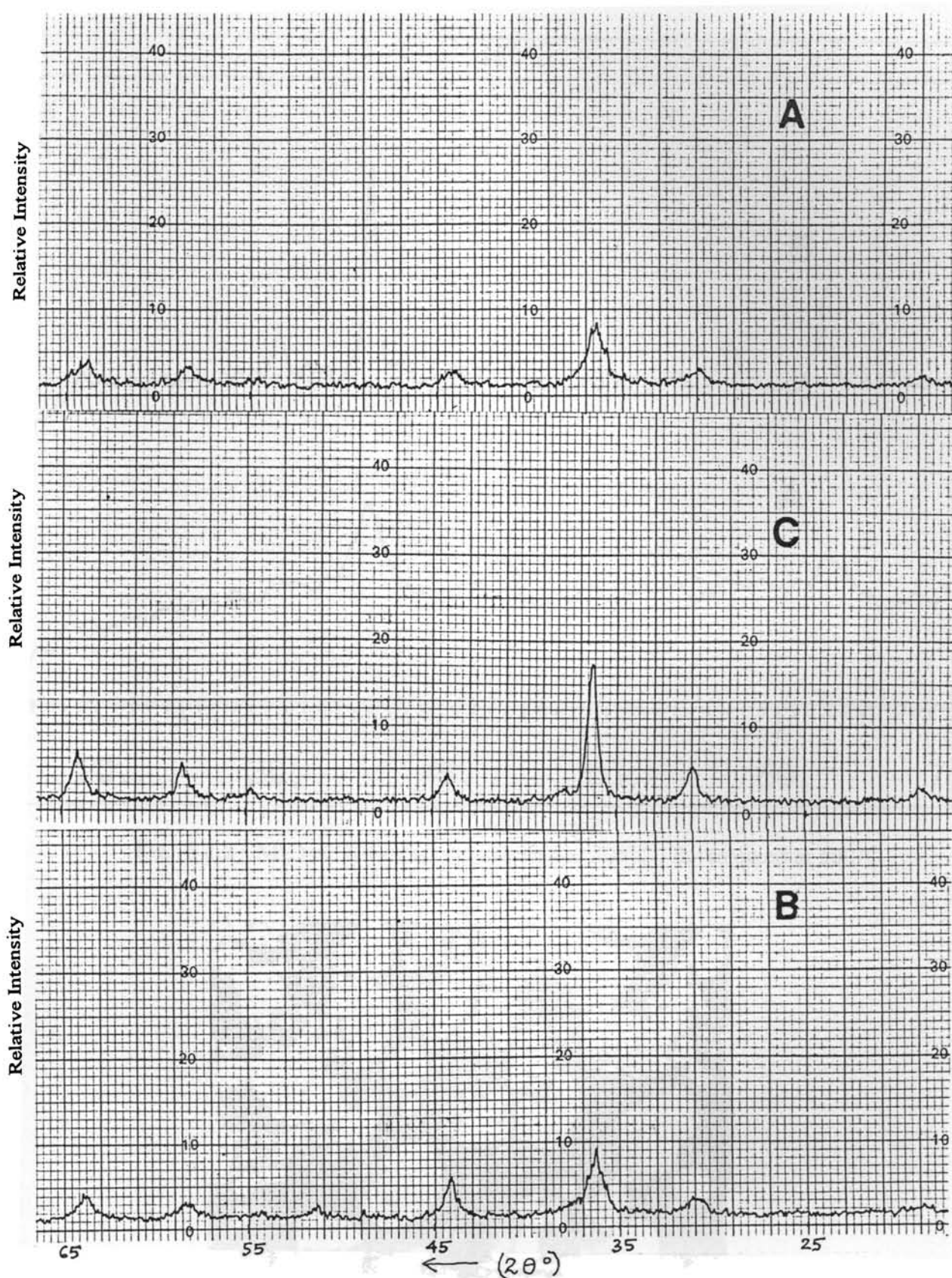


Fig. 3.1.2 XRD of $\text{Ni}_{0.3}\text{Cu}_{0.7}\text{Fe}_2\text{O}_4$. **A**- unmodified, **B**- sulphate-modified, **C**- after use in the cyclohexanol decomposition reaction.

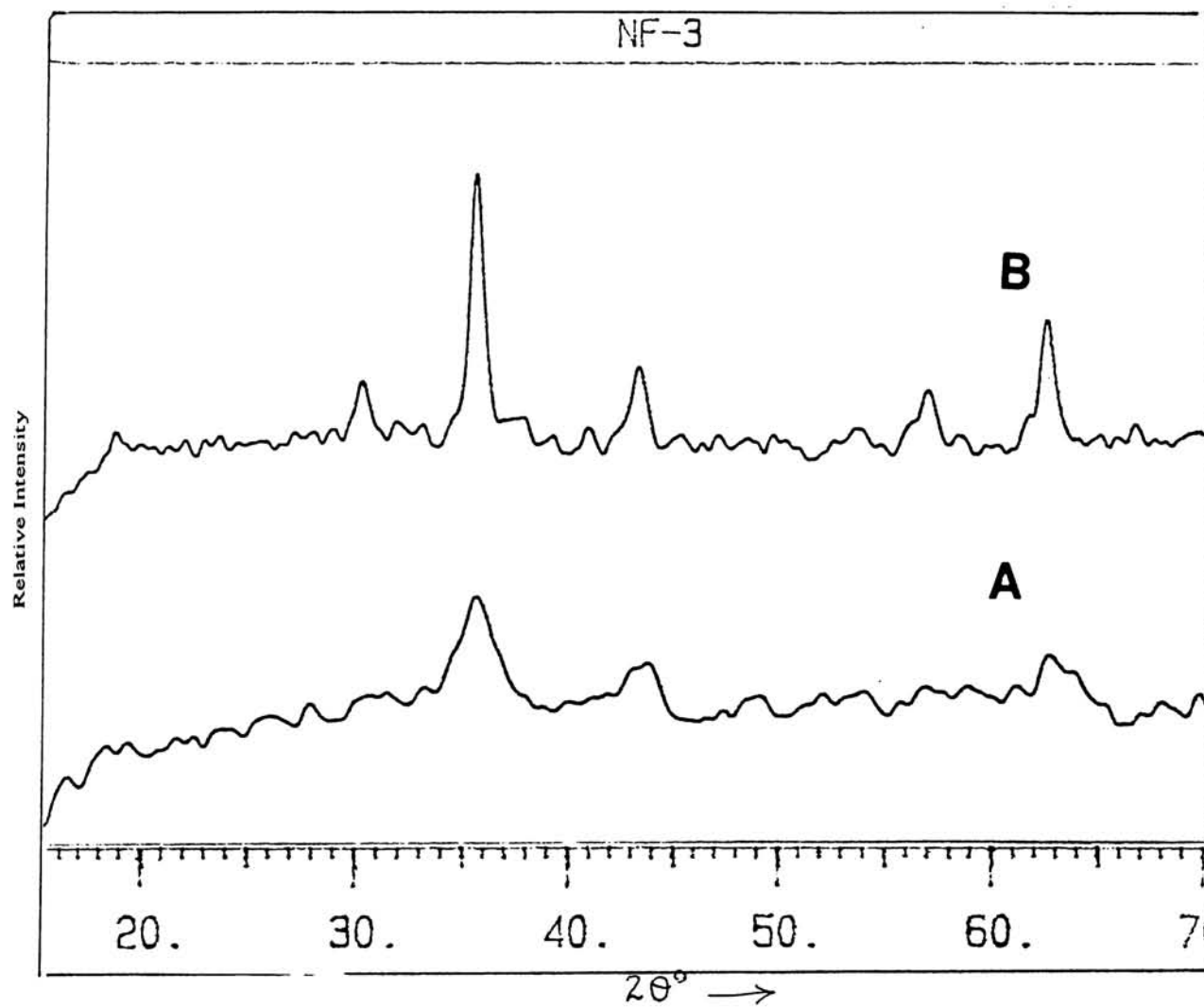


Fig. 3.1.3 XRD of NiFe_2O_4 . A. calcined at 300°C B. calcined at 500°C

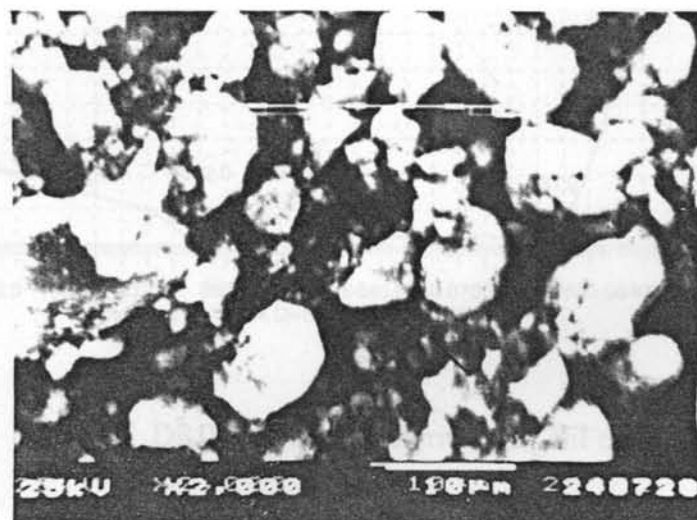


Fig. 3.1.14. Scanning Electron Micrograph (SEM) of CoFe_2O_4 calcined at 300°C

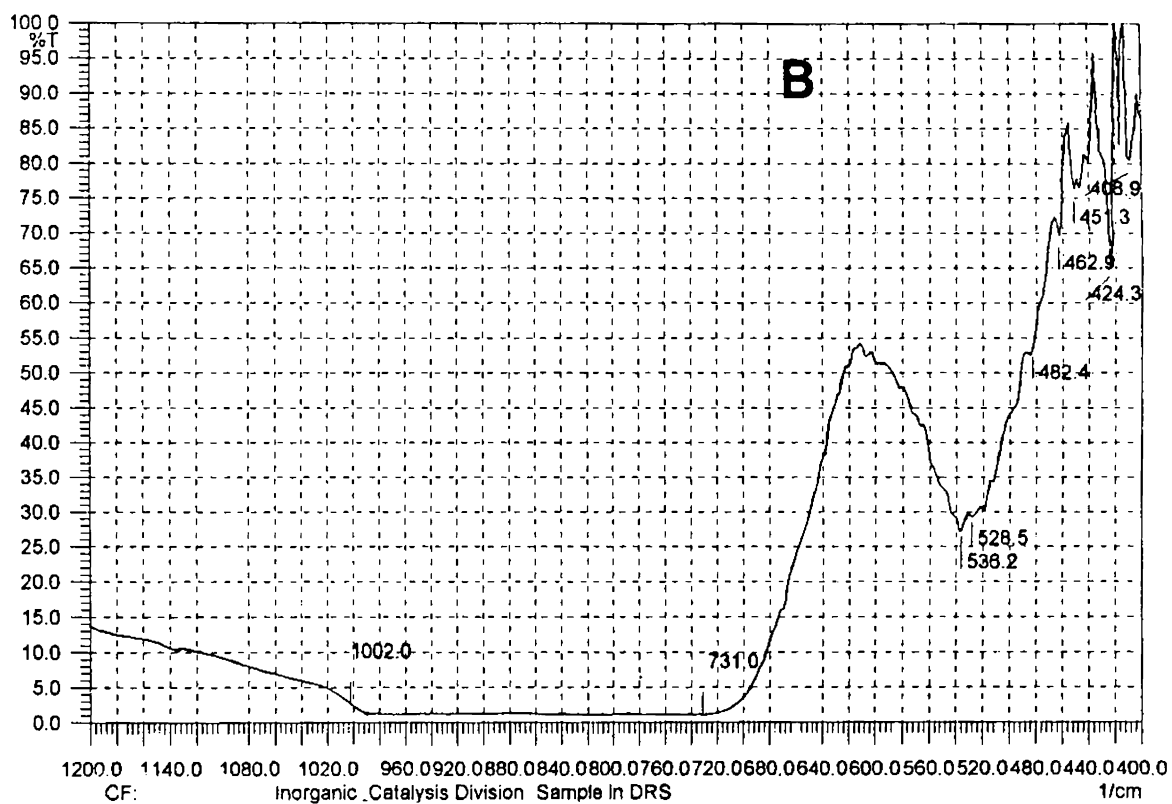
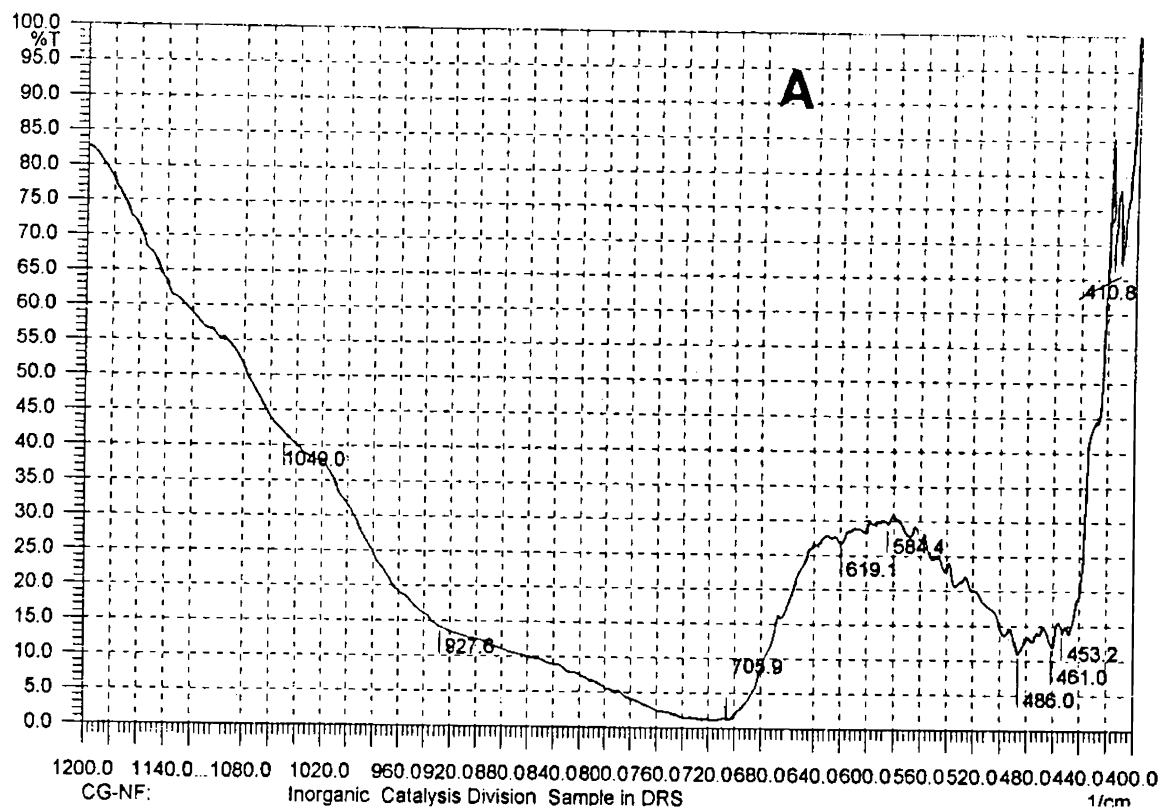


Fig. 3.1.4 DRIFT Spectra of ferrites. A: NiFe_2O_4 B: CoFe_2O_4

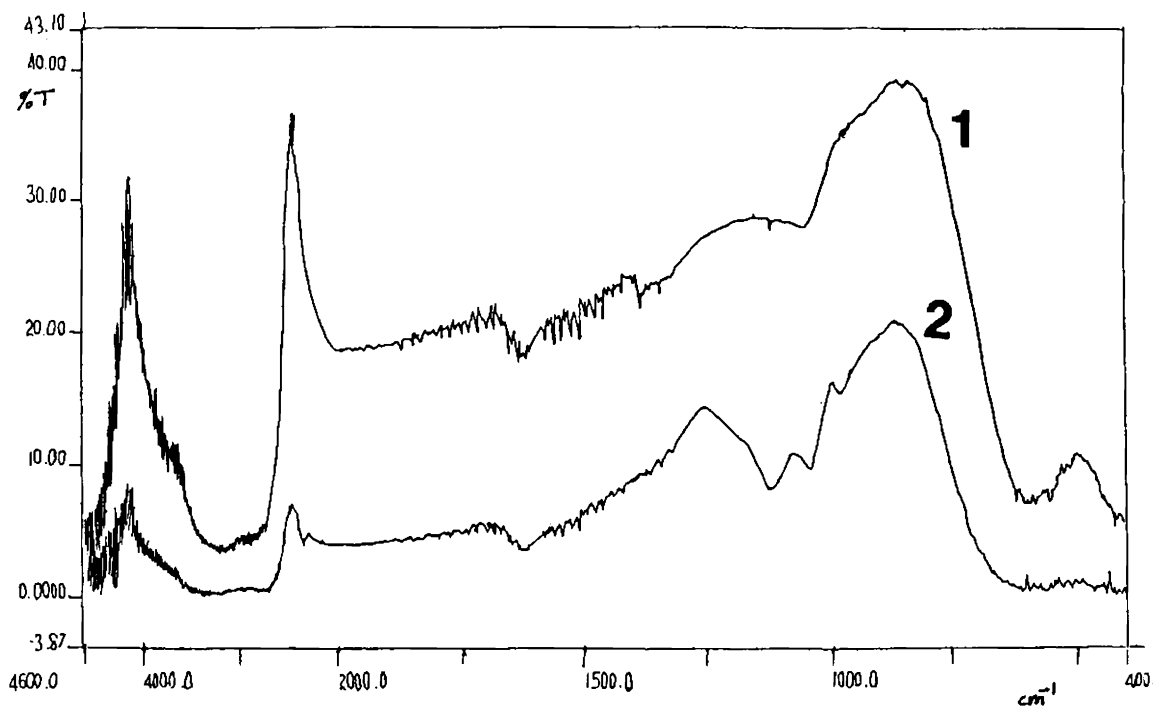


Fig. 3.1.5 FT-IR spectra of ferrites. 1. NiFe_2O_4 2. $\text{SO}_4^{2-}/\text{NiFe}_2\text{O}_4$, both calcined at 300°C

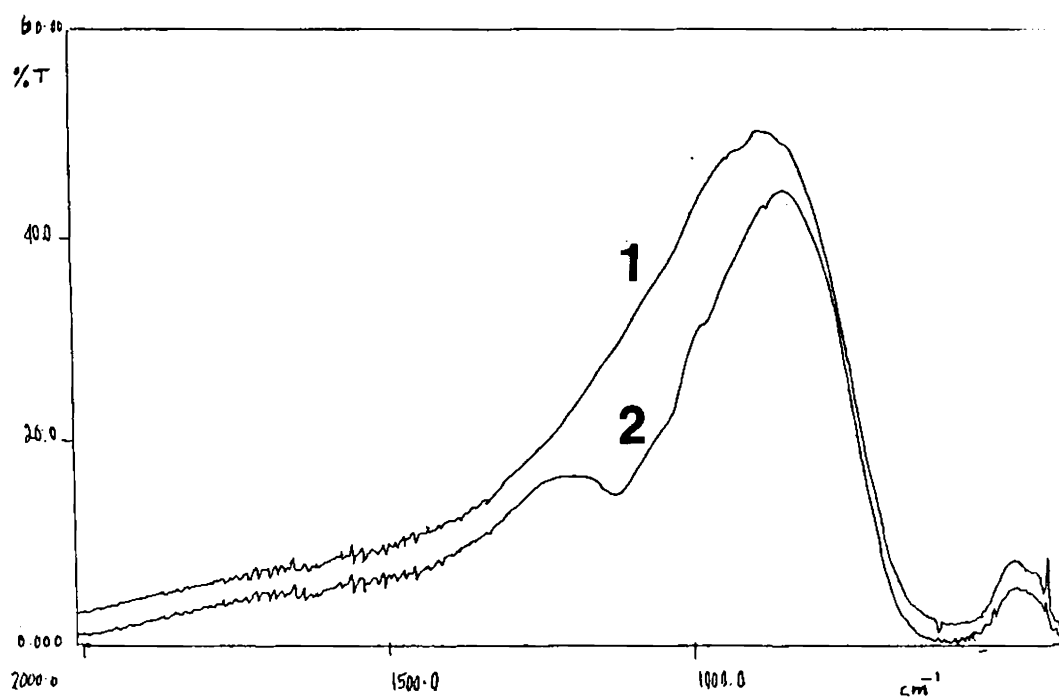


Fig. 3.1.6 FT-IR spectra of ferrites calcined at 500°C. 1. CoFe_2O_4 2. $\text{SO}_4^{2-}/\text{CoFe}_2\text{O}_4$

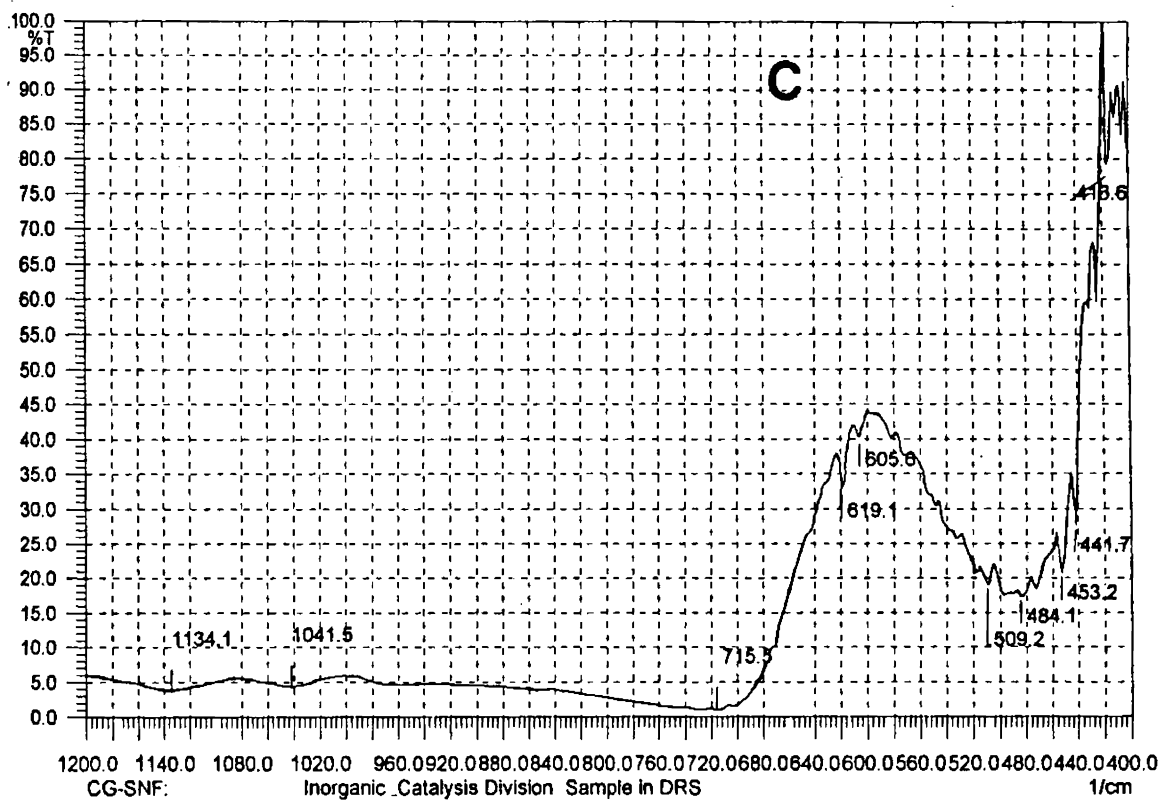


Fig. 3.1.4 DRIFT Spectra of ferrites. C: $\text{SO}_4^{2-}/\text{NiFe}_2\text{O}_4$

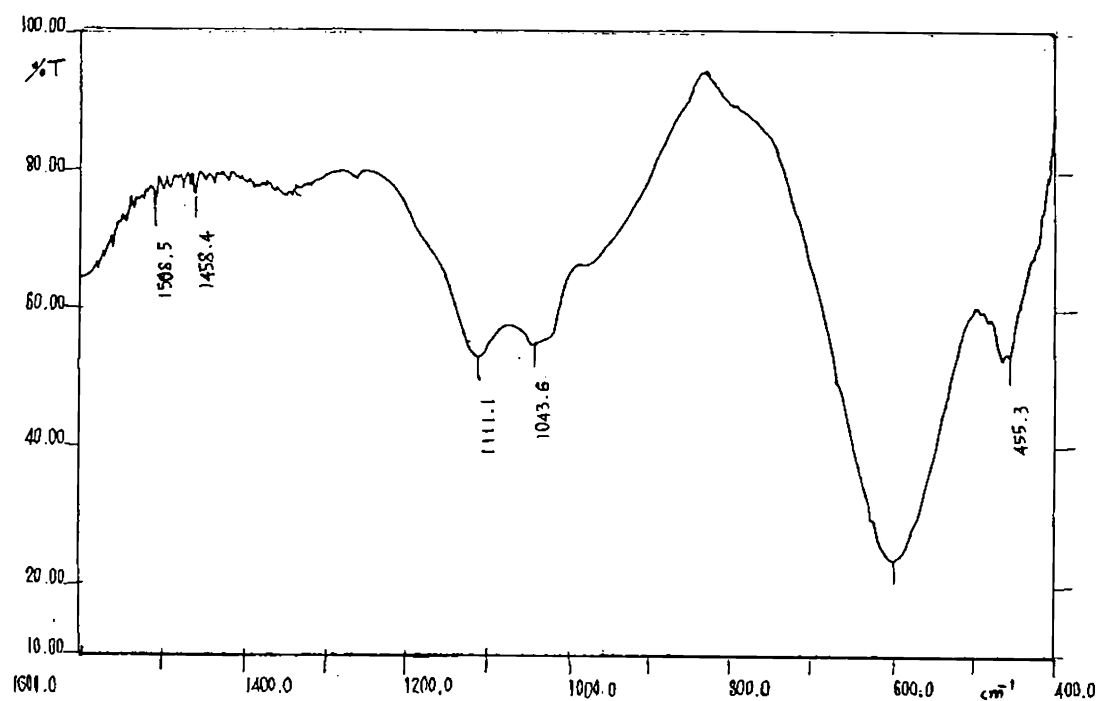
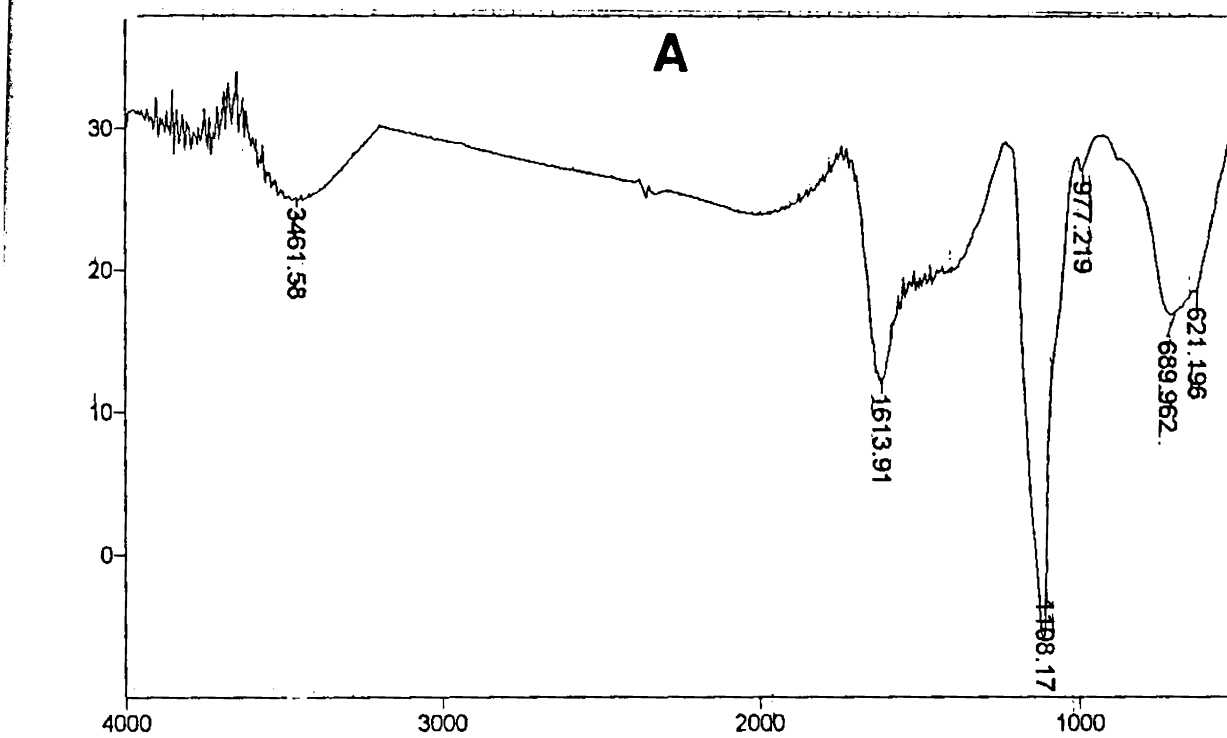
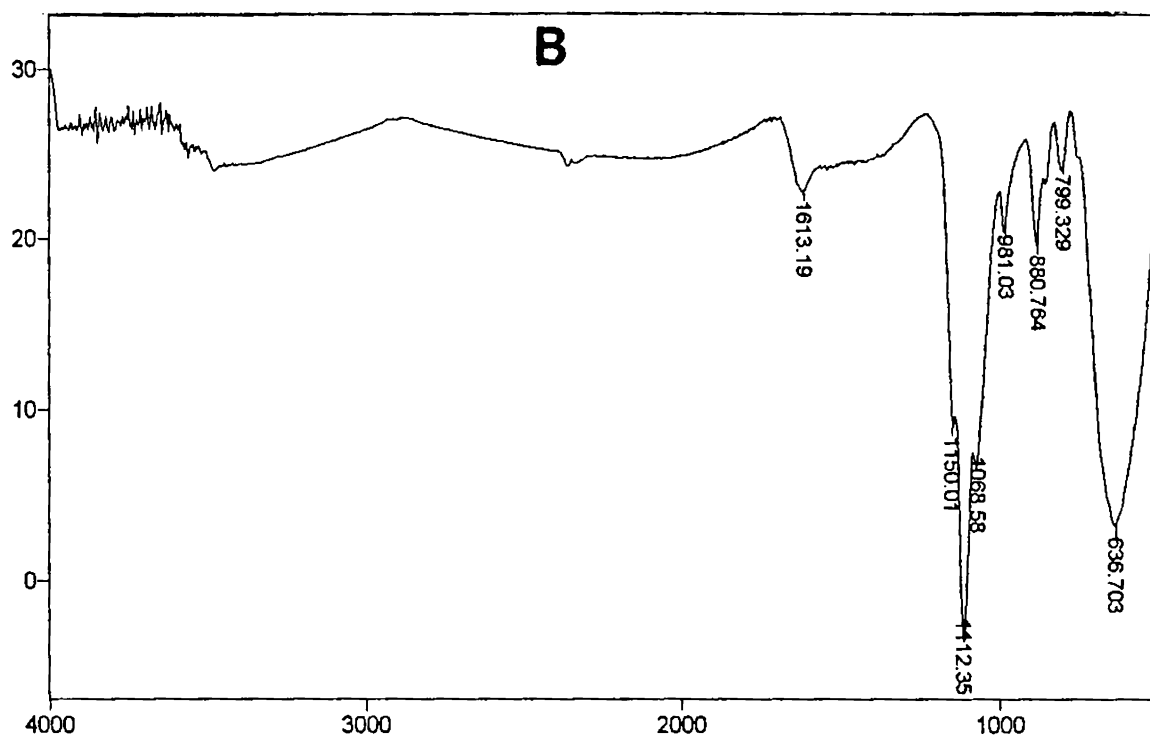


Fig. 3.1.7 FT-IR spectrum of $\text{SO}_4^{2-}/\text{Co}_{0.5}\text{Cu}_{0.5}\text{Fe}_2\text{O}_4$ calcined at 300°C



Transmittance / Wavenumber (cm-1)



Transmittance / Wavenumber (cm-1)

Fig. 3.1.8 FT-IR spectra of sulphated copper ferrite calcined at **A.** 300°C
and **B.** 500°C

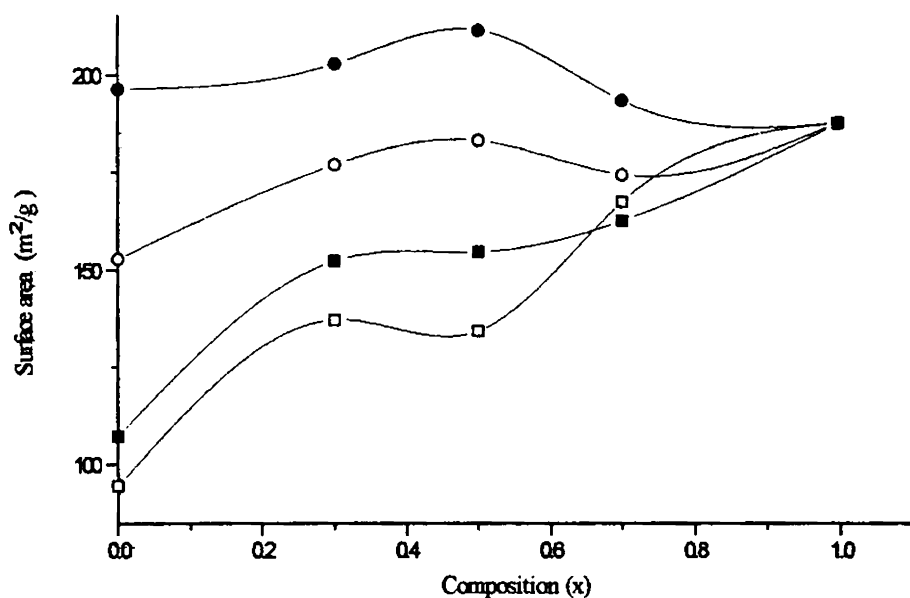


Fig. 3. 1.11 The trends in surface areas of the unmodified and sulphate modified ferrosinell systems activated at 300°C as a function of composition (x)

○ Unmodified Ni-Cu series ● Sulphate modified Ni-Cu series
 □ Unmodified Co-Cu series ■ Sulphate modified Co-Cu series

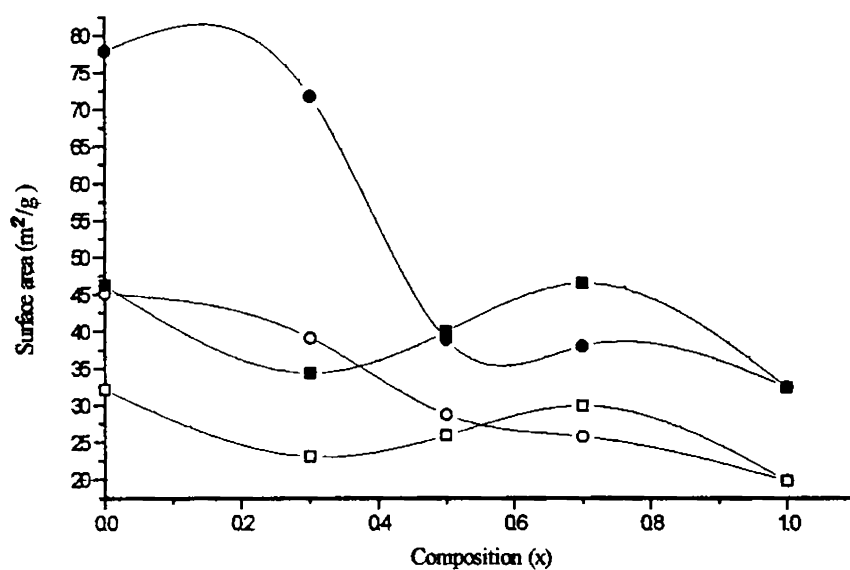


Fig 3. 1.12 The trends in surface areas of the unmodified and sulphate modified ferrosinell systems activated at 500°C, as a function of composition (x)

○ Unmodified Ni-Cu series ● Sulphate modified Ni-Cu series
 □ Unmodified Co-Cu series ■ Sulphate modified Co-Cu series

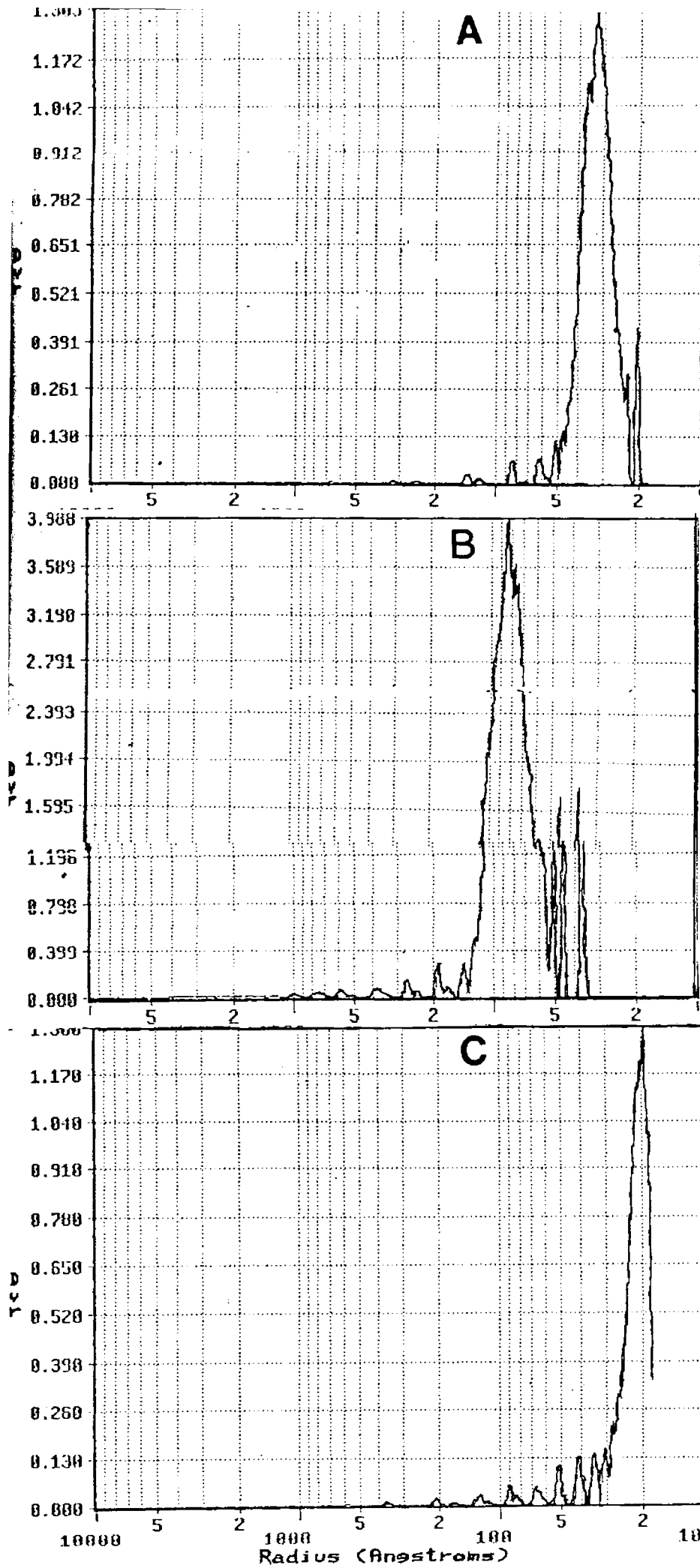
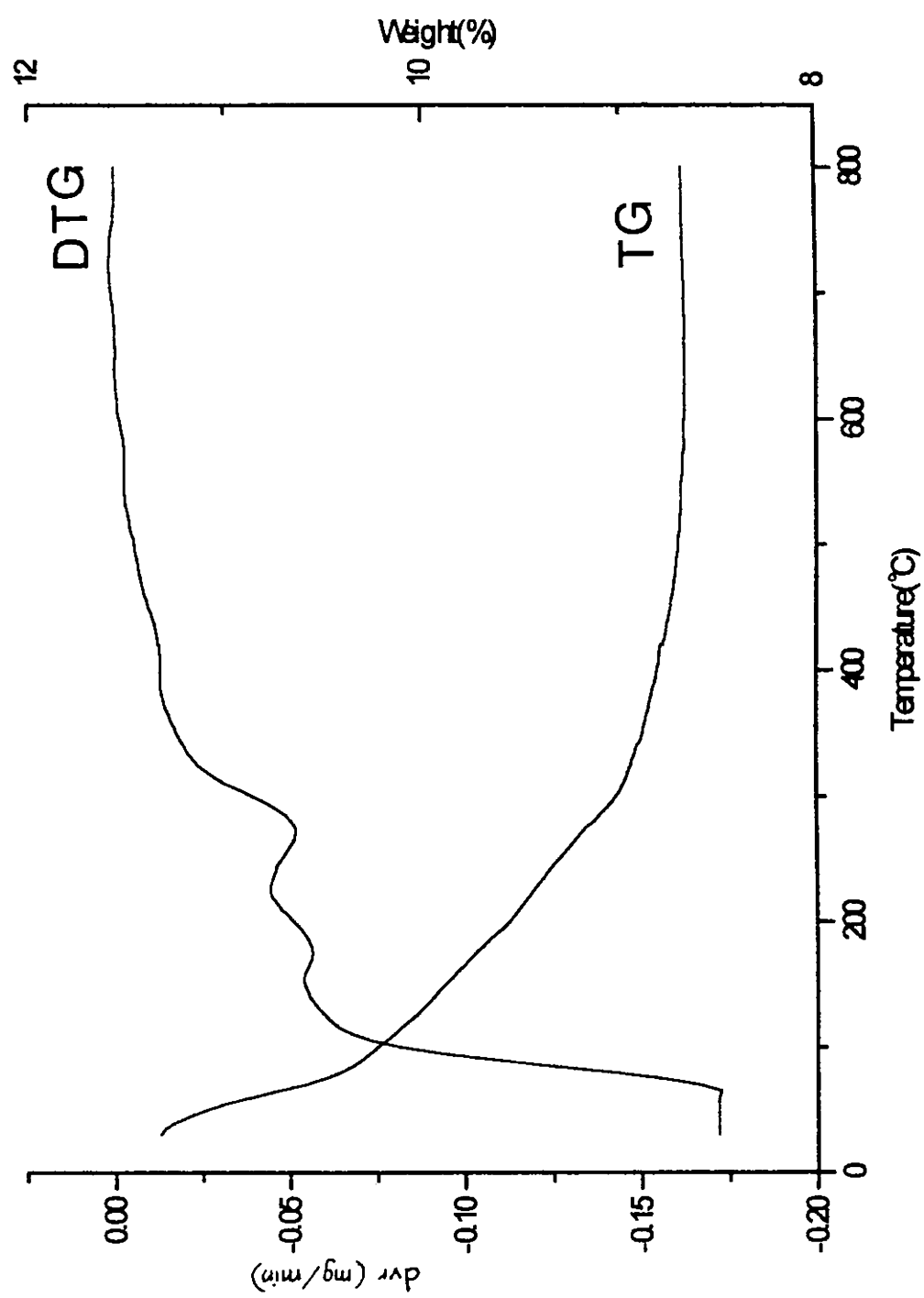


Fig. 3.1.13
 differential
 pore volume
 curves of
 A. $\text{NiFe}_2\text{O}_4(300^\circ\text{C})^*$
 B. $\text{NiFe}_2\text{O}_4(500^\circ\text{C})^*$
 C. $\text{SO}_4^{2-}/\text{NiFe}_2\text{O}_4(300^\circ\text{C})^*$
 * activation temp.

Fig. 3.1.15 TG – DTG curves of NiFe_2O_4

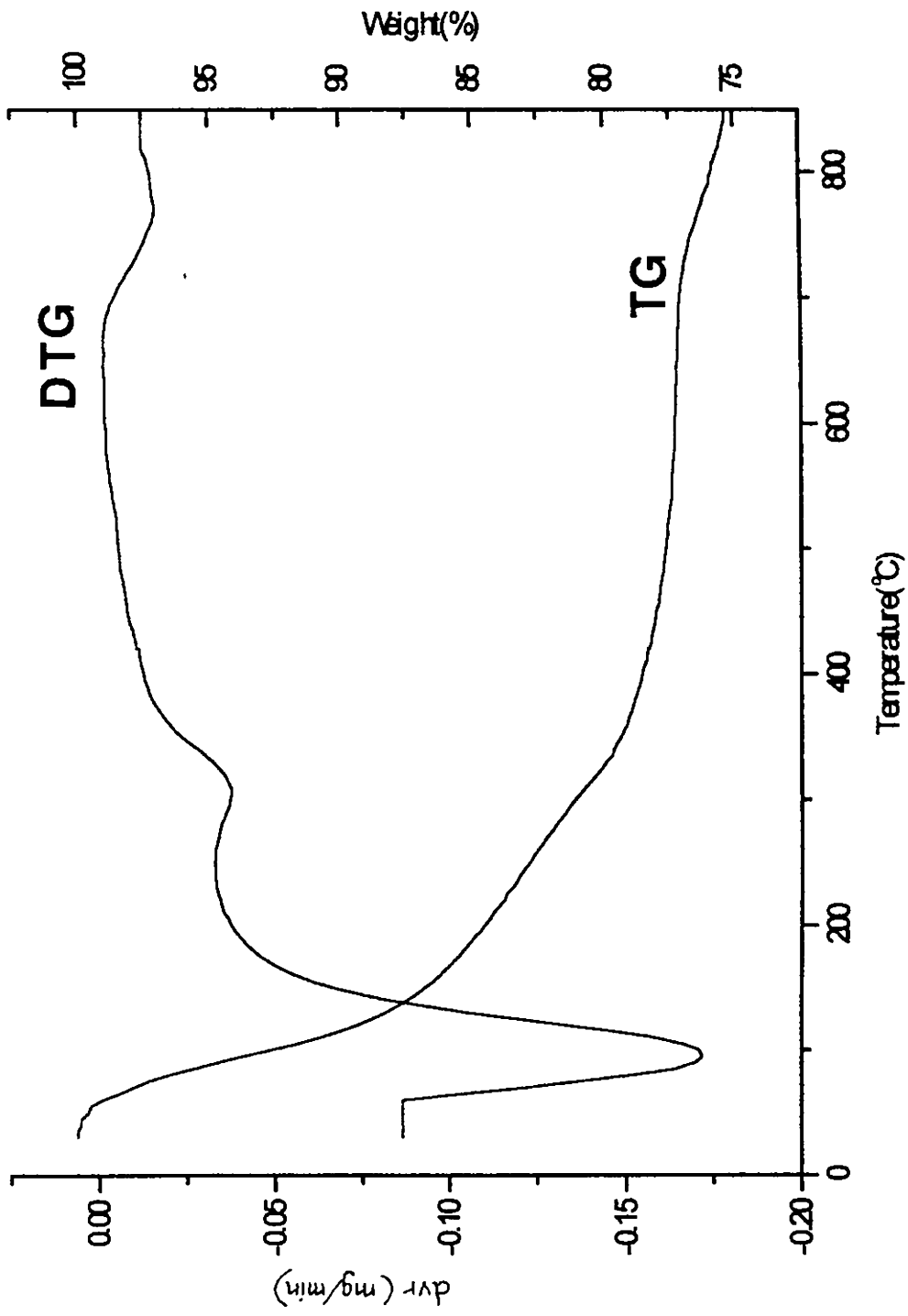


Fig. 3.1.16 TG – DTG curves of $\text{SO}_4^{2-}/\text{NiFe}_2\text{O}_4$

These parameters throw light on the oxidation state, electronic environment and magnetic properties of the iron nuclei in the ferrite samples and also on the particle size of these samples, as the following discussion shows.

All the isomer shift (I.S) values quoted in Table 3.1.7 are with respect to natural iron. Fe^{3+} ions in ferrites are d^5 systems and have zero crystal field stabilisation energy, both in tetrahedral and octahedral ligand fields due to oxygen anions. Its total spin, $S = 5/2$. The characteristic Mossbauer I.S. range for Fe^{3+} with $S = 5/2$ is within 0.2 to 0.5 mm s^{-1} with respect to natural iron [24]. There is a small but definite difference in the isomer shift values of T-site Fe^{3+} and O-site Fe^{3+} ions, the value at the T-site being about 0.08 mm s^{-1} less positive than that at O-site. This difference is attributable to a very slight sp^3 covalency, which the tetrahedral ions are known to experience. However, as the I.S values of Fe^{3+} in T- and O-sites are very close, the peaks overlap giving a single I.S. value for the iron in the ferrite samples. It is evident from the I.S. data given in Table 3.1.7, that all the iron atoms in our ferrite samples are in +3 oxidation state.

The Mossbauer spectra given in Fig 3.1.17 (a to d) are best fitted for doublets and thus show paramagnetic quadrupole patterns. The spectrum for CoFe_2O_4 (Fig. 3.1.17e) is distinct and is typical of a sample having superparamagnetic behaviour, a stage in between paramagnetic and ferrimagnetic nature. Its Mossbauer parameters are not computed.

The quadrupolar doublets prove the existence of an Electric Field Gradient (EFG) about the ^{57}Fe nuclei, which interacts with the electric quadrupole moment of the iron nuclei in the excited state. The EFG at a ^{57}Fe nucleus may arise from a non-spherical distribution of the 3d electrons of the ion itself and/or from the charges on neighbouring ions. However, since Fe^{3+} has a half-filled 3d shell, the EFG arises only from the neighbouring ions and thus exists only at those sites having non-cubic point symmetry. In the inverse spinel systems presently studied, the tetrahedral or A sites have no chemical disorder and thus experience no EFG. But the octahedral or B sites develop an EFG along the [111] zone direction, not only due to the chemical disorder from the surrounding metal cations but also from the oxygen ions. This is

because, the size of the tetrahedral ions in the small A sites causes an outward push and hence displacement of the four surrounding oxygen anions along the [111] directions. The cubic symmetry (T_d) of the A sites is maintained, but the cubic symmetry of the neighbouring octahedron (O_h) of oxygen anions around the B sites becomes distorted and changes to trigonal symmetry (D_{3d}), changing the trigonal component of the octahedral EFG [25]. (This is the cause of oxygen parameters greater than 0.375 for the simple ferros spinels of Co, Ni and Cu). The quadrupolar splitting constant (ΔE_Q) is a measure of the magnitude of the EFG. ΔE_Q values for the copper-containing spinels are relatively larger. This is due to an additional distortion of charge symmetry, due to Jahn-Teller distortion.

The Mossbauer line widths (expressed as FWHM) are a measure of the chemical disorder around the Mossbauer nuclei, which causes quadrupolar interaction inhomogeneity [25]. From Table 3.1.7, it is clear that high chemical disorder stays in $Ni_{0.5}Cu_{0.5}Fe_2O_4$ system. The distinct feature of the Mossbauer spectrum of $CoFe_2O_4$ (Fig 3.1.17e) can also be associated with the relaxation phenomenon.

It is well-known that the ferros spinels of Co, Ni and Cu are ferrimagnetic. However, the magnetic hyperfine splitting is missing in the spectra given in Fig. 3.1.17(a to d). This is because, the particle size in our samples is not large enough to show ferrimagnetic effects. As the grain size becomes smaller, the magnetisation direction of each particle of the ultra-fine ferrite powder fluctuates by virtue of thermal excitation energy kT and hence cannot be fixed as in large crystals. The Mossbauer transition, which takes place on a time scale of 10^{-8} s, feels an average magnetisation of zero [26,27]. For $CoFe_2O_4$ (Fig 3.1.17e), there is some emergence of a magnetic hyperfine pattern. This may be due to the sample being partially paramagnetic and partially ferrimagnetic simultaneously as some particles are too small to maintain ferrimagnetic properly while others, large enough to become ferrimagnetic. It is relevant to note here that the average particle size is the highest for $CoFe_2O_4$ among the simple ferros spinels, as from the XRD data (Table 3.1.3)

The Mossbauer spectra of CoFe_2O_4 and CuFe_2O_4 were taken, after these catalyst samples were used for the vapour-phase cyclohexanol decomposition reaction at 300°C , with a view to check whether there is any change in the particle size or in the oxidation state of iron, after the reaction. These spectra are given in Fig. 3.1.18(a&b). The characteristic 6 - line spectra (sextuplet) representing the magnetic hyperfine interaction have been obtained. This shows the inherent ferrimagnetic nature of the spinel samples, which could be manifested by the growth in particle size during the catalytic reaction. The I.S data show that iron maintains the +3 oxidation state even after the reaction. The spectra exhibit the well defined Zeeman pattern consisting of two separate 6 line patterns, one due to Fe^{3+} ions at the tetrahedral sites and the other due to the Fe^{3+} ions in the octahedral sites. As expected, when the magnetic interaction is operative, the quadrupolar interaction is very small and this explains the very small ΔE_Q values in the spectra shown in Fig. 3.1. 18 (a&b).

In a ferrimagnetic spinel, the intersublattice magnetic interaction is stronger than either of the intrasublattice interactions. The average nuclear magnetic field for Fe^{3+} ions in each of the two sublattices is proportional to the average magnetisation of the sublattice. The average normalised magnetisation (i.e. magnetisation per Fe^{3+} ion) of the tetrahedral sublattice will be smaller than that of the octahedral sublattice. This arises from the fact that each tetrahedral Fe^{3+} ion will have, on the average, one half of its intersublattice magnetic bonds with Co^{2+} or Cu^{2+} ions and the other half with Fe^{3+} ions, while every octahedral Fe^{3+} ion will have all of its intersublattice magnetic bonds with Fe^{3+} ions [25]. This explains why the sextet due to the tetrahedral Fe^{3+} ions is less widely split compared to that due to octahedral Fe^{3+} ions. (Fig.3.1.18).

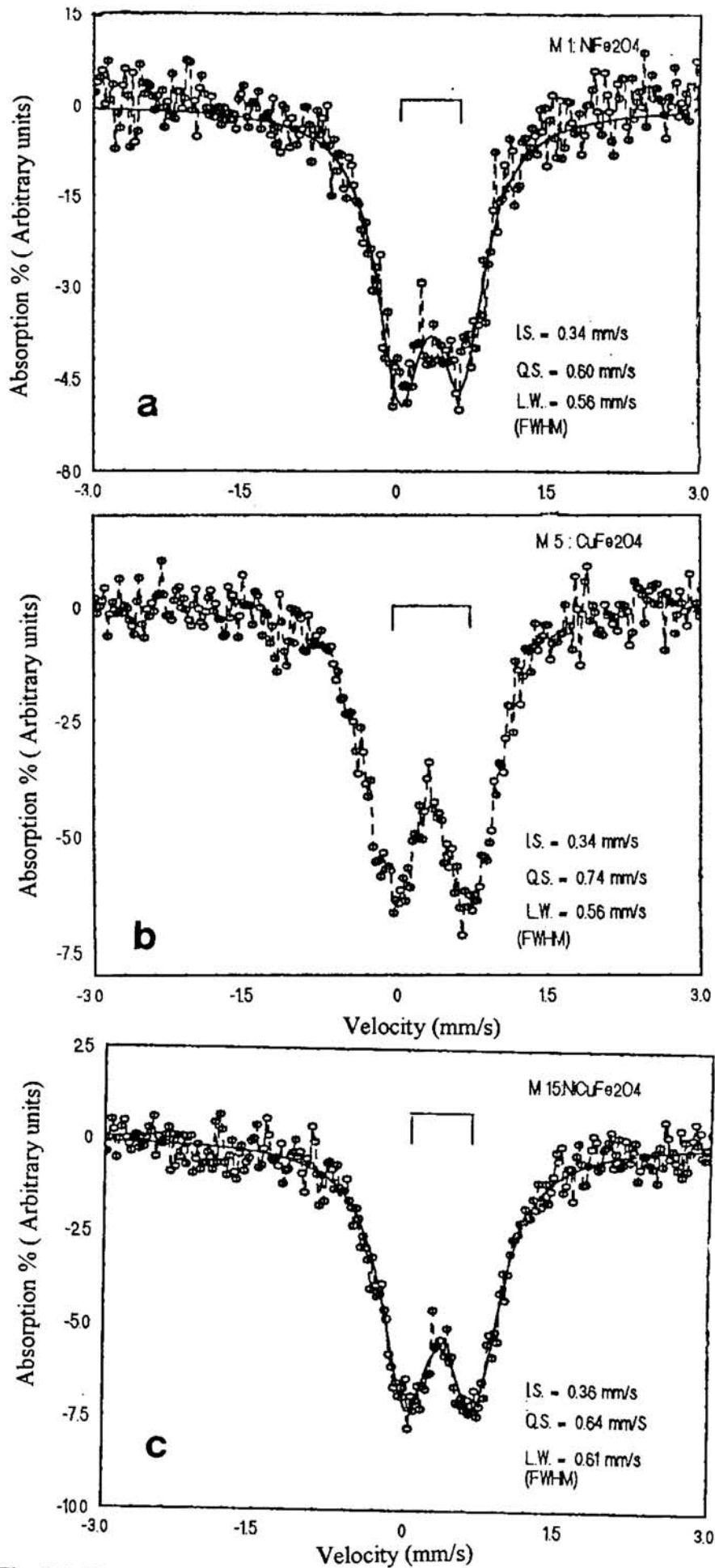


Fig. 3.1.17 Room temperature Mossbauer Spectra of spinel ferrites calcined at 300°C

a. NiFe_2O_4 b. CuFe_2O_4 c. $\text{Ni}_{0.5}\text{Cu}_{0.5}\text{Fe}_2\text{O}_4$

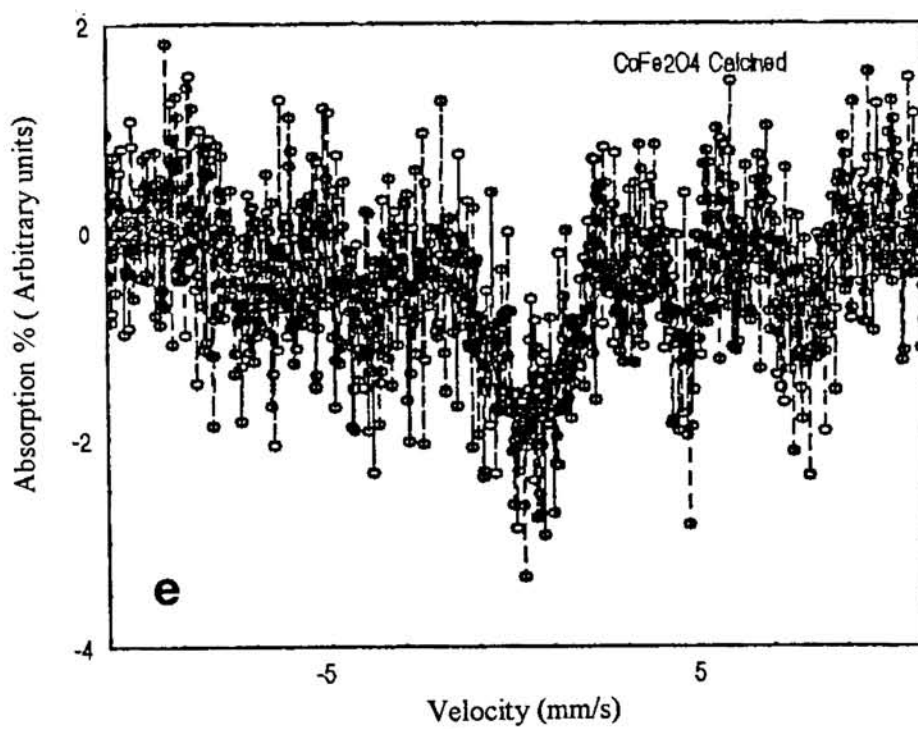
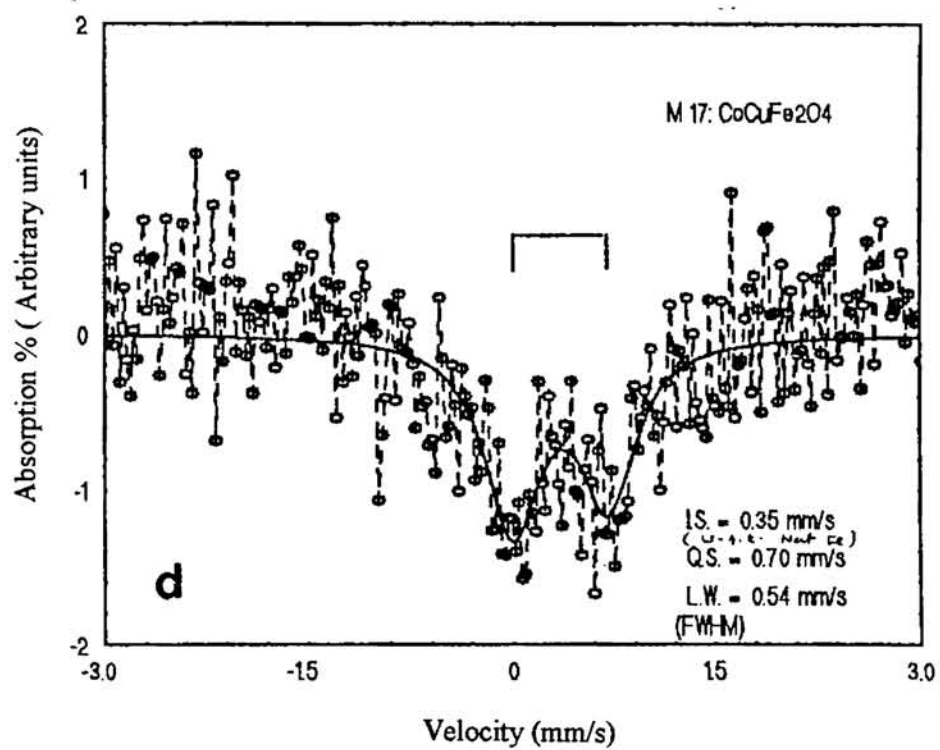
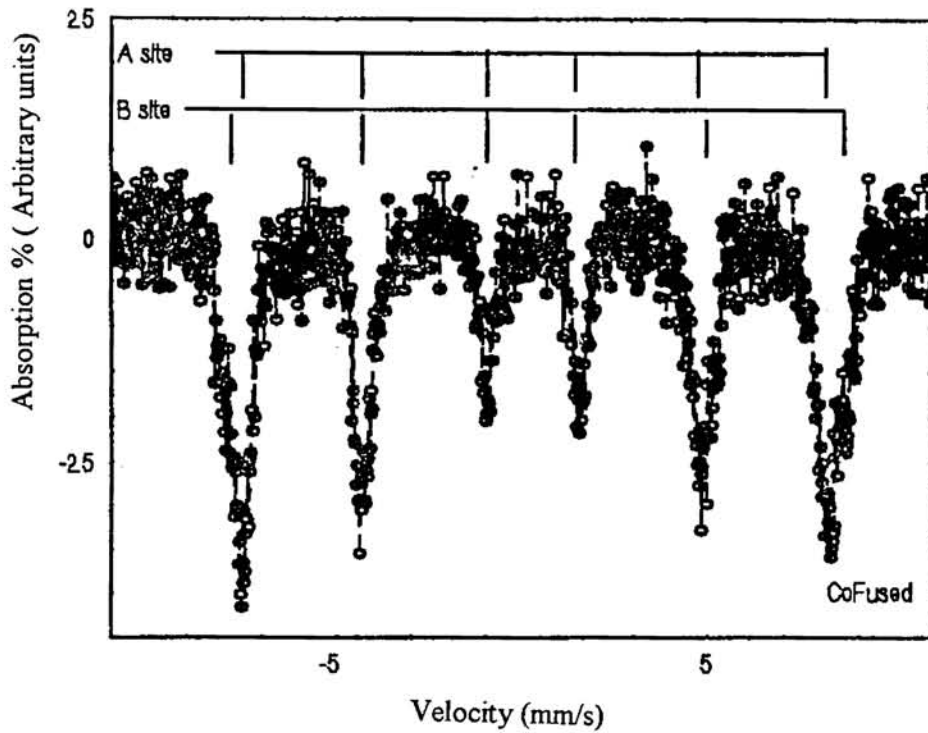
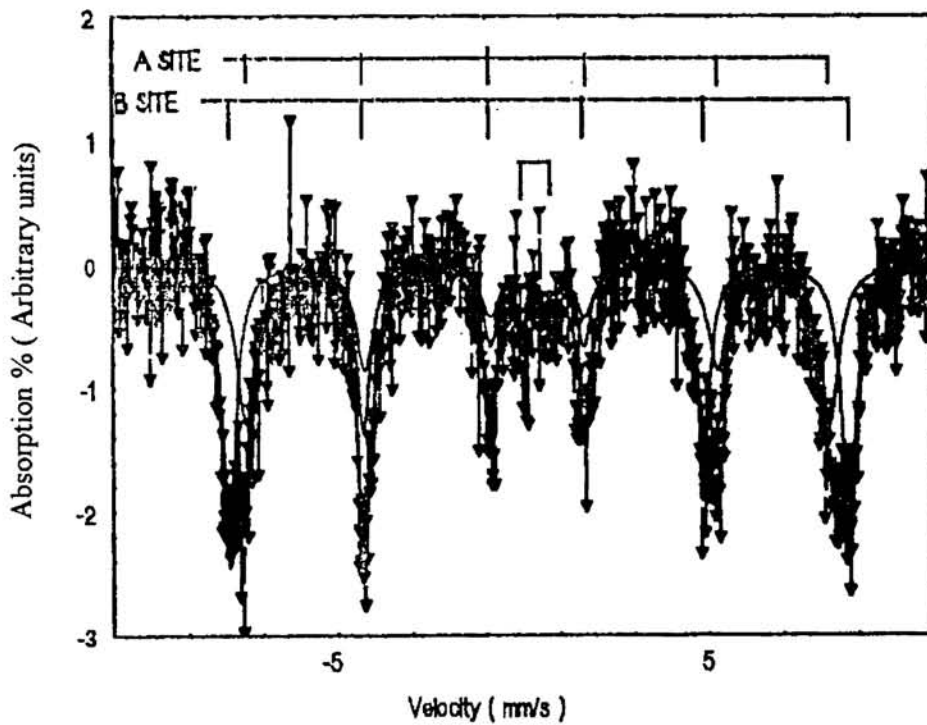


Fig. 3.1.17 Room temperature Mossbauer Spectra of spinel ferrites calcined at 300°C
d. $\text{Co}_{0.5}\text{Cu}_{0.5}\text{Fe}_2\text{O}_4$ e. CoFe_2O_4



a



b

Fig. 3.1.18 The Mossbauer spectra showing magnetic hyperfine patterns.

a. CoFe_2O_4 b. CuFe_2O_4

sample	site	I.S (± 0.02 mm/s)	Q.S (± 0.02 mm/s)	H_{Ni} (± 5 kOe)
(a) CoFe_2O_4	A site	0.06	0.03	485
	B site	0.41	0.02	510
(b) CuFe_2O_4	A site	0.18	-0.06	484
	B site	0.34	0.05	514

(central doublet negligibly small)

3.2 SURFACE PROPERTIES - ACIDITY/BASICITY

Surface acid-base properties of solids play an important role in determining their catalytic activities and selectivities in reactions. These surface properties vary with the composition of the catalytic system. Since all the catalyst systems in the present study have inverse spinel structure, the tetrahedral composition always remains the same and the change in composition (varying 'x' values) essentially represents the change in the composition of cations occupying the octahedral sites. Jacobs *et al.* [28], using low-energy ion scattering (LEIS) analysis, showed that the octahedral sites are exposed almost exclusively at the surface of the spinel oxide powders and that the catalytic performance is related only to the composition of the octahedral sites. In our samples, the octahedral cations are among Ni^{2+} , Co^{2+} , Cu^{2+} and Fe^{3+} and hence the relative acido-basic properties of these cations seem to be relevant during the discussion of the same properties of the ferrosinels systems. At the same time, the heterogeneity among the octahedral cations makes the situation qualitatively unpredictable from the independent properties of the parent oxides, also.

For the determination of the basicity of the systems, adsorption studies of electron acceptors of different electron affinity values were performed. To determine the surface acidity, two independent methods were adopted – (i) gravimetric adsorption of n-butylamine vapours followed by TGA and (ii) dehydration selectivity of cyclohexanol decomposition reaction.

3.2.1 Surface Electron Donating Properties (Evaluation of Lewis basicity)

Investigation of the strength and distribution of electron donor (ED) sites on oxide surface using electron acceptors (EA) having different electron affinity values has been well-established. The limiting amount of EA adsorbed depends on two factors: (i) the distribution of donor sites of different strengths on the surface and (ii) the electron affinity of the electron acceptor adsorbed. Thus a comparison of the limiting amount of EA adsorbed and the electron affinity values of the respective EA used, yields valuable information's regarding the strength and distribution of the ED sites. So, here we have attempted, by EA adsorption studies, to establish the ED

properties of the ferros spinel samples and the variation of these properties with the composition of the spinel samples.

The EA used for the adsorption studies are given in Table 3.2.1

Table 3.2.1. List of electron acceptors used for the adsorption study and their electron affinity values.

Electron Acceptors used (EA)	Electron Affinity values (eV)
7,7,8,8-tetracyanoquinodimethane (TCNQ)	2.84
2,3,5,6-tetrachloro-p-benzoquinone (Chloranil)	2.40
p-dinitrobenzene (PDNB)	1.77

Adsorption experiments were performed for all the catalyst samples activated at 300°C and, for a few catalyst samples, after activation at 500°C. All samples were activated for 3 hours prior to adsorption studies. The limiting amount of EA adsorbed is expressed in the unit of mmol m^{-2} of the oxide surface. The adsorption was found to be of Langmuir type. This was verified by using the linear form of Langmuir adsorption isotherm by plotting (equilibrium concentration/amount adsorbed) vs. equilibrium concentration. The limiting amount has been estimated from the Langmuir plot where amount of EA adsorbed (in mmol m^{-2}) is plotted against equilibrium concentration (in mmol dm^{-3}) of the EA in solution. These plots are shown in figures, Fig 3.2.1 to Fig 3.2.9. One of the linear Langmuir plots is given in Fig 3.2.10. Acetonitrile has been used as a solvent for adsorption studies.

The limiting amounts of TCNQ and chloranil adsorbed on the various catalytic systems are given in Table 3.2.2 and Table 3.2.3. Table 3.2.3 also gives the difference in the limiting amounts between TCNQ and chloranil. The adsorption of PDNB was so negligible that the amount adsorbed was hardly estimated.

Table 3.2.2 Adsorption data of TCNQ – Limiting amounts adsorbed

Catalyst series	A or x	Limiting amount(10^{-4} mmol/m ²)	Limiting amount(10^{-4} mmol/m ²)
		Act. Temperature:300° C	Act. Temperature:500° C
Simple ferros spinels			
i) AFe ₂ O ₄	Ni	18.3	29.9
	Co	19.0	28.6
	Cu	18.0	40.4
ii) SO ₄ ²⁻ / AFe ₂ O ₄	Ni	8.9	
	Co	5.7	*
	Cu	9.3	
Mixed ferros spinels			
i) Ni _{1-x} Cu _x Fe ₂ O ₄	0.3	16.7	32.4
	0.5	18.8	24.0
	0.7	18.0	28.0
ii) SO ₄ ²⁻ / Ni _{1-x} Cu _x Fe ₂ O ₄	0.3	9.9	
	0.5	8.6	*
	0.7	8.4	
iii) Co _{1-x} Cu _x Fe ₂ O ₄	0.3	19.2	24.3
	0.5	19.8	36.9
	0.7	16.6	34.3
iv) SO ₄ ²⁻ / Co _{1-x} Cu _x Fe ₂ O ₄	0.3	9.2	
	0.5	8.1	*
	0.7	9.2	

* Too low adsorption to be measured accurately

Table 3.2.3 Adsorption data – Limiting amounts of chloranil and (TCNQ – Chloranil) adsorbed at the activation temperature of 300°C

Catalyst series	A or x	Limiting amount (10^{-4} mmol/m ²)	
		Chloranil	TCNQ-Chloranil
Simple ferros spinels			
i) AFe ₂ O ₄	Ni	4.4	13.9
	Co	4.6	14.4
	Cu	6.7	11.3
ii) SO ₄ ²⁻ / AFe ₂ O ₄	Ni	3.0	5.9
	Co	1.0	4.7
	Cu	3.4	5.9
Mixed ferros spinels			
i) Ni _{1-x} Cu _x Fe ₂ O ₄	0.3	6.0	10.7
	0.5	6.2	12.6
	0.7	6.5	11.5
ii) SO ₄ ²⁻ / Ni _{1-x} Cu _x Fe ₂ O ₄	0.3	2.3	7.6
	0.5	1.5	7.1
	0.7	2.8	5.6
iii) Co _{1-x} Cu _x Fe ₂ O ₄	0.3	5.2	14.0
	0.5	6.0	13.8
	0.7	6.1	10.5
iv) SO ₄ ²⁻ / Co _{1-x} Cu _x Fe ₂ O ₄	0.3	1.1	8.1
	0.5	0.7	7.4
	0.7	0.9	8.3

The limiting amount of EA adsorbed is higher for TCNQ than for chloranil. Since TCNQ is a strong electron acceptor (electron affinity value 2.84 eV), it forms anion radicals on both strong and weak donor sites. In other words, the limiting amount of TCNQ adsorbed gives a measure of strong as well as weak donor sites on the catalyst surface. But, chloranil (electron affinity value 2.40 eV) can accept electrons from strong and moderately strong donor sites.

Negligible adsorption of PDNB in all systems indicates absence of very strong electron donor sites. This suggests that adsorption sites on the ferrosipinel systems act as electron donors to the EA molecule with electron affinity values less than 2.40 eV but greater than 1.77 eV. Accordingly the limit of electron transfer from ED sites of ferrosipinels to the EA molecule is located between 2.40 and 1.77 eV.

The difference between limiting amounts of TCNQ and Chloranil adsorbed can give an idea of the number of weak donor sites. From the data in tables 3.2.2 and 3.2.3 two aspects are clearly evident: (i) the increase in activation temperature results in an increase in the intrinsic basicity of the unmodified ferrosipinel samples and (ii) sulphation causes a drastic decrease in the surface basicity of all the samples. A critical survey of the adsorption data leads us to draw the following conclusions regarding the ED or Lewis basic sites of the catalyst samples.

(i) Simple ferrosipinel series

The limiting amount of chloranil adsorbed gives a measure of moderately strong and strong basic sites whereas the difference between the limiting amounts of TCNQ and chloranil adsorbed, represents a measure of weak basic sites. From the data on the limiting amount of EA adsorbed, the distribution of strength and order of basicity of oxides activated at 300°C follow the pattern:

Moderately strong and strong basic sites – $\text{CuFe}_2\text{O}_4 > \text{CoFe}_2\text{O}_4 \cong \text{NiFe}_2\text{O}_4$

Weak basic sites – $\text{CoFe}_2\text{O}_4 \cong \text{NiFe}_2\text{O}_4 > \text{CuFe}_2\text{O}_4$

Thus CuFe_2O_4 has the highest proportion of strong basic sites and lowest proportion of weak basic sites together. In other words, the basic sites in CuFe_2O_4 are mainly of the medium strong to strong type only. Sulphation affects both the weak and strong basic sites almost evenly and reduces these by nearly half in the case of

NiFe_2O_4 and CuFe_2O_4 and by nearly one fourth, in the case of CoFe_2O_4 . Sulphating agents being acidic preferentially attack at the basic sites converting these to acidic sites. The intrinsic basicities are higher at higher activation temperature as evident from the limiting amount values of TCNQ adsorbed at 500°C . The order of basicity at 500°C is $\text{CuFe}_2\text{O}_4 > \text{NiFe}_2\text{O}_4 \cong \text{CoFe}_2\text{O}_4$. The total basicity is the highest for CoFe_2O_4 among the simple ferrites and for $\text{Co-Cu}(x=0.5)$ -ferrite among the mixed ones, at the activation temperature of 300°C . But, at the activation temperature of 500°C , CuFe_2O_4 and $\text{Co-Cu}(x=0.5)$ ferrite rank as the most basic ones.

Determination of acidic and basic sites on solid surfaces is a multifaceted problem and unfortunately there exists no general theory of the acidity or basicity of the solids that could serve as a basis for their determination. Transition metal oxides are generally categorised as acidic oxides although basic sites too exist on these. Taking both Lewis and Brønsted definitions of acids and bases into account, it can be stated that all bases are essentially of Lewis character while acids can be of Lewis or Brønsted types [29].

Ferrospinel have both Lewis and Brønsted acid sites and Lewis basic sites. Electron donor sites can come from electrons trapped in intrinsic defects or from surface hydroxyl groups [30] or from coordinatively unsaturated oxide ion ($\text{O}_{\text{cus}}^{2-}$) associated with a neighbouring hydroxyl group [31]. Trapped electrons in intrinsic defects correspond to n-type semiconductors and are created at higher activation temperatures. At 300°C the basic sites are mainly due to surface hydroxyl groups. The surface hydroxyl groups on a given catalyst can vary in their electron donating properties and this amounts to distribution of basic strengths [30]

It will be interesting to analyse, in this context, the order of acidity/basicity among the octahedral cations of these ferrospinel on the basis of the usual theoretical parameters like charge to radius ratio, electronegativity etc. of the cations. It is the generally accepted notion that a greater degree of covalency of the oxide, originating from a higher charge to radius ratio of the metallic ion, gives a more acidic oxide. Conversely, a more ionic oxide originating from a lower charge to

radius ratio will be more basic. From the crystal radii given by Shannon [32], the charge to radius ratios of the cations Cu^{2+} , Ni^{2+} , Co^{2+} and Fe^{3+} in oxides have been calculated and these vary as $\text{Fe}^{3+} \gg \text{Ni}^{2+} > \text{Cu}^{2+} \cong \text{Co}^{2+}$. Thus the acidity of the oxides is expected to vary in this order and the basicity, in the reverse order. We can also expect that the acidity of a metal ion will be directly proportional to the electronegativity of the metal cation. Sanderson [33] has pointed out that the electronegativity of a metal ion (X_i) would change linearly with its charge according to, $X_i = (1+2Z) X_0$, where X_0 is the electronegativity of the neutral atom and Z is the charge of the metal ion. This parameter X_i may be regarded as a semiempirical acidity parameter of the metal ion. Using Pauling's electronegativity values [34], the X_i values of metal ions present in our ferrosinels samples have been computed and these vary as $\text{Fe}^{3+} \gg \text{Cu}^{2+} > \text{Ni}^{2+} \cong \text{Co}^{2+}$. Thus acidity varies in this order and basicity, in the reverse order. Based on the acidity parameters proposed by Smith [35], the acidity of the present transition metal oxides varies in the order $\text{Fe}_2\text{O}_3 \gg \text{NiO} > \text{CuO} \cong \text{CoO}$ and the basicity order is its reverse. By all the theoretical arguments, Fe^{3+} is the most acidic(least basic) while the order of acidity/basicity among Cu^{2+} , Co^{2+} and Ni^{2+} does not always correlate. This is due to the fact that the acido-basic properties of these ions are close to one another. However, our results from electron donor studies regarding the medium strong to strong basic sites are in fair agreement with these theoretical predictions. Again, one cannot expect the theoretical trends of acidity/basicity of single oxides to be followed by the mixed oxide systems which the ferrosinels are, where much modifications of the acido-basic properties can occur due to the mixing. On the assumption that moderately strong to strong basic sites are more important during base catalysed reactions, we can presume that the CuFe_2O_4 will be more effective in such reactions.

(ii) Mixed ferrosinels of Ni-Cu series

The limiting amount of chloranil adsorbed shows a steady increase with copper substitution in NiFe_2O_4 suggesting that a steady increase of moderately strong to strong basic sites occurs with copper substitution. But the difference between the limiting amounts of TCNQ and chloranil adsorbed which gives a measure of weak basic sites, does not suggest any pattern with copper substitution. However the average value of weak basic sites for Ni-Cu ferrosinels is less than that

of NiFe_2O_4 . Thus the property of copper ion in ferros spinels in increasing the strong basic sites and decreasing the weak basic sites is maintained in the mixed ferros spinel series also. Sulphation reduces the number of moderately strong to strong basic sites by nearly half for $x = 0.3$ and 0.7 while, by about one fourth for $x = 0.5$. But the weak basic sites are almost evenly reduced to about half with sulphation for the various compositions. Thus the strong basic sites of $\text{Ni}_{0.5}\text{Cu}_{0.5}\text{Fe}_2\text{O}_4$ are influenced to a greater extent by sulphation compared to the other compositions. Statistically there is a greater heterogeneity among the octahedral sites when $x = 0.5$ and this may make the basic sites more susceptible for sulphation.

(iii) Mixed ferros spinels of the Co-Cu series

Here also, the limiting amount of chloranil shows a steady increase with copper substitution in the CoFe_2O_4 . The difference of the limiting amounts of TCNQ and chloranil shows a steady decrease with 'x' value. Thus the same property viz. Cu^{2+} substitution increases the number of moderately strong to strong basic sites and decreases the weak basic sites is maintained in this series of catalyst samples also. The discussion of basicity given under simple ferros spinels applies to both the mixed ferros spinel series. Sulphation drastically reduces the number of strong basic sites, here. The weak basic sites are also reduced, the reduction being less pronounced compared to that for strong basic sites. Here also, the Co-Cu spinel with $x = 0.5$ experiences a greater influence of sulphation in decreasing the number of basic sites.

For samples activated at 500°C , the basicity shows an increase. This is due to the creation of new electron donor sites at the higher temperature. Ferros spinels are generally n-type semiconductors which lose lattice oxygen on heating causing anionic vacancies. The released electrons are accommodated by the conversion of Fe^{3+} to Fe^{2+} . The n-type semiconductivity is enhanced due to Cu^{2+} substitution in the ferros spinels as the Cu^{2+} ions can also get involved in redox processes like, $\text{Cu}^{2+} + \text{e}^- \leftrightarrow \text{Cu}^+$ or even $\text{Cu}^{2+} + 2\text{e}^- \leftrightarrow \text{Cu}$. The presence of free electrons in defect sites causes an increased basicity and this increase is found to be the highest for CuFe_2O_4 . For the mixed ferros spinel series, the limiting amounts of TCNQ at 500°C activation do not show any regular trend with composition; but the values are always much higher than those at 300°C activation.

Another contributing factor to the creation of anion vacancies in the copper – containing ferros spinels is the special co-ordination of Cu^{2+} ions on the surface described as (4+2) coordination [36] where the two oxygen anion ligands are rather loosely held due to Jahn – Teller distortion. Anion vacancy defects at the higher temperature not only creates free electrons but also creates very strong Lewis acid sites due to coordinatively unsaturated cations in the octahedral sites.

3.2.2 Gravimetric adsorption of n-butylamine followed by TGA

This method of determining acidity has been used for the unmodified and sulphate-modified simple ferros spinels of Co, Ni and Cu. Catalysts which have been activated at 300°C for three hours, were kept in a desiccator saturated with n-butylamine vapours at room temperature for 48 hours. These were then subjected to thermogravimetric analysis and the percentage weight loss per unit surface area were computed in three temperature ranges viz. $150\text{--}300$, $301\text{--}450$ and $451\text{--}600^\circ\text{C}$ which were considered to be measures of weak, medium and strong acid sites respectively. These data are given in Table 3.2.4. The following conclusions can be drawn from these data.

The total intrinsic acidity of the simple ferros spinels varies in the order $\text{Co} > \text{Ni} > \text{Cu}$. Among the sulphate-modified analogues, the order of total acidity is $\text{Co} > \text{Cu} > \text{Ni}$. The distribution of the strength of acid sites is rather wide for CoFe_2O_4 , the sites being distributed in comparable proportions among the weak, medium and strong sites. But for NiFe_2O_4 and CuFe_2O_4 , the distribution is narrow, the weak sites being larger in number than the other sites. Sulphation shows an increase in the number of medium strong acid sites in all cases and also an increase in weak sites except for NiFe_2O_4 . The number of strong acid sites is maximum for CoFe_2O_4 . Sulphation slightly reduces the number of strong acid sites for NiFe_2O_4 and CoFe_2O_4 while leaves that of CuFe_2O_4 almost unchanged. Acidic properties of oxides originate from surface hydroxyl groups (Brønsted acidity) and overexposed metal cations (Lewis acidity). For activation temperatures of above 500°C , most of the Brønsted sites might have disappeared. Transition metal oxides are primarily redox

catalysts and the acido-basic properties are only of secondary importance. Hence much less work has been done on investigating the acid-base properties of transition metal oxides. Both acidic and basic sites exist on transition metal oxides. But these are generally classed as acidic oxides or the A-type oxides as described by Auroux *et al.* [37]. For a mixed oxide like ferrosinell, the acido-basic properties can be very decisive in determining their catalytic activities. Usually, the weak and medium strong acid sites have a high proportion of Brønsted type while the strong acid sites are mainly of the Lewis type.

Table 3.2.4. Data of acidity measurement by gravimetric adsorption of n-butylamine

Systems (activated at 300 °C)	% weight loss (10 ⁻² m ⁻²)			
	Weak (150-300 °C)	Medium (300-450 °C)	Strong (450-600 °C)	Total (150-600 °C)
Ni Fe ₂ O ₄	3.09	1.33	0.66	5.08
Co Fe ₂ O ₄	2.58	1.40	1.15	5.13
Cu Fe ₂ O ₄	3.25	0.63	0.40	4.23
SO ₄ ²⁻ / Ni Fe ₂ O ₄	2.46	1.92	0.55	4.93
SO ₄ ²⁻ / Co Fe ₂ O ₄	6.08	2.54	0.87	9.50
SO ₄ ²⁻ / Cu Fe ₂ O ₄	4.80	2.22	0.38	7.40

3.2.3 Dehydration Selectivity in Cyclohexanol decomposition reaction

The vapour-phase cyclohexanol decomposition reaction has been done as a test reaction to determine the functionality of the catalyst samples. From the dehydration activities of this reaction, we have been planning to assess the acidity,

especially the Brønsted acidity of the catalyst samples as a function of their composition. The results are discussed in Chapter V. However, the conclusions drawn regarding the acidities of the samples are relevant to be reproduced here.

From the dehydration rate constants (Table 5.1.1), it is clear that the acidities of the simple ferros spinels vary in the order $\text{Co} > \text{Ni} > \text{Cu}$ while those of the sulphated analogues follow the order $\text{Co} > \text{Cu} > \text{Ni}$. Exactly the same trends have been obtained by n-butylamine adsorption studies described earlier. But the dehydration activity of CuFe_2O_4 is too low to be caused by low Brønsted acidity alone. This feature of very low dehydration activity (or the complementary very high dehydrogenation activity) prevails throughout the mixed ferros spinel samples containing copper. But the sulphated samples of the same always show high dehydration activities suggesting increase of Brønsted acidic sites by sulphation. The trends in dehydration activity among the mixed ferros spinel series are not very impressive to suggest any correlation with composition. We propose that the redox properties of Cu^{2+} ion in copper containing ferros spinel samples become more decisive in controlling dehydration/dehydrogenation activities than their acido-basic properties. But sulphation seems to render the redox aspects somewhat dormant. Thus it is concluded that the true acidities of copper containing ferros spinel samples cannot be determined from the dehydration activities of cyclohexanol decomposition reaction.

The acidity and basicity distribution of the simple ferros spinels of Co, Ni and Cu can be analysed together by combining the relevant parts of n-butylamine adsorption data (Table 3.2.4) and limiting amount values of EA adsorbed (Table 3.2.2 & 3.2.3) into a single table and this is given in Table 3.2.5. From the data in Table 3.2.5, it is evident that a fair amount of reciprocity exists in the number of acid and basic sites of corresponding strengths among the catalyst samples. By reciprocity, we mean that, when the number of acid sites increases, the number of the basic sites of corresponding strength decreases.

Table 3.2.5 Distribution of acid and basic sites in the ferrosinels of Co, Ni and Cu at 300°C activation.

System	Acid sites (n-butylamine adsorption, % wt. loss, 10^{-2} m^{-2})		Basic sites (EA adsorption limiting amount, $10^{-4} \text{ mmol m}^{-2}$)	
	Weak	(medium + strong)	Weak	(medium + strong)
Ni Fe ₂ O ₄	3.09	1.99	13.9	4.4
Co Fe ₂ O ₄	2.58	2.55	14.4	4.6
Cu Fe ₂ O ₄	3.25	1.03	11.3	6.7
SO ₄ ²⁻ /Ni Fe ₂ O ₄	2.46	2.47	5.9	3.0
SO ₄ ²⁻ /Co Fe ₂ O ₄	6.08	3.41	4.7	1.0
SO ₄ ²⁻ /Cu Fe ₂ O ₄	4.80	2.60	5.9	3.4

For catalyst technology, the most sensitive probe of catalysts performance will continue to be the rate and selectivity of a chemical reaction. We have tested the catalyst performance of our samples for benzylation of aromatics and cyclohexanol decomposition. These are described and discussed in chapter IV and chapter V respectively.

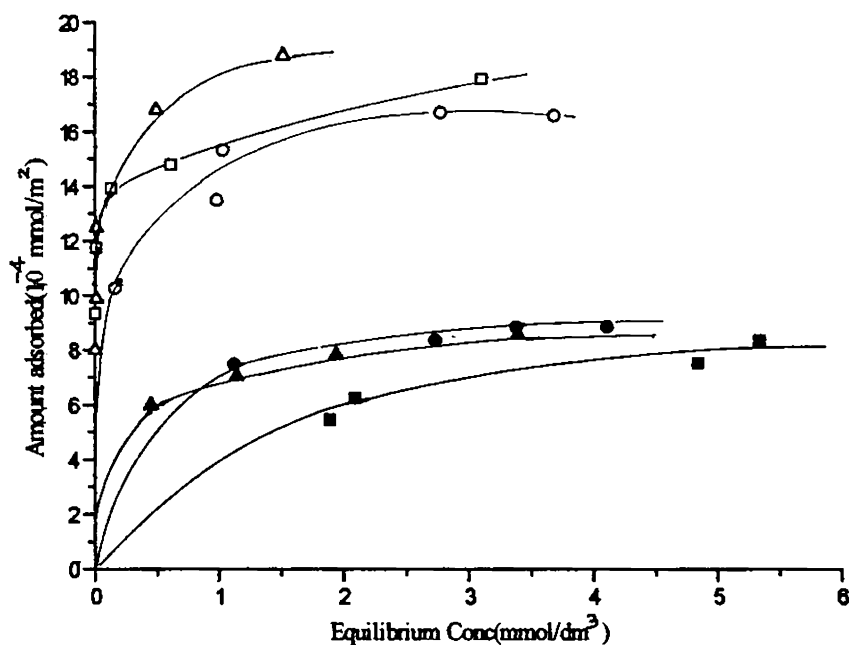


Fig.3.2. 3 Adsorption isotherms of TCNQ in acetonitrile over unmodified and sulphate modified mixed ferrosipinel systems of Ni-Cu series activated at 300°C

○ $\text{Ni}_{0.7}\text{Cu}_{0.3}\text{Fe}_2\text{O}_4$ Δ $\text{Ni}_{0.5}\text{Cu}_{0.5}\text{Fe}_2\text{O}_4$ □ $\text{Ni}_{0.3}\text{Cu}_{0.7}\text{Fe}_2\text{O}_4$
 ● $\text{SO}_4^{2-}/\text{Ni}_{0.7}\text{Cu}_{0.3}\text{Fe}_2\text{O}_4$ \blacktriangle $\text{SO}_4^{2-}/\text{Ni}_{0.5}\text{Cu}_{0.5}\text{Fe}_2\text{O}_4$ \blacksquare $\text{SO}_4^{2-}/\text{Ni}_{0.3}\text{Cu}_{0.7}\text{Fe}_2\text{O}_4$

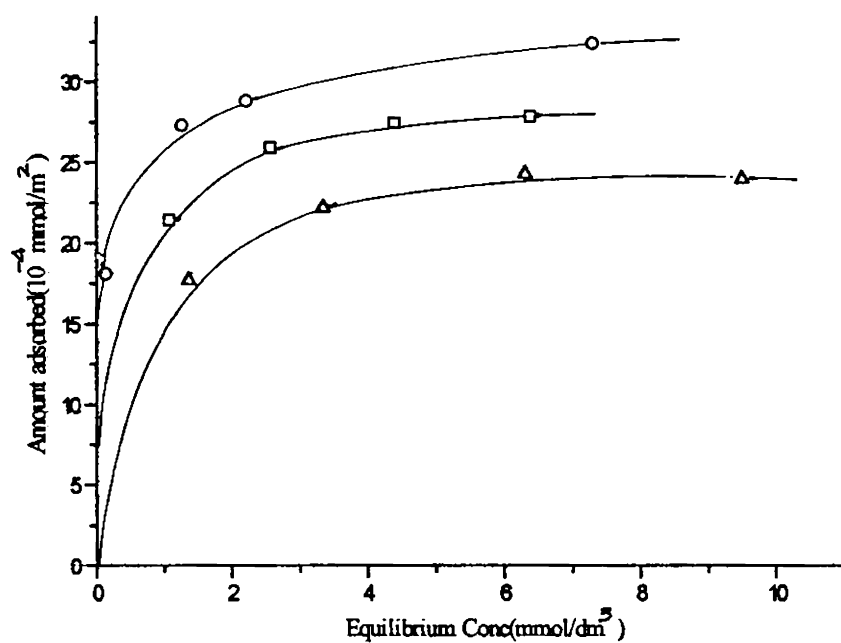


Fig.3.2. 4 Adsorption isotherms of TCNQ in acetonitrile over mixed ferrosipinel systems of Ni-Cu series activated at 500°C

○ $\text{Ni}_{0.7}\text{Cu}_{0.3}\text{Fe}_2\text{O}_4$ Δ $\text{Ni}_{0.5}\text{Cu}_{0.5}\text{Fe}_2\text{O}_4$ □ $\text{Ni}_{0.3}\text{Cu}_{0.7}\text{Fe}_2\text{O}_4$

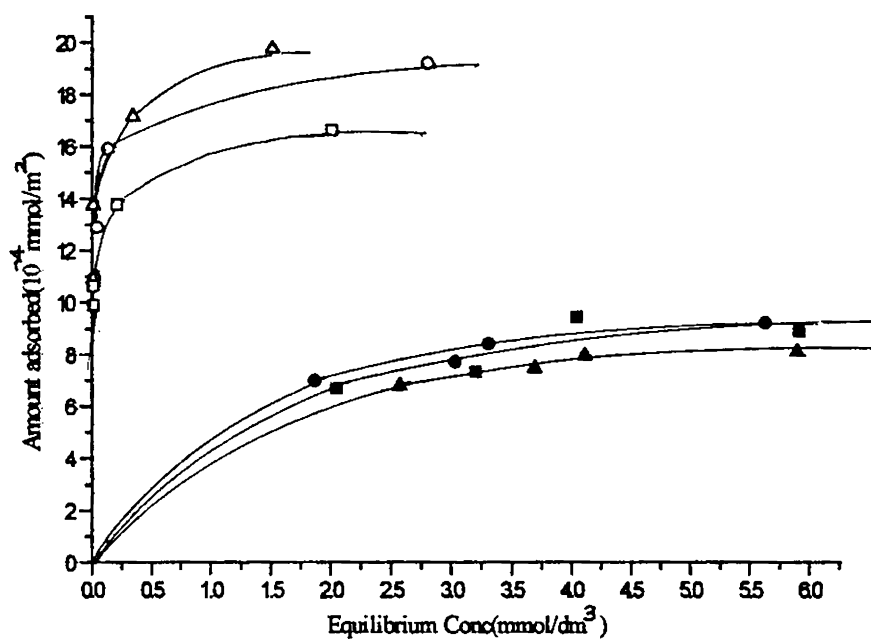


Fig.3.2. 5 Adsorption isotherms of TCNQ in acetonitrile over unmodified and sulphate modified mixed ferrosipinel systems of Co-Cu series activated at 300°C

○ Co_{0.7}Cu_{0.3}Fe₂O₄ △ Co_{0.5}Cu_{0.5}Fe₂O₄ □ Co_{0.3}Cu_{0.7}Fe₂O₄
 ● SO₄²⁻/Co_{0.7}Cu_{0.3}Fe₂O₄ ▲ SO₄²⁻/Co_{0.5}Cu_{0.5}Fe₂O₄ ■ SO₄²⁻/Co_{0.3}Cu_{0.7}Fe₂O₄

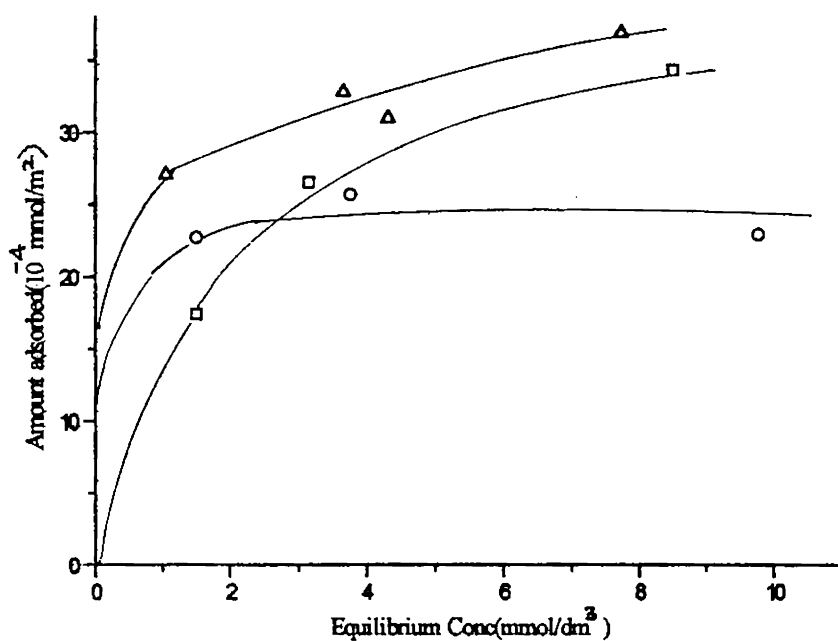


Fig.3.2. 6 Adsorption isotherms of TCNQ in acetonitrile over mixed ferrosipinels of Co-Cu series activated at 500°C

○ Co_{0.7}Cu_{0.3}Fe₂O₄ △ Co_{0.5}Cu_{0.5}Fe₂O₄ □ Co_{0.3}Cu_{0.7}Fe₂O₄

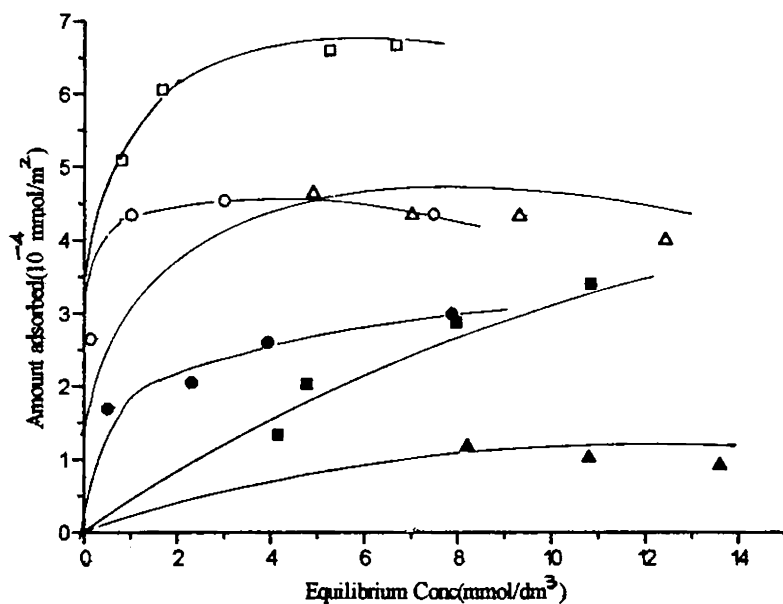


Fig.3.2. 7 Adsorption isotherms of chloranil in acetonitrile over unmodified and sulphate modified simple ferrosipinel systems activated at 300°C

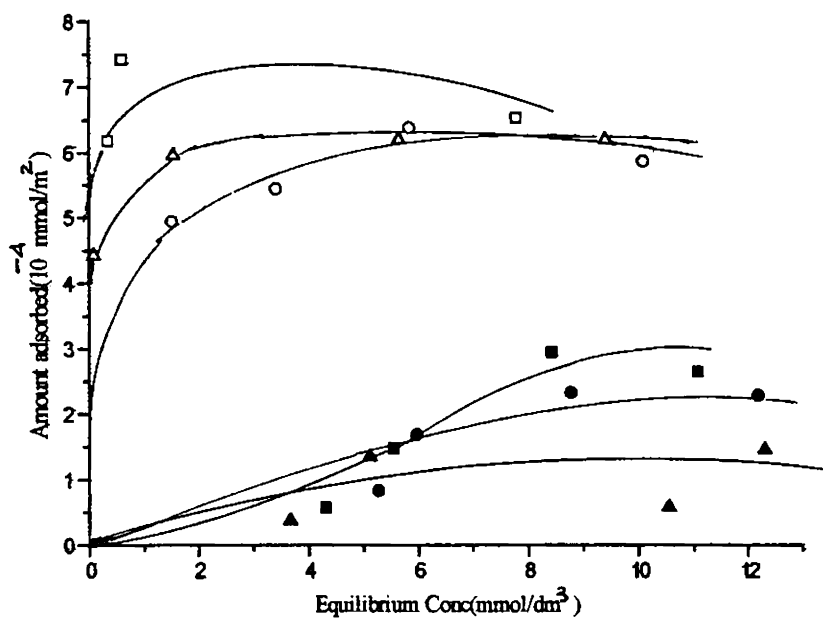
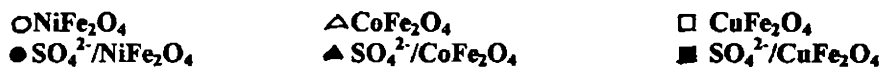


Fig.3.2. 8 Adsorption isotherms of chloranil in acetonitrile over unmodified and sulphate modified mixed ferrosipinel systems of Ni-Cu series activated at 300°C



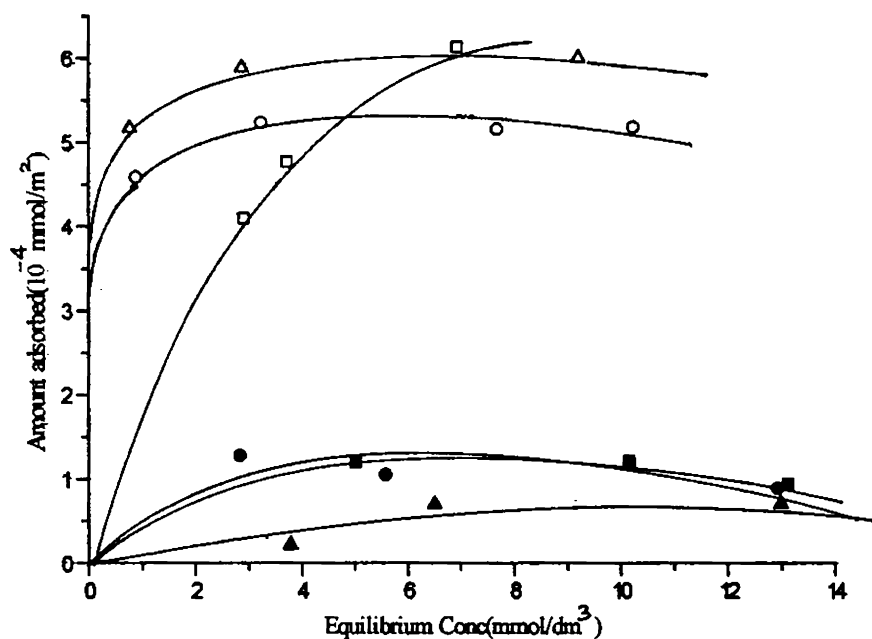


Fig.3.2. 9 Adsorption isotherms of chloranil in acetonitrile over unmodified and sulphate modified mixed ferrosphenel systems of Co-Cu series activated at 300°C

○ $\text{Co}_{0.7}\text{Cu}_{0.3}\text{Fe}_2\text{O}_4$ △ $\text{Co}_{0.5}\text{Cu}_{0.5}\text{Fe}_2\text{O}_4$ □ $\text{Co}_{0.3}\text{Cu}_{0.7}\text{Fe}_2\text{O}_4$
 ● $\text{SO}_4^{2-}/\text{Co}_{0.7}\text{Cu}_{0.3}\text{Fe}_2\text{O}_4$ ▲ $\text{SO}_4^{2-}/\text{Co}_{0.5}\text{Cu}_{0.5}\text{Fe}_2\text{O}_4$ ■ $\text{SO}_4^{2-}/\text{Co}_{0.3}\text{Cu}_{0.7}\text{Fe}_2\text{O}_4$

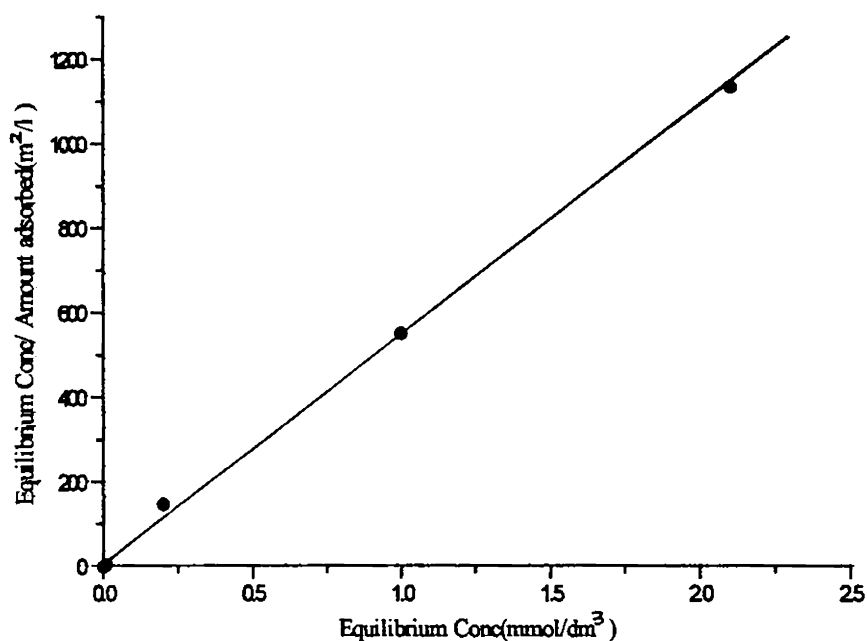


Fig.3.2. 10 Linear Langmuir plot for the adsorption of TCNQ in acetonitrile over NiFe_2O_4 systems activated at 300°C

REFERENCES

1. L. S. Dent Glasser, "Crystallography and its Applications", Van Nostrand Reinhold Company Ltd., New York, 1977, p. 114
2. Clive Whiston, "X – ray Methods" (Editor: F. E. Prichard), John Wiley & Sons, New York, 1991, p. 142
3. G. Blasse, Philips Research Reports Supplements, 3 (1964) 22
4. Clive Whiston, "X – ray Methods", (Editor: F. E. Prichard), John Wiley & Sons, New York, 1991, p. 110
5. R. D. Waldron, Phys. Rev., 99 (1995) 1727
6. W. B. White and B. A. De Angelis, Spectrochim. Acta, 23A (1967) 985
7. J. Preudhomme and P. Tarte, Spectrochim. Acta, 27A (1971) 961
8. K. Nakamoto, " Infrared Spectra of Inorganic and Coordination Compounds", 3rd Edition, Wiley, New York, 1978, p. 241
9. O. Saur, M. Bensital, A. B. M. Saad, J. C. Lavalley, C. P. Tripp and B. A. Morrow, J. Catal., 99 (1986) 104
10. B. A. Morrow, R. A. McFarlane, M. Lion and J. C. Lavalley, J. Catal., 107 (1987) 232
11. M. Bensitel, O. Saur, J. C. Lavalley and B. A. Morrow, Mater. Chem. Phys., 19 (1988) 147
12. M. Waquif, J. Bachelier, O. Saur and J. C. Lavalley, J. Mol. Catal., 72 (1992) 127
13. X. Song and A. Sayari, Catal. Rev.- Sci. Eng., 38(3) (1996) 329
14. J. R. Sohn and H. J. Jang, J. Mol. Catal., 64 (1991) 349
15. C. Miao, W. Hua, J. Chen and Z. Gao, Catal. Lett., 37 (1996) 187
16. F. Babou, G. Goudurier and J. C. Vadrine, J. Catal., 152 (1995) 341
17. K. Tanabe, Mater. Chem. Phys., 13 (1985) 347
18. L. H. Lunsford, H. Sang, S. M. Campbell, C. H. Liang and R. G. Anthony, Catal. Lett., 27 (1994) 305
19. C. Monterra, G. Cerrato, F. Pinna, M. Signoreto and G. Strukul. J. Catal., 149 (1994) 181
20. K. Nakamoto, " Infrared and Raman Spectra of Inorganic and Co-ordination Compounds", 4th Edition, Wiley, New York, 1986, p. 249
21. K. Nishiwaki, N. Kakuta, A. Ueno, H. Nakabayashi, J. Catal., 118 (1989) 498
22. F. R. Chen, G. Coudurier, J. F. Joly and J. C. Vadrine, J. Catal., 143 (1993) 616

23. K. Morishige, K. Kittaka and T. Morimoto, *Bull. Chem. Soc. Jpn*, 53 (1980) 2128
24. E. V. A. Ebsworth, D. W. H. Rankin and S. Cradock, "Structural Methods in Inorganic Chemistry", ELBS/Blackwell Scientific Publications, Great Britain, 1987, p. 287
25. J. M. Daniels and A. Rosencwaig, *Canadian Journal of Physics*, 48(4) (1970) 381
26. J. G. Lee, J. Y. Park and C. S. Kim, *J. Mater. Sci.*, 33 (1998) 3965
27. J. W. Niemantsverdriet and W. N. Delgass, *Topics in Catalysis*, 8 (1999) 133
28. J. P. Jacobs, A. Maltha, J. G. H. Reintjes, J. Drimal, V. Ponc and H. H. Brongersma, *J. Catal.*, 147 (1994) 294
29. J. Kijenski and A. Baiker, *Catal. Today* 5 (1989) 1
30. K. Meguro and K. Esumi, *J. Adhesion Sci. Technol.*, 4(5) (1990) 393
31. D. Cordischi and V. Indovina, *J. Chem. Soc. Faraday Trans.*, 72(10) (1976) 2341
32. R. D. Shannon, *Acta. Cryst.*, A32 (1976) 751
33. R. T. Sanderson, "Chemical Periodicity", Reinhold, New York, 1960
34. J. E. Huheey, E. A. Keiter and R. L. Keiter, "Inorganic Chemistry", Fourth Edition, Addison-Wesley, 1993, p. 188
35. D. W. Smith, *J. Chem. Educ.*, 64 (1987) 480
36. A. F. Wells, "Structural Methods in Inorganic Chemistry" 4th Edition, ELBS, London, 1979, p. 890
37. A. Auroux and A. Gervasini, *J. Phys. Chem.* 94 (1990) 6371

CHAPTER-IV
FRIEDEL-CRAFTS BENZOYLATION REACTION OF
TOLUENE AND BENZENE

4.0 INTRODUCTION

Benzoylation of aromatics is an important reaction in synthetic organic chemistry. It is unfortunate that many industries continue using the harmful halogen-containing Lewis acids such as AlCl_3 , BF_3 etc. as catalysts to perform this reaction. These homogeneous catalysts are needed in more than molar amounts to complete the reaction and are not reusable. The spent catalyst disposal is a real problem as these chemicals are environmentally hazardous, especially to aquatic life. The need to replace such catalysts with the more eco-friendly heterogeneous ones is felt all the more in recent years. In our work, we have found that our ferros spinel samples function as efficient heterogeneous catalysts for benzoylation of toluene and even benzene. No report has been found so far in the literature of the benzoylation of toluene and benzene catalysed by ferros spinel systems. In this part of the thesis, we report the results of our study on benzoylation of toluene and benzene using the ferros spinel catalyst systems and attempt to rationalise the results on the basis of the physico-chemical properties of the catalyst samples.

4.1 BENZOYLATION OF TOLUENE

Liquid-phase benzoylation of toluene was conducted by refluxing a mixture of toluene and benzoyl chloride in the molar ratio 3.6:1 in an oil bath at the boiling point of the mixture (120°C). The product yield was found to be proportional to the amount of the catalyst taken and the duration of the reaction run. We had optimised the conditions such that a reaction run for half an hour employing 0.1 g of the catalyst each time gave sufficient range in the yield of products that proper comparison of the catalytic activities of the various samples could be made. The reaction always yielded mainly two products which were estimated by GC and identified as 2-methylbenzophenone (2-MBP) and 4-methylbenzophenone (4-MBP) by GC-MS. (A trace amount of a third product, probably 3-MBP, was also observed in the GC as a tiny peak very much overlapping with the GC peak of the major product. This was not separately estimated but was counted along with the major product.) The reaction is represented schematically by the following figure (Fig. 4.1.1)

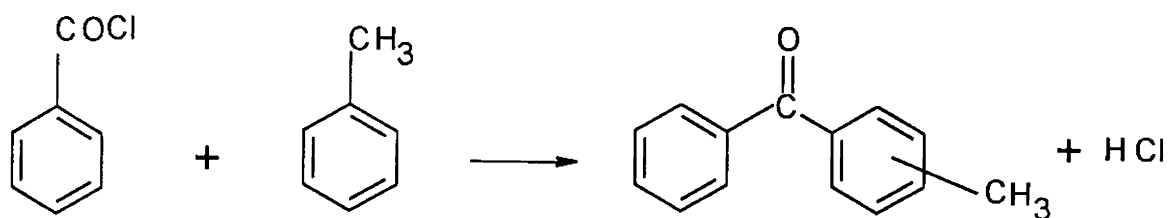


Fig. 4.1.1. Schematic representation of the benzoylation of toluene.

The results and their discussions are conveniently done under three headings: (i) simple ferrosphenel systems (ii) mixed ferrosphenels of the Ni-Cu series and (iii) mixed ferrosphenels of the Co-Cu series. The sulphated analogues of the samples were also tested for their catalytic activities. The rate in the units of ($\text{h}^{-1}\text{m}^{-2}$) was computed for each catalyst sample.

The product yield and rate constant from the primary GC data have been calculated by the following procedure. Using standard mixtures of toluene, benzoyl chloride and methylbenzophenone, GC calibration curve was made for each chemical species from which a GC response factor was made available for each. The experimental GC peak area percentage of each component in the reaction mixture was multiplied by the response factor and new peak area percentages were computed. From the molar ratio of reactants employed, it was calculated that a GC peak area percentage of 45.04 for the product corresponded to 100% yield in the reaction. Thus, % yield of products in any reaction run is simply equal to $(100x/45.04)$ where 'x' is the experimental peak area % of the products. From the product yield, the intrinsic rate constant was calculated using the formula,

$$k \text{ (h}^{-1} \text{ m}^{-2}\text{)} = \frac{2.303}{t w A} \log \frac{100}{(100 - \% \text{yield})}$$

where t = time the reaction (0.5 h), w = weight of the catalyst sample taken (0.1 g) and A = BET surface area of the catalyst ($\text{m}^2 \text{g}^{-1}$).

4.1.1 AFe_2O_4 (A = Ni, Co, Cu) – type systems

(a) RESULTS. The results of studying benzoylation of toluene over the simple ferrosphenel systems are given in Table 4.1.1. An activity profile diagram is given in Fig. 4.1.2(A).

Table 4.1.1 Benzoylation of toluene with benzoyl chloride over simple ferrosphenels of Ni, Co and Cu

Catalyst systems	T=573 K			T=773 K		
	Product yield (%)	Rate constant ($10^{-2}\text{h}^{-1}\text{m}^{-2}$)	Select. of 4-MBP	Product yield (%)	Rate constant ($10^{-2}\text{h}^{-1}\text{m}^{-2}$)	Select. of 4-MBP
NiFe_2O_4	23.4	3.5	83.0	17.1	8.3	84.2
CoFe_2O_4	44.5	12.5	84.2	25.4	18.2	84.4
CuFe_2O_4	59.5	9.6	85.6	42.3	55.6	84.4
$\text{SO}_4^{2-}/\text{NiFe}_2\text{O}_4$	36.6	4.7	83.8	15.7	4.4	84.6
$\text{SO}_4^{2-}/\text{CoFe}_2\text{O}_4$	45.6	11.3	85.0	27.0	13.6	85.9
$\text{SO}_4^{2-}/\text{CuFe}_2\text{O}_4$	57.1	9.0	85.1	35.2	26.7	86.2

T=activation temperature, toluene - benzoyl chloride molar ratio = 3.6:1, reaction temperature = 120°C , reaction time = 0.5 h, amount of catalyst = 0.1 g.

From the data given in Table 4.1.1, the following conclusions can be drawn.

- (i) Both for the unmodified and sulphate-modified simple ferrosipinel systems, the order of catalytic activity towards benzoylation of toluene is $\text{Co} > \text{Cu} \gg \text{Ni}$ at the activation temperature of 300°C while the order is $\text{Cu} \gg \text{Co} > \text{Ni}$ at 500°C activation. Thus CoFe_2O_4 is the most active catalyst at the lower activation temperature while CuFe_2O_4 is the most active one at the higher activation temperature. In any case, NiFe_2O_4 is the least active.
- (ii) Sulphation does not influence much the catalytic activity at the activation temperature of 300°C , while it brings down the catalytic activity at the activation temperature of 500°C , compared to the activity of the unmodified samples.
- (iii) Except for $\text{SO}_4^{2-}/\text{NiFe}_2\text{O}_4$, there is always an increase in the catalytic activity with the increase in activation temperature from 300 to 500°C . This increase is more prominent for the unmodified systems than for the sulphate-modified ones. The activity of CuFe_2O_4 increases nearly five-fold.
- (iv) The selectivity of the isomeric products remains more or less constant in the range 83-86% for 4-MBP and 17-14% for 2-MBP.

(b) DISCUSSION. Benzoylation of toluene has been reported over various heterogeneous catalysts such as calcined iron sulphate [1], sulphated zirconia [2], sulphated alumina [3], acidic zeolites [4], sulphated alumina-zirconia [5], a variety of sulphated metal oxides [6] and Si - MCM - 41 supported gallia and india [7]. Among these systems, all but the last mentioned are superacidic and the authors attribute the catalytic activity for acylation reaction to the superacidic Lewis or Brønsted sites. These ferrosipinel samples are not expected to be superacidic as such, nor such a quality has been created by sulphation as evidenced by IR studies. n-Butylamine adsorption data [Table 3.2.4] show that there is a considerable increase in weak and medium strong acid sites as a result of sulphation for the catalysts activated at 300°C . But the benzoylation activity data [Table 4.1.1] show that sulphation does not very much affect

the catalytic performance. Thus we infer that weak and medium strong acid sites are not involved in benzylation reaction. That leaves the strong acid sites which are usually of the Lewis type [8]. Aramendia *et al.* [9], using temperature programmed desorption mass spectrometry (TPD-MS) techniques with pyridine, 2,6-dimethylpyridine and carbon dioxide as probe molecules, showed that the effect of calcination temperature on acidity of metal oxide surfaces was to reduce the number of Brønsted sites and to leave only Lewis type sites among the strongest acid sites. Thus, at higher temperature of calcination, most of the Brønsted acid sites on metal oxides would have disappeared due to dehydroxylation. At the same time, the strength and the number of Lewis acid sites per unit surface area would have increased due to the creation of surface defects and more co-ordinatively unsaturated cations. The catalytic activity for benzylation increases with increase in the activation temperature of the catalysts (Table 4.1.1). Based on these observations, we can come to the conclusion that the catalytic activity of the ferrosin samples for benzylation reaction is due to the strong Lewis acidic sites present in the systems.

Ghorpade *et al.* [10], in their study of liquid-phase Friedel – Crafts benzylation of benzene with benzyl chloride over $\text{CuCr}_{2-x}\text{Fe}_x\text{O}_4$ spinel catalysts, showed that both Lewis and Brønsted acid sites are present on the surface of the spinels as proved by pyridine adsorption followed by FT-IR studies. These authors found that CuFe_2O_4 gave the highest yield of products and concluded that the Lewis acid sites were responsible for the good catalytic performance. As sulphation delays dehydroxylation [11], the creation of strong and new Lewis sites on sulphated samples will be less efficient compared to the unmodified samples, as the activation temperature is increased from 300 to 500°C. This explains the smaller influence of activation temperature on the catalytic performance of the sulphated samples compared to the influence on the unmodified systems (Table 4.1.1). Consequently, at the activation temperature of 500°C, the effect of sulphation on the catalytic activity is to decrease it by nearly half.

The acidity of electron deficient defects on metal oxide surface depends on the position of the particular metal in the periodic system of elements, i.e. on the

electronegativity of the metal cation [8,12]. The strength of Lewis acidity of the octahedral cations in the ferrosipinel systems can also be expected to depend on the electronegativities of these ions [13]. According to Sanderson [14], the electronegativity of a metal ion, X_i is given by the formula, $X_i = (1 + 2Z) X_0$ where Z is the charge of the metal ion and X_0 is the electronegativity of the metal atom ($Z = 0$). Substituting Pauling's electronegativity values [15] into the above equation, the X_i values of the metal ions present in these ferrosipinel systems are computed. These are given in Table 4.1.2

Table 4.1.2 Electronegativities of the octahedral metal ions in the ferrosipinel systems, calculated by Sanderson's [14] method.

Metal ion	Pauling's Electronegativity of the metal (X_0)	Electronegativity of the metal ion, X_i
Fe ³⁺	1.96	13.72
Cu ²⁺	2.00	10.00
Ni ²⁺	1.91	9.55
Co ²⁺	1.88	9.40

Thus the electronegativities of the cations vary in the order, $Fe^{3+} \gg Cu^{2+} > Ni^{2+} \cong Co^{2+}$. Evidently, the strong Lewis acidity of the ferrites originates primarily from the presence of tripositive ferric ions. Among the dipositive ions, Cu^{2+} provides the strongest Lewis acid sites. This may be due to its acquiring a stable, completely filled d- subshell on receiving an electron.

The rate of benzoylation depends both on the number and strength of the Lewis acid sites. By n-butylamine adsorption study of the acidity of the ferrosipinels, we know that the number of strong acid sites vary in the order $Co \gg Ni > Cu$. This correlates with

the highest catalytic activity of CoFe_2O_4 for the benzoylation reaction at the activation temperature of 300°C . The higher catalytic activity of CuFe_2O_4 over NiFe_2O_4 can be explained on the assumption that the benzoylation reaction requires the presence of strong Lewis acid sites of a certain minimum strength. The proportion of the Lewis acid sites above this minimum is higher in CuFe_2O_4 due to the higher electronegativity of Cu^{2+} over the Ni^{2+} ions. Thus, although the number of strong acid sites in CuFe_2O_4 is somewhat less than that in NiFe_2O_4 (Table 3.2.4), the presence of higher proportion of sufficiently strong Lewis acid sites catalyse the reaction, and CuFe_2O_4 proves to be more active than NiFe_2O_4 for benzoylation. Samples of CuFe_2O_4 activated at 500°C show the highest catalytic activity. This is due to the fact that CuFe_2O_4 is more vulnerable for the creation of anion vacancy defects on calcination than the other ferrites. The higher reducibility of Cu^{2+} ions [16] and its special coordination described as (4+2) [17] in octahedral complexes are responsible for this susceptibility. Coupled with this, there is a drastic decrease in its surface area from $187.87 \text{ m}^2/\text{g}$ to $19.77 \text{ m}^2/\text{g}$ as the activation temperature is changed from 300 to 500°C . Consequently CuFe_2O_4 will have the highest surface density of Lewis acid sites of the proper strength at the activation temperature of 500°C and hence the highest rate.

4.1.2 $\text{Ni}_{1-x}\text{Cu}_x\text{Fe}_2\text{O}_4$ ($x=0.3, 0.5, 0.7$) – type systems

(a) RESULTS. The product yield and rate constant of the benzoylation of toluene with the above catalytic systems are given in Table 4.1.3. An activity profile diagram is given in Fig. 4.1.2(B).

Table 4.1.3 Benzoylation of toluene with benzoyl chloride over $\text{Ni}_{1-x}\text{Cu}_x\text{Fe}_2\text{O}_4$ - type systems.

Catalyst systems	T=573 K			T=773 K		
	Product yield (%)	Rate constant ($10^{-2}\text{h}^{-1}\text{m}^{-2}$)	Select. of 4-MBP	Product yield (%)	Rate constant ($10^{-2}\text{h}^{-1}\text{m}^{-2}$)	Select. of 4-MBP
$\text{Ni}_{0.7}\text{Cu}_{0.3}\text{Fe}_2\text{O}_4$	50.8	8.0	85.2	26.7	15.9	84.1
$\text{Ni}_{0.5}\text{Cu}_{0.5}\text{Fe}_2\text{O}_4$	45.8	6.7	84.8	41.4	37.1	84.4
$\text{Ni}_{0.3}\text{Cu}_{0.7}\text{Fe}_2\text{O}_4$	55.4	9.3	84.6	36.1	34.7	85.8
$\text{Ni}_{0.7}\text{Cu}_{0.3}\text{Fe}_2\text{O}_4^*$	49.8	6.8	86.1	32.0	10.8	84.5
$\text{Ni}_{0.5}\text{Cu}_{0.5}\text{Fe}_2\text{O}_4^*$	57.5	8.1	85.4	39.8	26.1	84.5
$\text{Ni}_{0.3}\text{Cu}_{0.7}\text{Fe}_2\text{O}_4^*$	71.0	12.8	84.7	41.2	27.9	84.6

* Sulphated sample, T = activation temperature, toluene - benzoyl chloride molar ratio = 3.6:1, reaction temperature = 120°C, reaction time = 0.5 h, amount of catalyst = 0.1 g.

Analysis of the data given in Table 4.1.3 and comparison of these with the data in Table 4.1.1 lead us to the following conclusions.

(i) The catalytic activity of NiFe_2O_4 for benzoylation of toluene is almost doubled with the substitution by even a small amount of copper ($x = 0.3$) in the spinel matrix. The rate shows a general increase with copper content, both for the unmodified and sulphate-modified samples. This situation prevails both at the activation temperatures of 300 and 500°C.

(ii) As the activation temperature is increased from 300 to 500°C, the rate constant for the reaction is also increased for all the catalytic systems. The increase in rate constant is about two-fold when $x = 0.3$ but by many folds when $x = 0.5$ or 0.7 . However, the increase in rate for the sulphate-modified samples with activation temperature is less impressive than for the unmodified systems.

(iii) Sulphation has no significant effect on the rate at the activation temperature of 300°C, but somewhat reduces the rates at the activation temperature of 500°C, compared to the rates of the unmodified systems.

(iv) The selectivity of the products remains almost unchanged at 83-87 % of 4-MBP

(b) DISCUSSION. Many of the explanations given under the simple ferrosphenel systems are applicable here also. Thus, the increased activity of the copper-containing samples is due to the increase in strong Lewis acid sites provided by the Cu^{2+} ions. As more and more Cu^{2+} ions replace Ni^{2+} ions, the proportion of Lewis acid sites of the proper strength increases and the rate constant also increases. Sulphation has no positive effect on rate because sulphation of ferrosphenels only increases the number of weak and medium strong acid sites (Table 3.2.4) which are usually of the Brønsted type and are not involved in benzoylation reaction. The increased rates at the activation temperature of 500°C are due to the general increase in the number of strong Lewis acid sites per m^2 , which, in turn, is due to the creation of new coordinatively unsaturated cationic sites in the system.

4.1.3 $\text{Co}_{1-x}\text{Cu}_x\text{Fe}_2\text{O}_4$ ($x = 0.3, 0.5, 0.7$) – type systems

(a) RESULTS The data of catalytic activities of the above systems for benzoylation of toluene are shown in Table 4.1.4. An activity profile diagram is given in Fig. 4.1.2(C).

Table 4.1.4 Benzoylation of toluene with benzoyl chloride over $\text{Co}_{1-x}\text{Cu}_x\text{Fe}_2\text{O}_4$ - type systems.

Catalyst systems	T=573 K			T=773 K		
	Product yield (%)	Rate constant ($10^{-2}\text{h}^{-1}\text{m}^{-2}$)	Select. of 4-MBP	Product yield (%)	Rate constant ($10^{-2}\text{h}^{-1}\text{m}^{-2}$)	Select. of 4-MBP
$\text{Co}_{0.7}\text{Cu}_{0.3}\text{Fe}_2\text{O}_4$	56.2	12.1	86.3	54.8	68.8	84.3
$\text{Co}_{0.5}\text{Cu}_{0.5}\text{Fe}_2\text{O}_4$	63.7	15.1	84.5	43.8	44.3	84.6
$\text{Co}_{0.3}\text{Cu}_{0.7}\text{Fe}_2\text{O}_4$	57.2	10.1	86.3	35.7	29.5	84.3
$\text{Co}_{0.7}\text{Cu}_{0.3}\text{Fe}_2\text{O}_4^*$	58.5	11.6	85.4	47.6	37.6	86.1
$\text{Co}_{0.5}\text{Cu}_{0.5}\text{Fe}_2\text{O}_4^*$	59.7	11.8	86.0	55.4	40.5	86.8
$\text{Co}_{0.3}\text{Cu}_{0.7}\text{Fe}_2\text{O}_4^*$	53.7	9.5	85.2	36.4	19.4	84.4

* Sulphated sample, T = activation temperature, toluene - benzoyl chloride molar ratio = 3.6:1, reaction temperature = 120°C, reaction time = 0.5 h, amount of catalyst = 0.1 g.

Going through these data, we can arrive at the following findings.

(i) Introduction of Cu^{2+} ions into the spinel matrix of CoFe_2O_4 does not cause any substantial change in the rates, both for the unmodified and sulphate modified samples of 300°C activation, except in the case of $\text{Co}_{0.5}\text{Cu}_{0.5}\text{Fe}_2\text{O}_4$ where the rate shows a maximum. In fact, there is a small but obvious decrease in the rate constants with increase of copper-doping.

(ii) But, at 500°C activation, the effect of copper-doping is different. As per the general behaviour, all the rates are higher at the higher activation temperature. Added to this, copper-doping increases the rates by about two or three-folds from the value for pure

cobalt ferrite at 500°C. The maximum increase in rate occurs with the minimum introduction of copper namely $x = 0.3$; then the effect diminishes with further amounts of copper.

(iii) Sulphation of ferros spinels shows little influence on the liquid-phase benzoylation of toluene at the activation temperature of 300°C but it decreases the rates at 500°C activation, compared to the values of the unmodified systems.

(iv) The selectivity of the isomeric products remains unchanged at 83-87% of 4-MBP.

(b) DISCUSSION. We notice a fair amount of agreement in the conclusions of results between this system and those described earlier. Naturally, the explanations given for the results of the three types of systems are also expected to have many aspects in common. The rate constant for benzoylation reaction is a function of both the number and the strength of the strong acid sites. From n-butylamine adsorption data (Table 3.2.4), we observe that CoFe_2O_4 has the highest number of strong acid sites at 300°C activation and CuFe_2O_4 , the least. But, from electronegativity considerations, Cu^{2+} ions can provide stronger Lewis acid sites than Co^{2+} . The combined effects of these two factors operate on the catalytic activities of Co-Cu ferros spinels. The net result is that, introduction of copper does not very much affect the rates at 300°C activation. In other words, the decrease in the rate arising from the decrease in the number of active sites as Co^{2+} ions are being substituted by Cu^{2+} ions, almost matches the increase in the rate arising from the presence of stronger Lewis acid sites brought in by Cu^{2+} ions. But the picture is entirely different at 500°C activation. An increase in Lewis acid sites with respect to both number and strength is expected for copper-containing ferros spinels at 500°C activation, due to the susceptibility of copper-containing spinel lattice to yield more coordinately unsaturated cation sites at the higher calcination temperature. The catalytic activity culminates to a maximum for $\text{Co}_{0.7}\text{Cu}_{0.3}\text{Fe}_2\text{O}_4$ at 500°C activation, from among all the systems described so far.

The explanation of the influence of sulphation is the same as given under the earlier systems. Thus, sulphation creates new acid sites of the weak or medium strong

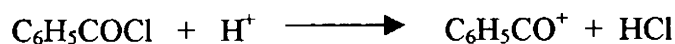
Brønsted type, which fail to catalyse the benzoylation reaction. The rates at 500°C activation is less for the sulphated samples than those of the unmodified ones because, sulphation delays dehydroxylation. Hence creation of new Lewis acid sites will be less efficient compared to the case of the unmodified systems.

Among all the catalytic systems described, the most active catalyst for benzoylation of toluene is $\text{Co}_{0.7}\text{Cu}_{0.3}\text{Fe}_2\text{O}_4$ and the second most active is CuFe_2O_4 , both activated at 500°C. But, for process catalysts, high activity should be coupled with large surface area so as to give high yields. In this respect, the best process catalyst will be $\text{SO}_4^{2-}/\text{Ni}_{0.3}\text{Cu}_{0.7}\text{Fe}_2\text{O}_4$ (71% yield) and the second best will be $\text{Co}_{0.5}\text{Cu}_{0.5}\text{Fe}_2\text{O}_4$ (63.7% yield), both activated at 300°C. The latter is also the most active at 300°C activation.

4.1.4 Mechanism of benzoylation reaction

The mechanism of homogeneous Friedel-Crafts acylation is not completely understood, but at least two mechanisms are probably operative, depending on the conditions. In most cases, the attacking species is the acyl cation RCO^+ formed by reaction with the Lewis acid. In the other mechanism, an acyl cation is not involved but a 1:1 complex, formed between RCOCl and the Lewis acid, acts as the attacking species. Evidence for RCO^+ intermediate has been obtained in polar solvents but in non-polar medium only the complex exists [18].

Many of the earlier studies on the benzoylation of toluene by heterogeneous catalysts involve superacidic sulphated metal oxides as catalysts. [2,3,5 & 6]. Superacidity requires a trace of adsorbed water and has been attributed to highly acidic Brønsted sites adjacent to strong Lewis sites [19]. Benzoylation of toluene, according to some of the authors [2, 3 & 5], takes place through the creation of benzoyl cation by the reaction of superacidic Brønsted sites of the catalyst with benzoyl chloride, according to the reaction step,



But, there is no evidence for superacidity in our catalytic systems. The catalytic activity, effect of sulphation and effect of activation temperature of these ferrosphinel systems for benzoylation of toluene, strongly suggest that the reaction involves interaction of the Lewis acid sites of the catalysts with benzoyl chloride. As the reaction mixture has a net non-polar nature, a complex between the catalyst and C_6H_5COCl is a more likely intermediate than a free benzoyl cation. A plausible mechanism can be represented by the following figure (Fig 4.1.3)

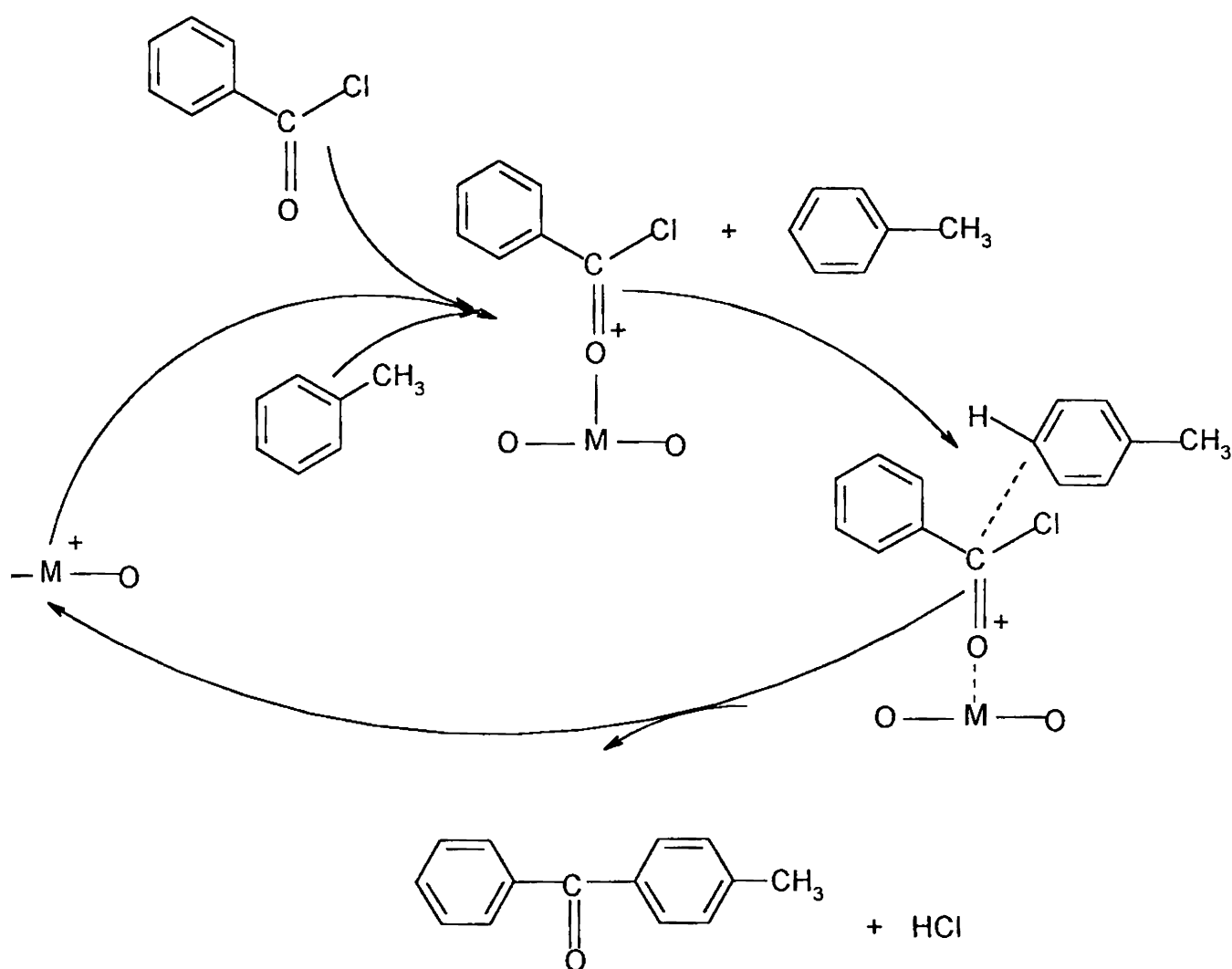


Fig 4.1.3 A plausible mechanism for benzoylation of toluene by ferrosphinel catalysts

The formation of predominant para isomer is due to steric considerations. The formation of only para and ortho isomers as the main products can be rationalised by considering the symmetry of the highest occupied molecular orbital (HOMO) of toluene involved in the interaction with the intermediate complex. An interaction can take place only on bonds formed by orbitals bearing the same sign, i.e. 1-2, 1-6, 3-4 and 4-5, but not 2-3 and 5-6. Of the four allowed sets, the attack on the former two can lead only to ortho substitution whereas the latter two will give the para isomer and less meta [20]. This is evident from the following figure (Fig. 4.1.4)

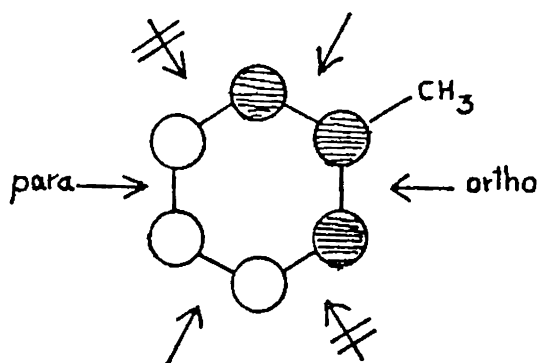


Fig. 4.1.4. The HOMO of toluene suggesting only the ortho and para substituted products.

It is worthwhile to compare the yields of the most active catalysts for Friedel-Crafts benzoylation of toluene using benzoyl chloride reported by some of the earlier workers with our results. Such a comparison has been done in Table 4.1.5.

Table 4.1.5 Comparison of the reaction data for the Friedel-Crafts benzylation of toluene using benzoyl chloride

Catalyst	Amount of toluene & benzoyl chloride	Reaction temp. (°C)	Reaction time (h)	Amount of catalyst	Yield (%)	Reference
SO ₄ ²⁻ /Al ₂ O ₃	15 ml 7.1mmol	110	3	0.5	37.0	[3]
SO ₄ ²⁻ /ZrO ₂ /Al ₂ O ₃	20 ml 1 ml	110	2	0.5	58.7	[5]
SO ₄ ²⁻ /ZrO ₂	141 mmol 2 mmol	100	3	0.5	60.0	[6]
SO ₄ ²⁻ /SnO ₂	141 mmol 2 mmol	100	3	0.5	52.0	[6]
SO ₄ ²⁻ /TiO ₂	141 mmol 2 mmol	100	3	0.5	17.0	[6]
Zeolite H- beta	molar ratio 5:1	115	1	1.0	45.9	[4]
Fe ₂ (SO ₄) ₃ calcined at 700°C	0.5 M benzoyl chloride in toluene	110	1	0.4-0.6	30.0	[1]
Co-Cu ferrite with x=0.5 ^a	molar ratio = 3.6:1	120	0.5	0.1	63.7	Present work
Sulphated Ni-Cu ferrite with x = 0.7 ^a	„	„	„	„	71.0	„

^a activation temperature of the catalyst = 300°C

It is very clear from the Table 4.1.5 that these ferrosinell samples are excellent catalysts for the benzylation of toluene.

4.2 BENZOYLATION OF BENZENE

The absence of any activating group in the ring makes the acylation of benzene more difficult. There are, in fact, few reports of Friedel-Crafts acylation of benzene using heterogeneous catalysts. We have done the benzylation of benzene with benzoyl chloride over our catalyst samples in order to verify their activities and to reaffirm the conclusions made during the study of benzylation of toluene. Our results, discussed in the following sections, are indeed encouraging and show good correlations with the results obtained for the benzylation of toluene.

The experimental procedure and the calculation method were almost the same as in the case of toluene. But, in the present case, the optimisation of conditions required the reaction to be run for 1.5 hours with 0.15 g catalyst so as to get comparable yields. The molar ratio between benzene and benzoyl chloride was 4.3:1. The GC peak area percentage of 41.51 for the product, after correction with the GC response factor, corresponded to 100 % yield in the reaction. The reaction is represented by the following scheme. (Fig 4.2.1)

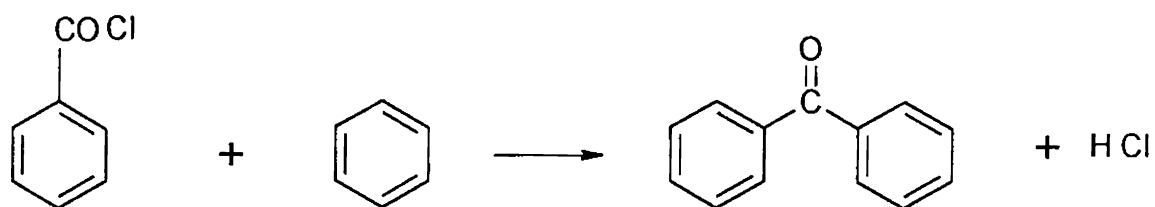


Fig 4.2.1 Scheme for the benzylation of benzene

4.2.1 Results

The yields of benzophenone and the rate constants over the various ferrosphenel samples are given in Table 4.2.1. Activity profile diagrams are given in Fig. 4.2.2(AtoC)

Table 4.2.1 Benzoylation of benzene. Product yield and rate constants

Catalyst series	A or x	Activation temperature		Activation temperature	
		300°C		500°C	
		Product yield (%)	Rate const. ($10^{-3}h^{-1}m^{-2}$)	Product yield (%)	Rate const. ($10^{-3}h^{-1}m^{-2}$)
Simple ferros spinels					
i) A Fe ₂ O ₄	Ni	7.4	2.3	4.3	4.3
	Co	7.5	3.7	5.6	8.0
	Cu	16.2	4.2	9.8	23.3
ii) SO ₄ ²⁻ /A Fe ₂ O ₄	Ni	7.8	1.8	4.1	2.4
	Co	5.0	2.1	6.1	6.1
	Cu	12.5	3.2	9.8	14.1
Mixed ferros spinels					
i) Ni _{1-x} Cu _x Fe ₂ O ₄	0.3	9.2	2.4	5.6	6.1
	0.5	10.6	2.7	6.4	10.2
	0.7	8.7	2.3	5.5	9.8
ii) SO ₄ ²⁻ / Ni _{1-x} Cu _x Fe ₂ O ₄	0.3	13.9	3.3	5.0	3.2
	0.5	8.8	1.9	5.1	6.0
	0.7	11.1	2.8	7.8	9.5
iii) Co _{1-x} Cu _x Fe ₂ O ₄	0.3	13.0	4.5	5.1	10.1
	0.5	5.9	2.0	9.4	17.0
	0.7	9.8	2.7	7.4	11.4
iv) SO ₄ ²⁻ / Co _{1-x} Cu _x Fe ₂ O ₄	0.3	8.7	2.7	5.0	6.6
	0.5	7.2	2.2	6.2	7.1
	0.7	10.4	3.0	7.6	7.6

Benzene:benzoyl chloride molar ratio=4.3:1, reaction temp.: 85°C, reaction time: 1.5 h, amount of catalyst=0.15 g.

A critical analysis of the data given in Table 4.2.1 leads us to the following conclusions.

(a) Simple ferros spinels

- (i) The rate constants for the simple ferros spinels and their sulphated analogues, at both activation temperatures of 300 and 500°C, always increase in the order, $\text{Cu} > \text{Co} > \text{Ni}$.
- (ii) The effect of activation temperature is to increase the rate for both the unmodified and sulphate-modified systems, the increase being the highest (almost five times) for copper ferrite.
- (iii) The effect of sulphation is to bring down the rates at both activation temperatures.

(b) Mixed ferros spinels of the Ni-Cu series

- (i) The effect of copper substitution in nickel ferrite is to leave the rates practically unaffected for both the unmodified and sulphate-modified samples at 300°C activation temperature. But at 500°C activation, the Ni-Cu ferrites show higher rates and the activity increases with increase of copper content, for both the unmodified and sulphate-modified samples.
- (ii) The effect of sulphation is to leave the rates almost unaffected at 300°C activation but to reduce the rates at 500°C activation.
- (iii) The effect of activation temperature is always to increase the rates both for the unmodified and sulphate-modified samples, the rates of the unmodified samples being increased by larger factors.

(c) Mixed ferros spinels of the Co-Cu series

- (i) At 300°C activation, the effect of copper-doping in cobalt ferrite is to a slight increase in the rate initially but then the rate declines with further quantities of copper introduced. There is no pronounced effect on the rates of sulphated cobalt ferrites due to copper substitution. But, at 500°C activation, the rates are somewhat higher for the copper containing samples, the sample $\text{Co}_{0.5}\text{Cu}_{0.5}\text{Fe}_2\text{O}_4$ showing a maximum rate. But the sulphated varieties do not show much change in their activities due to copper-doping.

(ii) At 300°C activation, sulphation of Co-Cu ferros spinels results in a decrease in the rate at $x = 0.3$; but the rates remain almost unchanged at $x = 0.5$ or 0.7 . At 500°C activation, the rates of sulphated samples are lower than the values for the unmodified ones.

(iii) The effect of activation temperature is to increase the rates of all the samples, the unmodified samples experiencing an increase by larger factors.

4.2.2 Discussion of results

In the discussion of results for the benzoylation of toluene, we had reasoned out that the strong Lewis acid sites provided by the octahedral cations of the ferros spinel structure were the active sites for the reaction and that the Cu^{2+} ions provided stronger Lewis acid sites compared to Ni^{2+} or Co^{2+} ions. These two findings are further supported by the activity trends of the catalyst samples in the benzoylation of benzene reaction.

Benzene, being less reactive than toluene towards electrophilic substitution, requires stronger Lewis acid sites in the catalysts so that an intermediate complex with higher polarity of bonds is available for attack of the benzene ring. Thus, strength of Lewis acid sites is a more important factor here than the number of strong acid sites. This aspect is reflected in the trend of catalytic activity among the simple ferros spinels. Copper ferrite, possessing stronger Lewis acid sites than nickel or cobalt ferrites shows a greater catalytic activity in any situation like modified/unmodified or activated at 300/500°C. The increase in catalytic activity with activation temperature is maximum for copper ferrite. This is due to the fact that CuFe_2O_4 has greater susceptibility for the creation of anion vacancies and thus the number of coordinatively unsaturated cations increases with calcination temperature, than in the case of nickel or cobalt ferrite so that copper ferrite possesses stronger and more abundant active sites at 500°C activation. This is supported by the well-documented thermal instability of copper oxide [23, 24]

Copper-doping has a minor influence on the rates of the mixed ferros spinel series at 300°C activation both for unmodified and sulphate- modified systems, with one or two

exceptions. This is readily explicable because CuFe_2O_4 has the lowest number of strong acid sites at 300°C activation compared to nickel or cobalt ferrites as revealed by n-butylamine adsorption studies (Table 3.2.4). So copper-doping causes a depletion in the number of strong acid sites although the sites provided by the Cu^{2+} ions are stronger. The two effects more or less compensate so that the net influence will be only some minor modifications in the rate constants. But at 500°C activation, the inherent quality of copper-containing ferros spinels in providing new and stronger Lewis acid sites with calcination temperature, exhibits itself and the rates of all the mixed ferros spinel series are higher than the values for simple ferros spinels at 500°C . This influence is more for the Ni-Cu series than for the Co-Cu series. This is understandable because cobalt ferrite, due to the presence of greater number of strong acid sites, is more active than nickel ferrite and hence will show smaller influence in rates by copper-doping.

At 500°C activation temperature, the effect of sulphation is to bring down the rates compared to those of the unmodified systems at the same activation temperature. Sulphation delays dehydroxylation of the catalyts on calcination. So the creation of new Lewis acid sites takes place less efficiently. Thus the rates are smaller compared to those of the unmodified samples.

It is seen that the most active catalyst for benzoylation of benzene is CuFe_2O_4 and the second most active catalyst is $\text{Co}_{0.5}\text{Cu}_{0.5}\text{Fe}_2\text{O}_4$, both calcined at 500°C . But as process catalyts, the samples giving highest yields are preferred. In this respect, the best catalyst is again CuFe_2O_4 calcined at 300°C . The second best catalyst is $\text{SO}_4^{2-}/\text{Ni}_{0.7}\text{Cu}_{0.3}\text{Fe}_2\text{O}_4$, closely followed by $\text{Co}_{0.7}\text{Cu}_{0.3}\text{Fe}_2\text{O}_4$, both calcined at 300°C .

It is relevant to compare the yields of heterogeneous Friedel-Crafts benzoylation of benzene using benzoyl chloride in some early reports with our present results. This is given in Table 4.2.2. This comparison shows that the present ferros spinel catalyts are highly promising for the benzoylation of benzene under heterogeneous conditions

Table 4.2.2 Comparison of the reaction data for the Friedel-Crafts benzoylation of benzene using benzoyl chloride over some heterogeneous catalysts reported.

Catalyst	Amounts of reactants	Reaction temp. (°C)	Reaction time (h)	Amount of catalyst	Yield (%)	Reference
Fe ₂ (SO ₄) ₃ calcined at 700°C	0.5 M benzoyl chloride solution in benzene	80	1.0	0.4-0.6	4.8	[1]
Rare-earth supported K10 Montmorillonite	not specified	75	not given	0.01	zero	[21]
Ga ₂ O ₃ and In ₂ O ₃ supported on Si-MCM-41	13 ml benzene + 1ml benzoyl chloride	80	4.8	0.4	50	[7]
Zeolite H- beta	catalyst / benzoyl chloride ratio=0.33	80	18.0	-	54	[22]
CuFe ₂ O ₄ activated at 300°C	benzene-benzoyl chloride molar ratio = 4.3:1	85	1.5	0.15	16.2	Present work

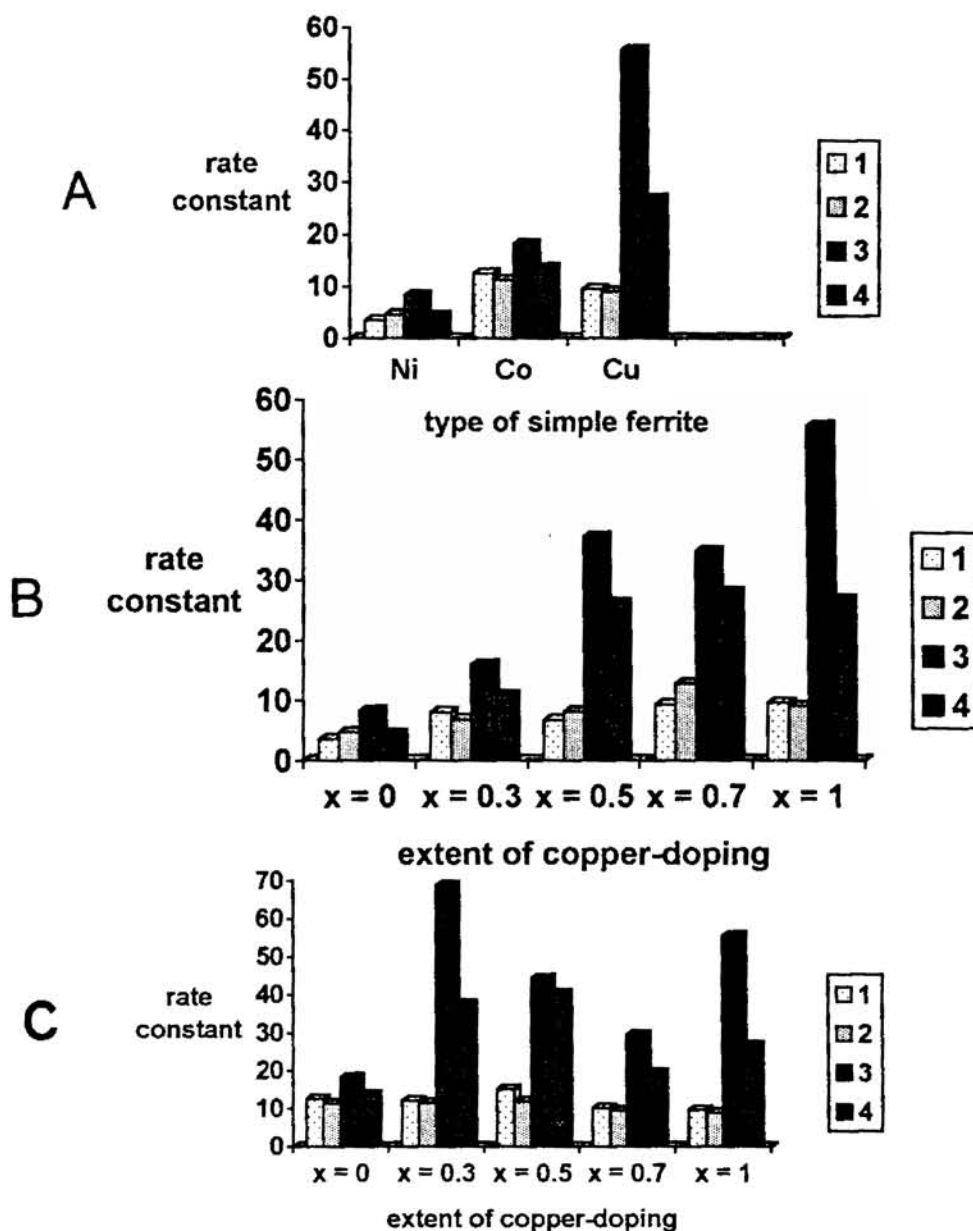


Fig. 4.1.2. Activity Profile Diagrams for the benzoylation of toluene with benzoyl chloride over various ferrite systems. (A) : Simple ferrites (B): Ni-Cu ferrites (C): Co-Cu ferrites

Sample conditions: 1. unmodified, activation temperature-300°C. 2. Sulphated, activation temperature-500°C. 3. unmodified, activation temperature-300°C. 4. Sulphated, activation temperature-500°C.

Reaction conditions: toluene-benzoyl chloride molar ratio: 3.6:1, reaction temperature: 120°C, reaction time: 0.5 h, amount of catalyst: 0.5 g.

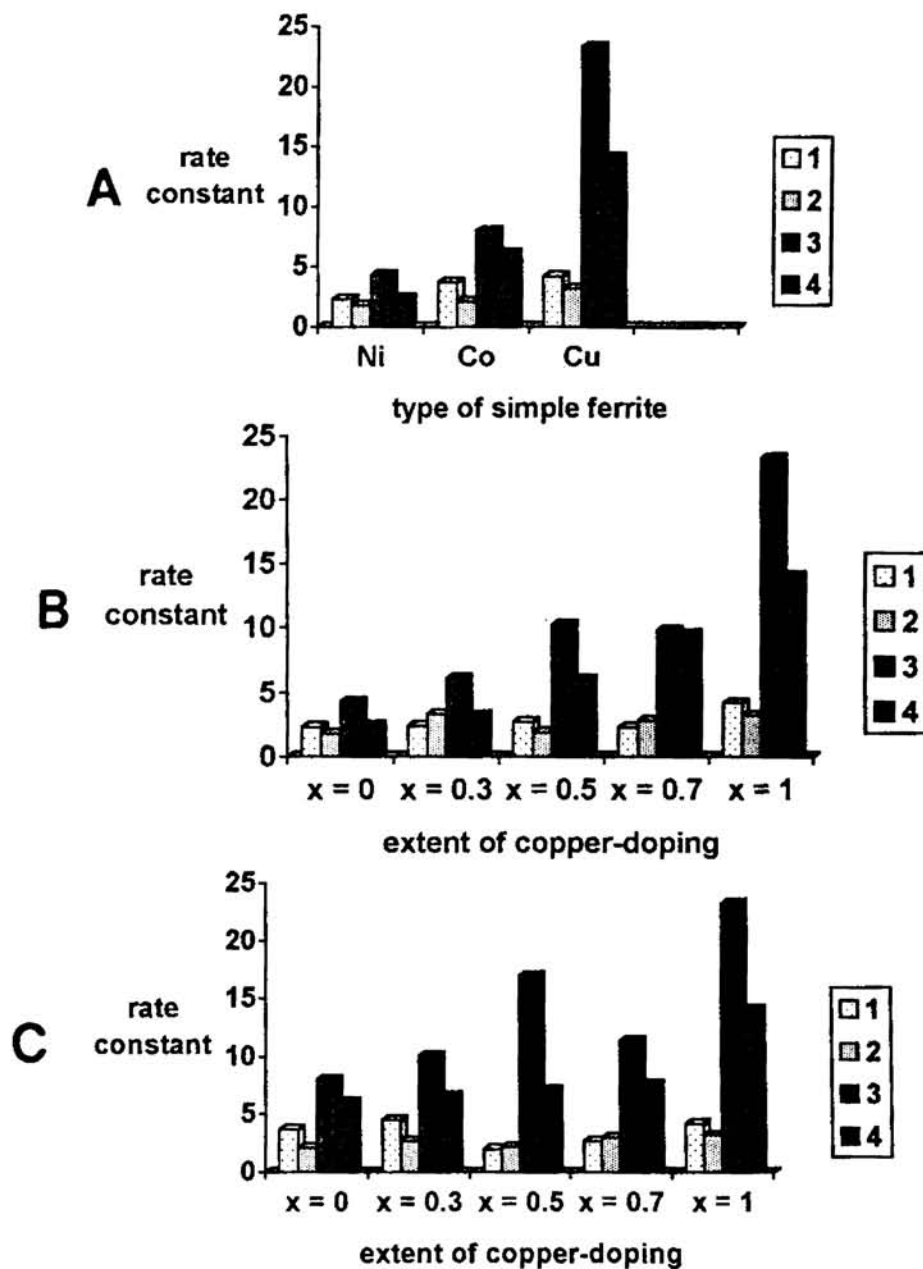


Fig. 4.2.2 Activity profile diagram for the benzoylation of benzene with benzoyl chloride over various ferrite systems. (A) : simple ferrites, (B): Ni-Cu ferrites, (C): Co-Cu ferrites.

Sample conditions: 1. unmodified, activation temperature: 300°C, 2. Sulphated, activation temperature: 300°C 3. unmodified, activation temperature: 500°C 4. Sulphated, activation temperature: 500°C

Reaction conditions: benzene-benzoyl chloride molar ratio: 4.3:1, reaction temperature: 85°C, reaction time: 1.5 h, amount of catalyst: 0.15 g.

REFERENCES

1. K. Arata, K. Yabe and I. Toyoshima, *J. Catal.*, 44 (1976) 385
2. M. Hino and K. Arata, *J. Chem. Soc., Chem. Commun.*, (1985) 112
3. K. Arata and M. Hino, *Appl. Catal.*, 59 (1990) 197
4. A. P. Singh, D. Bhattacharya and S. Sharma, *J. Mol. Catal.*, 102 (1995) 139
5. Y. Xia, W. Hua and Z. Gao, *Catal. Lett.*, 55 (1998) 101
6. K. Arata, H. Nakamura and M. Shouji, *Appl. Catal.*, 197 (2000) 213
7. V. R. Choudhary, S. K. Jana and B. P. Kiran, *J. Catal.*, 192 (2000) 25
8. J. Kijenski and A. Baiker, *Catal. Today*, 5 (1989) 1
9. M. A. Aramendia, V. Borau, I. M. Garcia, C. Jimenez, A. Marinas, J. M. Marinas, A. Porras and F. J. Urbano, *Appl. Catal.*, 184 (1999) 115
10. S. P. Ghorpade, V. S. Darshane and S. G. Dixit, *Appl. Catal.*, 166 (1998) 135
11. X. Song and A. Sayari, *Catal. Rev. – Sci. Eng.*, 38(3) (1996) 329
12. A. Auroux and A. Gervasini, *J. Phys. Chem.*, 94 (1990) 6371
13. A. B. Boffa, C. Lin, A. T. Bell and G. A. Somorjai, *Catal. Lett.*, 27 (1994) 243
14. R. T. Sanderson, “Chemical Periodicity”, Reinhold, New York, 1960
15. J. E. Huheey, E. A. Keiter and R. L. Keiter, “Inorganic Chemistry”, Fourth Edition, Addison-Wesley, 1993, p. 118
16. P. W. Atkins, “Physical Chemistry”, Third Edition, ELBS, UK, 1987, p.268
17. A. F. Wells, “Structural Inorganic Chemistry”, 4th Edition, ELBS, 1975, p.890
18. J. March, “Advanced Organic Chemistry”, Fourth Edition, John Wiley and Sons, New York, 1999, p. 541
19. J. H. Lunsford, H. Sang, S. M. Campbell, C. H. Liang and R. G. Anthony, *Catal. Lett.*, 27 (1994) 305
20. G. A. Olah, S. Kobayashi and M. Tashoro, *J. Am. Chem. Soc.*, 94,21 (1972) 7448
21. D. B. Barbier, A. Dormond and F. D. Montagne, *J. Mol. Catal.*, 149 (1999) 215
22. A. P. Singh and D. Bhattacharya, *Catal. Lett.*, 32 (1995) 327
23. M. Iwamoto, Y. Yoda, N. Yamazoe and T. Seiyama, *J. Phys. Chem.*, 82 (1978) 2564
24. J. L.G. Fierro and J. F. Garcia de la Branda, *Catal. Rev.–Sci. Eng.*, 28(2&3)(1986) 265

CHAPTER - V
VAPOUR-PHASE CYCLOHEXANOL
DECOMPOSITION REACTION

5.0 INTRODUCTION

The best method for characterising industrial acid catalysts seems to be through model reactions [1,2]. The greatest advantage here is that operating conditions similar to those in industrial processes can be chosen, which is not the case with the usual method of chemisorption of basic compounds where the studies are done mostly under vacuum and at room temperature. Model reactions are not only useful for checking the suitability of industrial catalysts, but also are efficient means for determining surface acid-base properties. Alcohol decomposition reaction has been widely studied because it is a simple method to determine the functionality of an oxide catalyst. Decomposition of isopropanol [3-7] and of cyclohexanol [8-13] are the most widely studied reactions in this category. Dehydration activity is linked to acidic property and dehydrogenation activity to the combined effects of both acidic and basic properties.

5.1 DECOMPOSITION OF CYCLOHEXANOL

In this chapter, we describe our study of the vapour-phase decomposition of cyclohexanol over the ferrosinels systems. The reaction was studied in a fixed-bed, down-flow, vertical silica reactor of 2 cm diameter and 30 cm length inside a double zone furnace, using 3 g of pelletised and then broken catalyst. In order to get good reproducibility, the catalyst samples were activated *in situ* in air for 3 hours before each experiment. Cyclohexanol was fed by a syringe pump at the rate of 3.6 ml h⁻¹. The products, condensed to a liquid by a water condenser, were analysed by GC and identified by comparison of the GC retention times of the sample and pure components, expected during the reaction.

The percentage yield of cyclohexene (CHENE) and cyclohexanone (CHONE) were calculated from the selectivity of each, using the formula:

$$\% \text{ yield} = \frac{\text{conversion} \times \text{selectivity}}{100}$$

The reaction can be represented by the scheme given in Fig 5.0.1

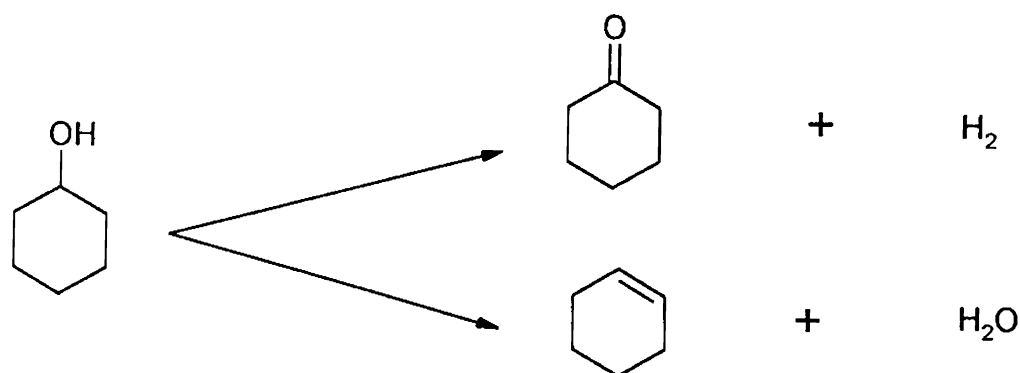


Fig. 5.0.1 Reaction scheme for the decomposition of cyclohexanol

Apart from the main products CHENE and CHONE, the reaction also gave minor amounts of some other products which included benzene and phenol. With one or two exceptions, the amount of benzene ranged between 0.5 to 2% while that of phenol, between 0 to 1.5 % . As we were mainly interested in assessing the dehydration and dehydrogenation activities of the catalyst samples, all the minor products were set aside under one banner, namely ‘other products’, during the calculation of selectivities.

It is assumed that the dehydration and dehydrogenation processes represent a set of parallel reactions obeying first order kinetics. The integrated rate equation for a first order process in a flow system is similar to that in a static system provided the ‘time’ of the reaction is replaced by the ‘contact time’ [14]. Hence an intrinsic rate constant for each of CHENE and CHONE formation is calculated using the relation,

$$k = \frac{2.303}{w A t} \log \frac{100}{(100 - \% \text{ yield})}$$

where w = mass of the catalyst, A = surface area and t = contact time

5.1.1 AFe_2O_4 ($A = Ni, Co, Cu$) – type systems

(a) **RESULTS:** The percentage conversion, product selectivity and rate constants during cyclohexanol decomposition over the above mentioned catalytic systems are given in Table 5.1.1. An activity profile diagram is given in Fig. 5.1.1 (A).

Table 5.1.1 Reaction data on the cyclohexanol decomposition over simple ferrites of general formula, AFe_2O_4 ($A = Ni, Co$ and Cu).

system	% conversion	Product selectivity(%)			Rate constants ($10^{-4}h^{-1}m^{-2}$)		$\frac{k_{CHONE}}{k_{CHENE}}$	$k_{CHONE} + k_{CHENE}$
		CHENE	CHONE	OTHERS	k_{CHENE}	k_{CHONE}		
$NiFe_2O_4$	61.39	50.92	47.40	1.68	9.30	8.52	0.92	17.82
$CoFe_2O_4$	49.02	47.20	50.72	2.08	10.54	11.45	1.09	21.99
$CuFe_2O_4$	67.59	14.82	83.78	1.40	2.10	16.78	7.99	18.88
$NiFe_2O_4^*$	93.63	61.04	26.53	12.43	16.35	5.51	0.34	21.86
$CoFe_2O_4^*$	71.81	61.75	38.04	0.21	20.67	11.26	0.54	31.93
$CuFe_2O_4^*$	75.90	80.08	17.85	2.07	18.90	2.94	0.16	21.84

*sulphated samples. Activation temperature of the catalysts: 300°C, reaction temperature: 300°C, amount of catalyst: 3 g, feed rate: 3.6 ml h⁻¹, contact time: 0.88 h, WHSV = 1.14 h⁻¹

The data of Table 5.1.1 enable us to draw the following conclusions:

- (i) The dehydration activity of the unmodified simple ferrosinzel systems varies in the order $\text{Co} > \text{Ni} > \text{Cu}$ and of the sulphate-modified systems, in the order $\text{Co} > \text{Cu} > \text{Ni}$.
- (ii) The dehydrogenation activity follows the order $\text{Cu} \gg \text{Co} > \text{Ni}$ for the unmodified systems and the order $\text{Co} > \text{Ni} > \text{Cu}$ for the sulphated samples. The ratio of dehydrogenation to dehydration activity, which is considered as a basicity parameter, varies in the order $\text{Cu} \gg \text{Co} > \text{Ni}$ for the unmodified systems, while in the order $\text{Co} > \text{Ni} > \text{Cu}$ for the sulphated samples.
- (iii) Sulphation causes a noticeable enhancement in the dehydration activities of all the ferrites; this influence of sulphation is maximum for copper ferrite and minimum for nickel ferrite.
- (iv) The sum of the dehydration and dehydrogenation rate constants can be considered as a measure of the total catalytic activity of a sample. It is seen that sulphation causes an increase in the net catalytic activities of all the samples.

(b) DISCUSSION

Selectivity in the alcohol decomposition reaction has long been regarded as one of the 'indirect' methods for investigating the acid-base properties of the catalytic sites of metal oxides. As first suggested by Ai [15] in the case of isopropanol decomposition and later confirmed by several authors [16-18], dehydration was catalysed by acid sites whereas the dehydrogenation was catalysed by both acid and basic sites through a concerted mechanism. As a consequence, the dehydration rate could be regarded as a measure of the acidity of the catalyst, while the ratio of the dehydrogenation rate to the dehydration rate, as a rough index of the basicity of the catalysts. Thus, dehydration of cyclohexanol (CHOL) leading to cyclohexene (CHENE) would be catalysed by acid centres whereas its dehydrogenation leading to cyclohexanone (CHONE) would be catalysed both by acid and basic sites.

The effect of sulphation on the selectivities gives a clue regarding the type of acid sites involved in the dehydration activity. We have already determined the acidities of the simple ferrosphel systems by the 'direct' method of chemisorption of n-butylamine followed by gravimetric analysis of the desorbed probe molecules by TG. The results of this analysis are reproduced along with the CHENE rate constants in Table 5.1.2

Table 5.1.2 Comparison of the acidity parameters obtained by the 'direct' method of n-butylamine adsorption and the 'indirect' method of cyclohexanol decomposition.

Catalytic systems	Acid sites(n-butylamine adsorption , % weight loss in units, 10^{-2} m^{-2})			Acidity parameter k_{CHENE} ($10^{-4} \text{ h}^{-1} \text{ m}^{-2}$)
	Weak	medium	strong	
NiFe ₂ O ₄	3.09	1.33	0.66	9.30
CoFe ₂ O ₄	2.58	1.40	1.15	10.54
CuFe ₂ O ₄	3.25	0.63	0.40	2.10
NiFe ₂ O ₄ *	2.46	1.92	0.55	16.35
CoFe ₂ O ₄ *	6.08	2.54	0.87	20.67
CuFe ₂ O ₄ *	4.80	2.22	0.38	18.90

* sulphated samples.

From the data of Table 5.1.2, it is clear that sulphation of the ferrites has caused an increase in the number of weak and medium strong acid sites rather than of strong acid sites. Creation of strong acid sites by sulphation depends on the nature of the oxide. In many cases, sulphation does not enhance reactivity catalysed by strong acid sites. Thus, Hino and Arata [19] observed that, for many metal oxides including NiO and CuO, there is little catalytic activity enhancement corresponding to strong acid sites, on sulphation. Miao *et al.* [20], during their study of sulphate-promoted mixed oxide superacids, found that addition of Fe, Ni, Co, etc. to zirconia affected the catalytic activity only slightly.

Thus, in the present case, we can rule out the role of strong acid sites in deciding the dehydration activity because sulphation, while increasing the rate constants of dehydration, does not enhance the number of strong acid sites. The acidities of the weak acid sites do increase for cobalt and copper ferrites but not for nickel ferrite, by sulphation. Now, coming to the case of medium strong acid sites, all the acidities increase with sulphation; the effect being least for nickel ferrite and most for copper ferrite. The k_{CHENE} values also show a similar trend; the increase being the least for nickel ferrite, but the highest for copper ferrite, on sulphation. Thus, we observe that there is excellent correlation between the dehydration activities and the trends in the number of moderately strong acid sites and so come to the conclusion that the moderately strong acid sites of the ferrite samples are more decisive in controlling the dehydration activities. Aramendia *et al.* [7], during their investigation of different organic test reactions over acid-base catalysts, found that alcohol dehydration activity was appreciably correlated to Brønsted acidity and concluded that weak to medium acid sites were responsible for dehydration.

It is well-known that sulphation delays the transformation of substances from amorphous to crystalline phase [21]. The TG curve (Fig. 3.1.16) shows that the weight loss of sulphated nickel ferrite due to dehydration occurs somewhat beyond 300°C. Thus, at 300°C, the sulphated ferrosphenel samples are much more hydroxylated than the unmodified ones. Hydroxyl groups provide Brønsted type acid sites. So the increased acidity of medium strength, of sulphated samples is due to the increase in Brønsted acid sites and these sites are responsible for the increased dehydration activity. During their study of cyclohexanol conversion at 300°C, Martin and Duprez [12] noted that the presence of sulphate on zirconia increased its protonic acidity as proved by an increase in the CHENE activity. At the same time, sulphation on zirconia caused a decrease in the ratio of CHONE to CHENE activities. Bezouhonova and Al-Zihari [8] recommended the dehydration activity of cyclohexanol conversion as a simple test to measure the Brønsted acid sites in a metal oxide. The same opinion was also expressed by Martin and Duprez [12] and Aramendia *et al.* [7]. Russian workers [22,23], during their

investigation of selective oxidation over a series of transition metal oxides, found that acidic sites of only moderate strength were important in such oxidations.

It is to be noted that the dehydration activity of copper ferrite is too low compared to the activities of the other ferrites, to be caused by its low acidity alone. Factors, apart from acidity, are suspected to be operative here.

A similar comparison can be made between the surface basicities determined earlier by adsorption of electron acceptors of varying electron affinity values (Chapter III) and the present basicity parameter, namely, $k_{\text{CHONE}}/k_{\text{CHENE}}$. This comparison is compiled in Table 5.1.3. During sulphation, some of the Lewis basic sites are converted to Brønsted acid sites as evident from decreased basicities of the sulphated ferrites.

There is, indeed, a correlation between the (medium + strong) basicity parameters obtained from EA adsorption studies and the ratio of the rate constants during cyclohexanol conversion, for the unmodified ferrites. Yet, the ratio of rate constants for copper ferrite is too large compared to the values for the other ferrites, to be caused by the increase in basicity alone. There is no other correlation between the basicity parameters obtained by the two independent methods.

Table 5.1.3. Comparison of basicity parameters from surface electron donor studies and cyclohexanol decomposition reaction.

system	Basic sites (limiting amount of the electron acceptor adsorbed, 10^{-4} mmol m^{-2})		Basicity parameter, k_{CHONE}/k_{CHENE}
	Weak	(medium+strong)	
NiFe ₂ O ₄	13.9	4.4	0.92
CoFe ₂ O ₄	14.3	4.6	1.09
CuFe ₂ O ₄	11.3	6.7	7.99
NiFe ₂ O ₄ *	5.9	3.0	0.34
CoFe ₂ O ₄ *	4.7	1.0	0.54
CuFe ₂ O ₄ *	5.9	3.4	0.16

* sulphated samples.

According to Armendia *et al.* [7], the widely documented correlation found for alcohol dehydration is not so clear for alcohol dehydrogenation. Gervasini and Auroux attempted to correlate the dehydration and dehydrogenation activities of isopropanol decomposition [6] with the acid-base character obtained by the calorimetric investigation [24] of a large series of metal oxides. They failed to get any simple relationship between the alcohol decomposition activities and acid-base properties and attributed the cause of this failure to the wide heterogeneity of the oxides chosen. However, they obtained correlation between strength of acid sites of the oxides (calorimetric method) and the experimental activation energy for the dehydration. But, not even such a correlation was obtained for the basic sites with dehydrogenation.

The questionability regarding the use of alcohol decomposition activities as a measure of basicity seems to be applicable to our results also. Apart from this, the unusual activities of copper ferrite, namely, too low a dehydration activity and a complementary leap in dehydrogenation activity, are baffling.

Copper-based catalysts have attained considerable importance, owing to their selective properties in reactions involving hydrogen [25]. In their study of cyclohexanol decomposition over various transition metal oxides, Bezouhanova and Al-Zihari [8] noted that ZnO and CuO were the most active materials for dehydrogenation. Present industrial practice of cyclohexanone manufacture, the key intermediate for Nylon 6 or Nylon 66, involves catalytic dehydrogenation of cyclohexanol over commercial grade CuO/ZnO catalyst, known as Girdler-G-66B [26]. The double oxide system CuO/Cr₂O₃ supported on MgF₂ was found to be a very good catalyst for dehydrogenation of isopropanol and cumene [27]. Dehydrogenation activities of transition metal oxides are catalysed by basic as well as redox sites [27]. Isopropanol conversion is often sensitive to the redox properties of the catalysts [18,28,29]. Lahousse *et al.* [18] found that MgO (a very basic oxide) was totally inactive towards conversion of isopropanol to acetone while a less basic ZnO was very active and concluded that dehydrogenation required redox sites rather than basic sites.

Among the divopositive cations in the ferrosipinel systems under study, there is a wide difference in the redox properties of copper ion from those of Co²⁺ or Ni²⁺ ions. We propose that the unique behaviour of copper ferrite during cyclohexanol decomposition is contributed by this difference in redox properties. Cu²⁺ with a higher electrode potential is more reducible and hence more efficient an oxidizing agent than Ni²⁺ or Co²⁺ ions (Table 5.1.4)

Table 5.1.4 data on standard electrode potentials.

Redox system	E ⁰ value (V)
$\text{Cu}^{2+} + 2\text{e}^- \rightleftharpoons \text{Cu}$	0.34
$\text{Cu}^{2+} + \text{e}^- \rightleftharpoons \text{Cu}^+$	0.16
$\text{Co}^{2+} + 2\text{e}^- \rightleftharpoons \text{Co}$	-0.28
$\text{Ni}^{2+} + 2\text{e}^- \rightleftharpoons \text{Ni}$	-0.23

The ferrospinels of nickel, cobalt and copper are n-type semiconductors with the band gap or activation energy of 0.37 eV for NiFe_2O_4 [10], 0.52 eV for CoFe_2O_4 [30] and 0.19 eV for CuFe_2O_4 [31]. The very low activation energy for CuFe_2O_4 is a direct consequence of its increased reducibility and this makes the electron movements in the system easier, increasing its oxidation activity.

As the dehydration and dehydrogenation selectivities are complimentary, a high dehydrogenation activity leads to a low dehydration activity. We have invoked the redox properties along with the basic properties to explain the high dehydrogenation activity of copper ferrite. Hence the complimentary dehydration activity is reduced much lower than demanded by the true acidity. In other words, in the case of copper ferrite, the cyclohexanol dehydration rate cannot be taken as a true index of its acidity.

The structural stability of the spinel catalysts during cyclohexanol conversion has been tested by taking the Mossbauer spectra of cobalt and copper ferrites after these have been used in the continuous-flow reactor for nearly 5 hours. These spectra are given in Fig. 3.1.18. Unlike the fresh catalysts, the used catalysts show the magnetic hyperfine splitting expected of ferrimagnetic substances. The lack of magnetic splitting for the fresh catalysts is due to their very small particle size. But, after being used in the reaction, the particle size of the catalysts has increased as evident from the magnetic hyperfine structure shown in the Mossbauer spectra. The isomer shift value of iron is still typical of Fe^{3+} proving that no bulk reduction has occurred during the reaction. As n-type semiconductors have a tendency to lose lattice oxygen on heating [32], some electrons are released which may cause some surface reduction of Fe^{3+} ions. This explains the electron conduction by the 'hopping' mechanism between Fe^{3+} and Fe^{2+} sites. The fate of the hydrogen during dehydrogenation will be conversion to water by combining with the lattice oxygen. Using ^{18}O -tracer technique, the participation of lattice oxygen during catalytic oxidation by metal oxides has been proved [33].

5.1.2 Ni_{1-x}Cu_xFe₂O₄ and Co_{1-x}Cu_xFe₂O₄ (x = 0.3, 0.5, 0.7) – type systems

(a) **RESULTS** The reaction data for the vapour-phase decomposition of cyclohexanol over the Ni-Cu and Co-Cu series of mixed ferrosinels are given in Table 5.1.5. An activity profile diagram is given in Fig. 5.1.1 (B) & (C).

Table 5.1.5 Cyclohexanol decomposition reaction data over mixed ferrosinels of the Ni-Cu series and the Co-Cu series of general formula A_{1-x}Cu_xFe₂O₄ (A = Ni or Co and x = 0.3, 0.5 & 0.7)

Mixed ferrite samples	x	% conversion	Product selectivity(%)			Rare constant (10 ⁻⁴ h ⁻¹ m ⁻²)		$\frac{k_{\text{CHONE}}}{k_{\text{CHENE}}}$	$\frac{k_{\text{CHONE}} + k_{\text{CHENE}}}{k_{\text{CHENE}}}$
			CHENE	CHONE	OTHERS	k _{CHENE}	k _{CHONE}		
Ni-Cu	0.3	79.6	11.2	81.6	7.3	2.0	22.4	11.2	24.4
Ni-Cu	0.5	71.1	12.6	82.9	4.5	2.0	18.4	9.4	20.4
Ni-Cu	0.7	83.5	25.1	72.5	2.4	5.1	20.2	4.0	25.3
Ni-Cu*	0.3	83.8	17.0	80.4	2.6	2.9	20.9	7.2	23.8
Ni-Cu*	0.5	89.0	63.2	35.3	1.6	14.8	6.7	0.5	21.5
Ni-Cu*	0.7	84.9	77.0	21.2	1.7	20.8	3.9	0.2	24.7
Co-Cu	0.3	76.7	6.3	90.9	2.7	1.4	33.0	23.9	34.4
Co-Cu	0.5	78.7	9.3	89.3	1.4	2.1	34.2	16.0	36.4
Co-Cu	0.7	77.3	8.0	90.7	1.3	1.5	27.3	18.8	28.8
Co-Cu*	0.3	54.8	46.6	51.8	1.6	7.3	8.3	1.1	15.6
Co-Cu*	0.5	67.3	71.9	26.2	1.9	16.2	4.8	0.3	21.0
Co-Cu*	0.7	47.5	60.1	37.9	2.0	7.8	4.6	0.6	12.5

*Sulphated samples. Activation temperature of the catalyst: 300°C, reaction temperature : 300°C, amount of catalyst : 3 g, feed rate : 3.6 ml h⁻¹, contact time : 0.88 h, WHSV : 1.14 h⁻¹.

A critical analysis of the data given in Table 5.1.5 and Table 5.1.1 enables us to make the following comments.

- (i) The dehydration activities of all the copper-containing mixed ferros spinels are monotonously much lower and the dehydrogenation activities are much larger than the corresponding values for the pure ferrites of Ni and Co.
- (ii) Except for Ni-Cu ferrite with $x = 0.3$, sulphation of the mixed ferros spinel samples causes their dehydration activities to increase by many folds and their dehydrogenation activities to decrease by corresponding proportions.
- (iii) There is no definite trend in the dehydration or dehydrogenation activities of both unmodified and sulphate-modified samples, that can be described as a function of copper concentration within the range $x = 0.3$ to $x = 0.7$
- (iv) On the average, the dehydrogenation activities and the $k_{\text{CHONE}}/k_{\text{CHENE}}$ ratios are much larger for the Co-Cu ferros spinels than for the Ni-Cu ferros spinels.
- (v) The lower dehydrogenation activities of the sulphated samples parallels with the lower limiting amount values of EA adsorbed by the samples, as was described in chapter III. Apart from this general correspondence, there is no one to one correlation between the basicity parameters of cyclohexanol decomposition and the same parameters in terms of limiting amounts of EA adsorbed.

(b)DISCUSSION

The sudden fall in the rate of dehydration of nickel and cobalt ferrites by as much as one-fifth, due to the incorporation of even a small amount of copper as $x = 0.3$, cannot be due to the small acidity of copper alone. As mentioned elsewhere, we strongly feel that the involvement of redox properties of copper ion in the copper-containing ferros spinels in the dehydrogenation process is responsible for this anomalous behaviour. Thus any possibility for getting a respectable correlation between the dehydration/dehydrogenation activities and the acid-base properties of these systems is lost. Iwamoto *et al.* [34], during their investigation of oxygen adsorption properties of metal oxides by means of TPD technique, found that CuO showed the largest amount of oxygen desorption, much larger than shown by NiO, Co_3O_4 or Fe_2O_3 . This correlates

surface areas at the activation and reaction temperature of 300°C. Hence all these samples are potential catalysts for industries. The catalyst giving the highest conversion of cyclohexanol is sulphated nickel ferrite (93.6%), the one giving the highest yield of cyclohexene is sulphated Ni-Cu ferrite with $x = 0.7$ (65.4% yield) and the catalyst giving the highest yield of cyclohexanone is Co-Cu ferrite with $x = 0.5$ (70.3% yield). It should be mentioned that a few catalyst samples gave significant quantities of benzene and phenol as the other products. Thus Ni-Cu ($x = 0.3$) gave 4.7% phenol, Ni-Cu ($x = 0.5$) gave 2.3 % phenol and sulphated NiFe_2O_4 gave 8% yield of benzene. Benzene is formed by the disproportionation of cyclohexene [9] and phenol by further dehydrogenation of cyclohexanone at high contact time [10].

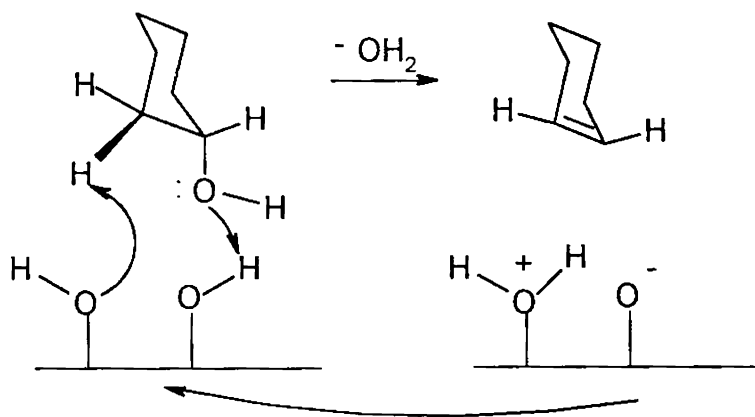
5.1.3 Mechanism of cyclohexanol decomposition

(a) Dehydration

It has been well-established that Brønsted acid sites of the catalyst are directly involved in the alcohol dehydration mechanism. The exact mechanism of gas-phase dehydration of cyclohexanol has proved difficult to study directly. But, by examining the dehydration of methyl-substituted cyclohexanols, two possible mechanistic schemes have been proposed for the dehydration of cyclohexanol [38,39]. These are given in Fig. 5.1.2

Scheme I is similar to E-2 elimination, in which the catalyst provides both an acidic site to attack the hydroxyl group and a basic site to abstract a proton. Scheme II is similar to E-1 elimination in which the reaction proceeds through initial formation of a carbocation)

Scheme I : Concerted dehydration.



Scheme II : Non-concerted (carbocation) dehydration

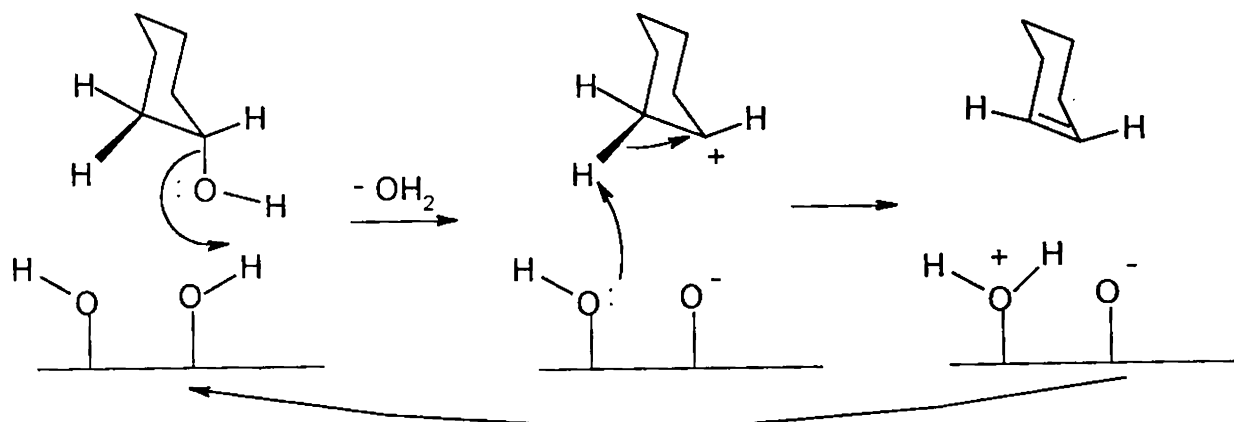


Fig. 5. 1. 2 Mechanism for the dehydration of cyclohexanol.

Recently the mechanism of gas-phase dehydration of cyclohexanol over a solid zirconium phosphate catalyst has been thoroughly studied by Costa *et al.*[13], by means of deuterium labeling experiments. In order to decide which one of these mechanisms (scheme I or scheme II of Fig. 5.1.2) is operating, a deuterium – labeled cyclohexanol was prepared and, after dehydration, scrambling of the label was investigated in the cyclohexene product. They [13] noticed the existence of scrambling of the label in the product cyclohexene. This was sufficient proof of the carbocation mechanism (Scheme II).

In cyclohexanol, the C-O bond is equatorial [40], and steric factors favour a perpendicular approach of the OH group of cyclohexanol to the surface of the catalyst, rather than a parallel approach. With such an approach of the equatorial hydroxyl group, the rest of the cyclohexanol molecule is at some distance from the catalyst surface and so is not involved in the reaction. Hence the reaction consists of the cleavage of the C – O bond to yield a carbocation, which is not necessarily involved with the catalyst surfaces.

(b) Dehydrogenation

Dehydrogenation of alcohols is catalysed by both redox and basic sites. We have suggested the redox properties of copper ferrite as an additional reason for its high dehydrogenation activity. It is well-known that the dehydrogenation process, explained in terms of acid-base properties of catalysts, takes place with the involvement of both acid and basic sites through a concerted mechanism [4,5,8,12]. This mechanism is represented by the following figure, Fig. 5.1.3 [8].

This mechanism, usually known as the ‘carbonyl’ mechanism, involves the fission of the O-H and C_α – H bonds. Most authors support this mechanism as against the rival ‘enolic’ mechanism involving the splitting of the C_β – H bond [41]. The metal cation is acting as a Lewis acid site accepting a hydride ion whereas the oxygen anion of the catalyst is acting as a Brønsted base accepting the proton of the OH group of the alcohol.

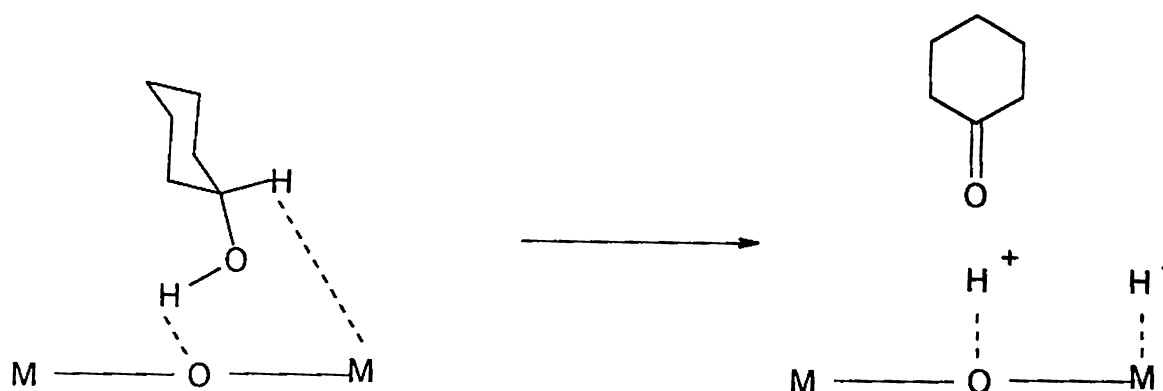


Fig 5.1.3 Mechanism of the dehydrogenation of cyclohexanol

When the proton acceptance precedes the splitting of the $C_{\alpha} - H$ bond, a surface alkoxide is formed as a reactive intermediate and the $C_{\alpha} - H$ bond is activated in the surface alkoxide facilitating its breakage [42, 43].

The high Lewis acidity of Cu^{2+} can be mentioned as a reason for the enhanced dehydrogenation activity of copper ferrite, as predictable from this mechanism. In fact, the high oxidising ability of Cu^{2+} ion parallels with its strong Lewis acidity. An idea from HSAB concept seems to be relevant to be mentioned here. Cu^{2+} is a soft acid and H^{-} is a very soft base so that the interaction between Cu^{2+} and H^{-} is expected to be very strong and natural. According to Klopman [44], soft acid – soft base interaction is controlled by the energies of the frontier orbitals involved in bonding and the binding forces are more of covalent character.

5.1.4 Effect of time on stream

The stability of the catalysts were tested by making the time on stream studies under the experimental conditions of WHSV and reaction temperature over a period of 5 hours. Most of the unmodified systems showed excellent stability (Fig 5.1.4). Sulphate-modified systems showed decrease in activity with time. This is usually the case with sulphate-modified catalysts and is attributed to easy coke formation [21].

5.1.5 Cyclohexanol decomposition and benzoylation of toluene

There is a fairly good correlation between the total catalytic activity for cyclohexanol decomposition ($k_{\text{CHENE}} + k_{\text{CHONE}}$) and the rate constant for benzoylation of toluene at 300° C. This is clear from Table 5.1.6. This may be due to the common role of Lewis acidity involved in both conversions.

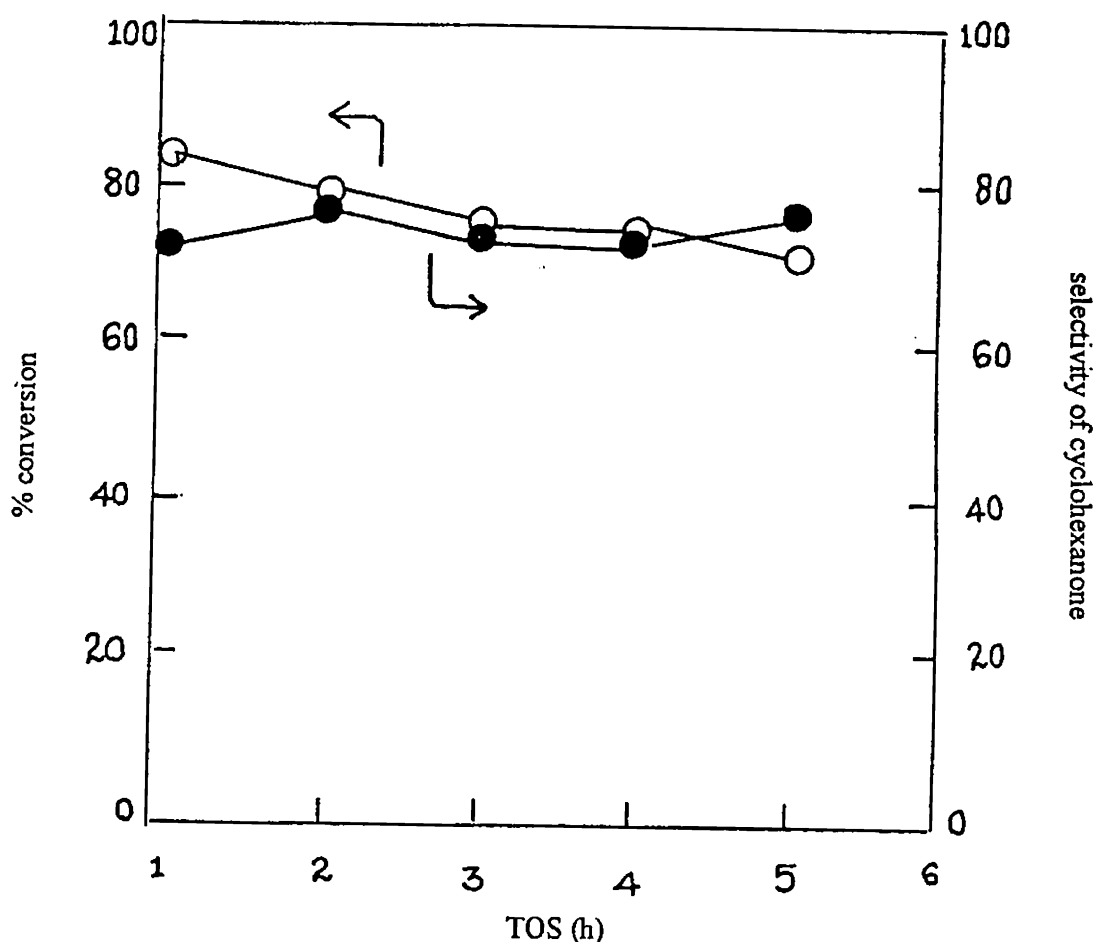


Fig. 5.1.4. Effect of time on stream (TOS) on cyclohexanol decomposition over the catalyst $\text{Ni}_{0.3}\text{Cu}_{0.7}\text{Fe}_2\text{O}_4$

Table 5.1.6 Comparison between the rate constants for the benzylation of toluene and the cyclohexanol decomposition over the various ferrosipinel systems

System, $A_{1-x}Cu_xFe_2O_4$ (A=Ni or Co)	x	Benzylation of toluene, rate constant, ($10^{-2} h^{-1} m^{-2}$)	Cyclohexanol decomposition ($k_{CHENE} + k_{CHONE}$) ($10^{-4} h^{-1} m^{-2}$)
Ni	0	3.5	17.8
Co	0	12.5	22.0
Cu	0	9.6	18.9
Ni*	0	4.7	21.9
Co*	0	11.3	31.9
Cu*	0	9.0	21.8
Ni - Cu	0.3	8.0	24.4
Ni - Cu	0.5	6.7	20.4
Ni - Cu	0.7	9.3	25.3
Ni - Cu*	0.3	6.8	23.8
Ni - Cu*	0.5	8.1	21.5
Ni - Cu*	0.7	12.8	24.7
Co - Cu	0.3	12.1	34.4
Co - Cu	0.5	15.1	36.4
Co - Cu	0.7	10.1	28.8
Co - Cu*	0.3	11.6	15.6
Co - Cu*	0.5	11.8	21.0
Co - Cu*	0.7	9.5	12.5

* sulphated samples.

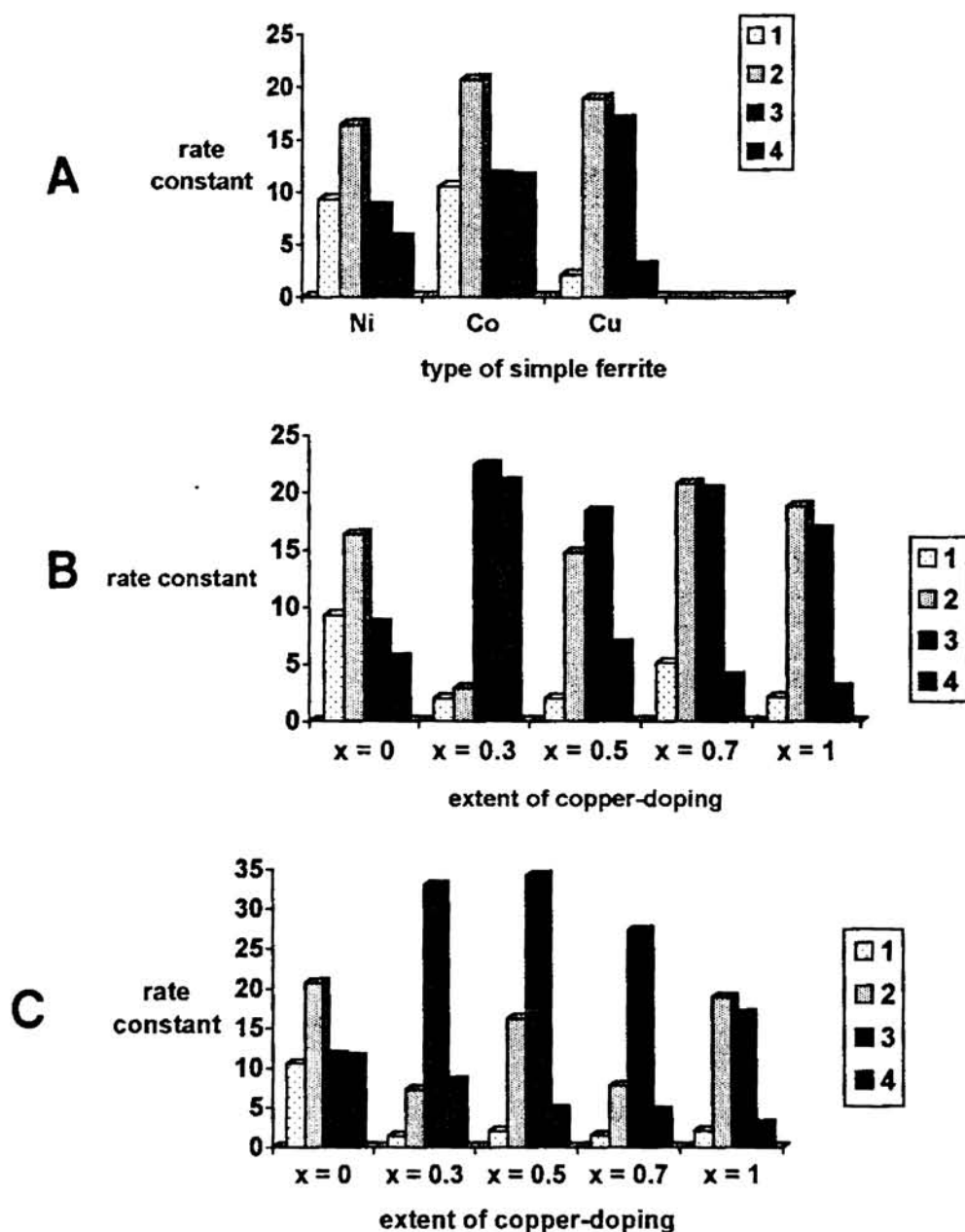


Fig. 5.1.1 Activity profile diagrams for the vapour-phase decomposition of cyclohexanol over the various ferrite systems of general formula, $A_{1-x}Cu_xFe_2O_4$ ($A = Ni$ or Co , $x = 0, 0.3, 0.5, 0.7$ and 1) (A) : simple ferrites, (B) : Ni-Cu ferrites, (C) : Co-Cu ferrites

1. Dehydration rate – unmodified systems. 2. Dehydration rate – sulphated systems.
 3. dehydrogenation rate – unmodified systems. 4. Dehydrogenation rate – sulphated systems. Reaction temperature: $300^\circ C$, contact time: 0.88 h, feed rate: 3.6 ml/h.

REFERENCES

1. M. Guisnet, "Catalysis by acids and Bases", B. Imelik *et al.* (Editors), Studies in Surface Science and Catalysis 20, Elsevier, Amsterdam, 1985, p.283
2. J. Kijenski and A. Baiker, *Catal. Today*, 5 (1989) 1
3. K. Tanabe, M. Misoto, Y. Ono and H. Hattori, "New Solid Acids and Bases", Kodansha, Tokyo and Elsevier, Amsterdam, 1989
4. M. Ai, *J. Catal.*, 40 (1975) 318
5. M. Ai, *Bull. Chem. Soc. Jpn.*, 50 (1977) 2579
6. A. Gervasini and A. Auroux, *J. Catal.*, 131 (1991) 190
7. M. A. Armendia, V. Borau, I. M. Garcia, C. Jimenez, A. Marinas, J. M. Marinas, A. Porras and F. J. Urbano, *Appl. Catal.*, 184 (1999) 115
8. C. P. Bezouhanova and M. A. Al-Zihari, *Catal. Lett.*, 11 (1991) 245
9. M. Dobrovolszky, P. Tetenyi and Z. Paal, *J. Catal.*, 74 (1982) 31
10. N. J. Jebarathinam and V. Krishnasamy, "Catalysis: Present & Future", P. Kanta Rao and R. S. Beniwal (Editors), Publication And Information Directorate /Wiley Eastern Ltd., New Delhi, 1995, p. 354
11. M. V. Joshi, S. G. Oak and V. S. Darshane in "Catalysis: Modern Trends", N. M. Gupta and D. K. Chakrabarthy (Eds) , Narosha Publishing House, New Delhi, 1995, p. 275
12. D. Martin and Duprez, *J. Mol. Catal.*, 118 (1997) 113
13. M. C. C. Costa, L. F. Hodson, R. A. W. Johnstone, J. Y. Liu and D. Whitaker, *J. Mol. Catal.*, 142 (1999) 349
14. K. J. Laidler, "Chemical Kinetics", Third Edition, Harper International Edition, 1987, p.33
15. M. Ai, *J. Catal.*, 40 (1975) 318
16. P. E. Hathaway and M. E. Davis, *J. Catal.*, 116 (1989) 279
17. A. L. Mc Kenzie, C. T. Fishel and R. J. Davis, *J. Catal.*, 138 (1992) 547
18. C. Lahousse, J. Bachelier, J. C. Lavalley, H. Lauron-Pernot and A. M. Le Govic, *J. Mol. Catal.*, 87 (1994) 329

19. K. Arata and M. Hino, *React. Kinet. Catal. Lett.*, 25(1-2) (1984) 143; K. Arata and M. Hino, *Appl. Catal.*, 59 (1990) 197
20. C. Miao, W. Hua, J. Chen and Z. Gao, *Catal. Lett.*, 37 (1996) 187
21. X. Song and A. Sayari, *Catal. Rev. – Sci. Eng.*, 38(3) (1996) 329
22. Yu. Belokopytov, K. M. Kholyavalenko and M. Ya. Rubanik, *Kin. i Kataliz (russ.)*, 14 (1973) 1280
23. Yu. Belokopytov, K. M. Kholyavalenko and M. Ya. Rubanik, *Kataliz i Katalizatory*, Vol. 8 (Russ.), *Naukovaya Dumka, Kiev*, 1971, p. 13
24. A. Auroux and A. Gervasini, *J. Phys. Chem.*, 94 (1990) 6371
25. S. Berckman, C. J. Morrel, and G. Egloff, “*Catalysis: Organic and Inorganic*”, Reinhold, New York, 1940
26. W. S. Chen and M. D. Lee, *Appl. Catal.*, 83 (1992) 201
27. M. Wojciechowska, J. Haber, S. Lomnicki and J. Stoch, *J. Mol. Catal.*, 141 (1999) 155
28. M. I. Zaki, G. A. M. Hussein, H. A. El Ammany, S. A. A. Mansour, J. Polz and H. Knozinger, *J. Mol. Catal.*, 57 (1990) 367
29. L. J. Lakshmi and P. Kanta Rao, in “*Catalysis: Present and Future*”, P. Kanta Rao and R. S. Beniwal (Editors), Publication And Information Directorate /Wiley Eastern Ltd., New Delhi, 1995, p. 354
30. G. R. Dube and V. S. Darshane, *Bull. Chem. Soc. Jpn.*, 64 (1991) 2449
31. S. P. Ghorpade, V. S. Darshane and S. G. Dixit, *Appl. Catal.*, 166 (1998) 135
32. R. L. Augustine, “*Heterogeneous Catalysis for the Synthetic Chemist*”, Marcel Dekker, Inc., New York, 1995, p.179
33. Y. Takasu, M. Matsui and Y. Matsuda, *J. Catal.*, 76 (1982) 61
34. M. Iwamoto, Y. Yoda, N. Yamazoe and T. Siewama, *J. Phys. Chem.*, 82 (1978) 2564
35. J. L. G. Fierro and J. F. Garcia de la Branda, *Catal. Rev. – Sci. Eng.*, 28 (2&3) (1986) 265
36. K. Meguro and K. Esumi, *J. Adhesion Sci. Technol.*, 4(5) (1990) 393
37. F. R. Chen, G. Coudurier, J. F. Joly and J. C. Vedrine, *J. Catal.*, 143 (1993) 616

38. J. Blanc and H. Pines, *J. Org. Chem.*, 33 (1968) 2035
39. C. L. Kibby, S. S. Lande and W. K. Hall, *J. Am. Chem. Soc.*, 94 (1972) 214
40. E. L. Eliel, N. L. Allinger, S. J. Angyal, G. M. Morrison, "Conformational Analysis", Wiley, New York, 1965, p.51
41. D. Gulkova and M. Kraus, *J. Mol. Catal.*, 87 (1994) 47
42. L. Nondek and J. Sedlacek, *J. Catal.*, 40 (1975) 34
43. M. Bowker, R. W. Petits and K. C. Waugh, *J. Catal.*, 99 (1986) 53
44. G. Klopman, *J. Am. Chem. Soc.*, 90 (1968) 223

CHAPTER-VI
SUMMARY AND CONCLUSION

6.1 SUMMARY

Ferros spinels have attracted much attention due to their special cation distribution, structural stability, catalytic activity and technologically useful electric and magnetic properties. The usual ceramic method of preparing ferros spinels gives aggregate particles with low surface areas and large particle size, which adversely affect their catalytic utility. The recently developed low temperature co-precipitation method yields homogeneous and fine ferrite particles with high surface areas. This has given a new impetus to the study of catalytic activities of the ferrite systems. The present thesis is devoted to the study of the surface properties and catalytic activities of the ferros spinels of Co, Ni and Cu, prepared by the low temperature co-precipitation route. The surface properties are evaluated by various physico-chemical methods and the catalytic activities are studied for the liquid-phase Friedel-Crafts benzoylation of toluene and benzene and for the vapour-phase decomposition of cyclohexanol. As sulphation of metal oxides often yields more acidic and active samples, we have also studied the effect of sulphation on the surface properties and catalytic activities of all the ferros spinel systems. The sulphation has been done by 'impregnation method' using ammonium sulphate solution. The catalyst systems studied are $\text{Ni}_{1-x}\text{Cu}_x\text{Fe}_2\text{O}_4$ and $\text{Co}_{1-x}\text{Cu}_x\text{Fe}_2\text{O}_4$ and their sulphated analogues with $x = 0, 0.3, 0.5, 0.7$ and 1 .

In **Chapter I**, an introduction to heterogeneous catalysis and a literature survey on catalysis by transition metal oxides and 2-3 oxidic spinels, with special reference to oxides of Ni, Co, Cu and Fe, are given. This chapter also includes literature surveys on heterogeneous Friedel-Crafts acylation reaction, alcohol decomposition reaction and the study of surface electron donor properties by adsorption of electron acceptors. A detailed description of the spinel structure and a review on methods of preparing catalysts are additional features of this chapter.

Chapter II deals with the various experimental procedures adopted for the present work. It also gives a brief account of the relevant theory of each method of characterization employed.

Chapter III is mainly oriented to giving the results and discussion of these characterization procedures. The results and discussion are conveniently done under three headings – simple ferros spinels, mixed ferros spinels of the Ni-Cu series and the mixed ferros spinels of the Co-Cu series. The spinel phase and the inverse spinel structure of the samples have been confirmed by the agreement between the experimental XRD data with the standard data given in JCPDS Data Cards. Average particle size from XRD data is in the range 15-25 nm. DRIFT spectra further confirms the spinel phase. Sulphation is qualitatively confirmed by FT-IR. The absence of a peak near 1400 cm^{-1} rules out any possible superacidity in the sulphated samples. IR data correspond to a surface sulphate structure of bidentate sulphato complex or bisulphate modified model. EDX analysis confirms the stoichiometry of the spinel samples and estimates the sulphate loading to an average amount of 1% by mass of sulphur. TGA proves that the dehydration of sulphated samples is delayed during calcination. Mossbauer spectra confirm the oxidation state of iron as +3. The lack of magnetic splitting is taken as evidence for the very small particle size of the samples while, the presence of quadrupolar splitting is evidence enough for the unsymmetrical octahedral electric field around the Mossbauer nucleus. The inherent ferrimagnetic quality of the sample is proved by the Mossbauer magnetic hyperfine splitting of used catalysts. This also proves the sintering of the particles during reaction. Study of ED properties with EA of varying electron affinity values shows that copper ferrite and copper containing mixed ferrites have high proportion of strong basic sites. Sulphation is found to decrease the ED properties of all the samples. The intrinsic ED properties are found to increase with the activation temperature and this effect is highest for copper ferrite. The results are rationalised in terms of charge to radius ratio of cations, electronegativity of cations and the unique properties of copper oxide such as thermal instability, special coordination described as (4+2) coordination, etc. Gravimetric adsorption of n-butylamine followed by TGA gives a distribution of acid sites of simple ferros spinels and their sulfated analogues. On the basis of the acidity results, CoFe_2O_4 is expected to be the best catalyst for acid-catalyzed reactions at 300°C .

Chapter IV narrates the results and discussion of the Friedel-Crafts benzoylation of toluene and benzene with benzoyl chloride over the ferros spinel systems. The reaction data show that sulphation has no positive effect on the benzoylation rates. From a critical analysis of the results, it is argued out that the strong Lewis acid sites provided by the octahedral cations of the spinel structure are directly involved in deciding the activities for benzoylation reaction. Three factors are to be considered to rationalise the catalytic activities. These are (i) the number of strong acid sites (ii) the exact strength of the strong acid sites and (iii) the effect of activation temperature on increasing the number and strength of the strong acid sites. In terms of these factors, the catalytic activities of all the samples for benzoylation reaction have been explained. The added electronegativity of the Cu^{2+} ion and the susceptibility of copper-containing ferros spinels to the creation of lattice defects on calcination, are also important factors in explaining the catalytic activities. The effects of sulphation, copper-doping and activation temperature on the rates of the catalytic systems for benzoylation have been thoroughly discussed in this chapter. Co-Cu ferrite with $x = 0.3$ activated at 500°C has the highest intrinsic activity while sulphated Ni-Cu ferrite ($x = 0.7$) activated at 300°C has the highest specific activity for benzoylation of toluene. In the case of benzoylation of benzene, CuFe_2O_4 activated at 500°C has the highest intrinsic activity while CuFe_2O_4 calcined at 300°C has the highest specific activity. A mechanism for benzoylation involving the formation of a complex intermediate between benzoyl chloride and the Lewis acid centre of the catalyst has been proposed.

In **Chapter V**, we have given the details of studying the vapour-phase decomposition of cyclohexanol at 300°C over the ferros spinel systems activated at 300°C . Intrinsic rate constants for cyclohexene (k_{CHENE}) and cyclohexanone (k_{CHONE}) formations have been calculated. In alcohol decomposition reaction, dehydration activity is related to the acid sites and dehydrogenation activity is related to the basic sites or redox sites of the catalysts. Good correlation is obtained between the dehydration activities of the simple ferros spinels and their acidities (medium strength) determined independently by the n-butylamine adsorption method. Except for a good correlation between the (medium + strong) basicity parameters obtained from EA adsorption studies and the ratio

$(k_{\text{CHONE}})/(k_{\text{CHENE}})$ for the unmodified simple ferrites, there is no correlation between the basicity parameters obtained by the two independent methods. The extremely low dehydration activity of copper-containing ferrites and the converse abnormally high dehydrogenation activity of the same samples for cyclohexanol decomposition cannot be due to the acidity/basicity factors alone. We strongly feel that, in copper-containing ferros spinels, the redox properties are involved in the dehydrogenation activity, 'blowing up' the basicity parameter. As a consequence, the dehydration selectivities no longer represent the true acidities of the samples in the mixed-ferrospinel series.

6.2 Conclusions

- Preparation of ferros spinels of Ni, Co and Cu by the low temperature co-precipitation method produced homogeneous and very fine particles with high surface areas.
- Sulphate modification has been done on all the catalytic systems. Sulphation studies on spinels are being reported for the first time. Sulphation caused an increase in the surface areas of most of the samples and delayed the dehydroxylation of the samples on calcination.
- Sulphation very much enhanced the dehydration activity of all the samples during the decomposition of cyclohexanol. However, sulphation did not show much influence on the catalytic activity for the benzoylation of aromatics.
- Study of distribution of acid sites by gravimetric adsorption of n-butylamine revealed that the number of medium strong and strong acid sites varied in the order $\text{Co} > \text{Ni} > \text{Cu}$ for the simple ferrites and in the order, $\text{Co} > \text{Cu} > \text{Ni}$ for the sulphated analogues. Sulphation caused a tremendous increase in the number of medium strong and weak acid sites while the strong acid sites were left unaffected.
- Adsorption experiments using electron acceptors of varying electron affinity values showed that CuFe_2O_4 has both the highest proportion of medium to

strong basic sites and also the lowest proportion of weak basic sites. In the mixed ferros spinel series, the effect of copper substitution was to increase the strong basic sites and to decrease the weak basic sites with copper content. However, the total basicity was highest for CoFe_2O_4 at the activation temperature of 300°C and for CuFe_2O_4 at the activation temperature of 500°C . Among the mixed ferros spinels, Co-Cu ferrite ($x = 0.5$) showed the maximum total basicity at both activation temperatures.

- The basicity of all the ferros spinel samples reduced significantly on sulphation.
- The effect of activation temperature of the catalyst was to increase the catalytic activity for benzoylation and to increase the electron donor properties of all the samples, the effects being very high for copper-containing samples.
- All the ferros spinel samples proved to be very good catalysts for benzoylation of toluene and also benzene with benzoyl chloride. The best yields were 71% for toluene catalysed by sulphated Ni-Cu ferrite with $x = 0.7$ and 16.2% for benzene catalysed by copper ferrite. Under our reaction conditions of short reaction time and small amounts of catalysts, these are promising yields in comparison to many other reported values.
- The intrinsic catalytic activity for benzoylation of toluene varied in the order $\text{Co} > \text{Cu} \gg \text{Ni}$ at the activation temperature of 300°C and in the order $\text{Cu} \gg \text{Co} > \text{Ni}$ at the activation temperature of 500°C for both unmodified and sulphate-modified ferrites. In the case of benzene, the catalytic activity for benzoylation was always in the order, $\text{Cu} > \text{Co} > \text{Ni}$ at both activation temperatures and for both unmodified and modified samples.
- There was a general increase in the catalytic activity for the benzoylation of aromatics with copper-doping, the effect being more pronounced in the Ni-Cu ferrites than in the Co-Cu ferrites.

- There was good correlation between the dehydration /dehydrogenation activities of cyclohexanol decomposition and the acid-base parameters determined by n-butylamine adsorption/electron donor studies, in the case of simple ferrites.
- During cyclohexanol decomposition, the best yield (70.3%) of cyclohexanone was given by Co-Cu ($x = 0.5$) ferrite and the best yield of cyclohexene (65.4%), by sulphated Ni-Cu ($x = 0.7$) ferrite.
- Copper-containing ferrites showed very high activities for dehydrogenation and very low activities for dehydration, during cyclohexanol decomposition. Along with the basic properties, the redox properties of copper ion are being suggested as the reason for this added dehydrogenation activity. Consequently, the dehydration activity, which is somewhat complementary to the dehydrogenation activity, cannot be regarded as a true index of Brønsted acidity of copper-containing systems.
- The afore-mentioned results agree to the generally accepted notions namely, alcohol dehydration is catalysed mainly by the medium strong Brønsted acid sites and the benzylation of aromatics is catalysed by the strong Lewis acid sites on the surface of the catalyst samples.
- The well-documented thermal instability of CuO imparts some thermal instability in copper-containing ferrosinels too. Calcination of such samples creates more surface defects in terms of co-ordinatively unsaturated cations and trapped electrons. This is the cause of the simultaneous increase in the Lewis acidity and Lewis basicity in such samples on calcination.